UNIVERSITY OF CALIFORNIA, SAN DIEGO

Acoustic sources of opportunity in the marine environment - applied to source localization and ocean sensing

A dissertation submitted in partial satisfaction of the
requirements for the degree
Doctor of Philosophy

in

Oceanography

by

Christopher M. Verlinden

Committee in charge:

William A. Kuperman, Chair
Michael J. Buckingham
William A. Coles
Bruce D. Cornuelle
William S. Hodgkiss
Walter H. Munk

2017

The dissertation of Christopher M. Verlinden is approved, and it is acceptable in quality and form for publication on microfilm and electronically:

_____

_____

_____

_____

_____

_____

Chair

University of California, San Diego

2017

TABLE OF CONTENTS

LIST OF FIGURES

ACKNOWLEDGEMENTS

Thank you to the Office of Naval Research for providing support for field work and to the United States Coast Guard Navigation Center Nationwide AIS database for providing AIS ship tracking data in support of this research initiative.

Chapter 2, in part has been published in the Journal of the Acoustic Society. Verlinden C. M. A., Sarkar J., Hodgkiss W. S., Kuperman W. A., and Sabra K. G.. Passive acoustic source localization using sources of opportunity. The Journal of the Acoustical Society of America, 138(1):EL54, 13 July, 2015. doi: http://dx.doi.org/10.1121/1.4922763. The dissertation author was a primary investigator and author of this material. Dr. William Kuperman, the chair of the committee, is a co-author.

Chapter 3, in part has been published in the Journal of the Acoustic Society. Verlinden C. M. A., Sarkar J., Cornuelle B.D., Kuperman W. A.. Determination of acoustic waveguide invariant using ships as sources of opportunity in a shallow water marine environment. The Journal of the Acoustical Society of America, 141, EL102, (2017). doi: http://dx.doi.org/10.1121/1.4976112. The dissertation author was a primary investigator and author of this material. Dr. William Kuperman, the chair of the committee, is a co-author.

Chapter 4, in part has been submitted for publication in the Journal of the Acoustic Society. Verlinden C. M. A., Sarkar J., Hodgkiss W. S., Kuperman W. A., and Sabra K. G.. Passive acoustic tracking using a library of nearby sources of opportunity. The Journal of the Acoustical Society of America. Submitted 06 March, 2017. The dissertation author was a primary investigator and author of this material. Dr. William Kuperman, the chair of the committee, is a co-author.

Chapter 5, in part is currently being prepared for submission for publication of the material. Kubicko J., Verlinden C., Sarkar J., Fagan, A., Nichols B., Martin J., Sabra K.. A feasibility study for passive acoustic estimation of vertical sound speed structure using sources of opportunity on a drifting volumetric array. The Journal of the Acoustical Society of America. Submitted 06 March, 2017. The dissertation author was a primary investigator and author of this material.

Chapter 6, has been published in the Journal of the Acoustic Society. Tipp-

mann, J., Sarkar, J., Verlinden, C., Hodgkiss, W., Kuperman, W.A.. Toward ocean attenuation tomography: Determining acoustic volume attenuation coefficients in seawater using eigenray amplitudes. The Journal of the Acoustical Society of America, 2016. The dissertation author was a primary investigator and author of this material. Dr. William Kuperman, the chair of the committee, is a co-author.

VITA

2008	B. S. in Marine and Environmental Science, United States Coast Guard Academy, New London, Connecticut
2014	M.S. in Oceanography, University of California, San Diego, La Jolla, California
2017	Ph. D. in Oceanography, University of California, San Diego, La Jolla, California

Verlinden C. M. A., Sarkar J., Hodgkiss W. S., Kuperman W. A., and Sabra K. G.. Passive acoustic source localization using sources of opportunity. The Journal of the Acoustical Society of America, 138(1):EL54, 13 July, 2015. doi: http://dx.doi.org/10.1121/1.4922763.

Verlinden C. M. A., Sarkar J., Cornuelle B.D., Kuperman W. A.. Determination of acoustic waveguide invariant using ships as sources of opportunity in a shallow water marine environment. The Journal of the Acoustical Society of America, 141, EL102, (2017). doi: http://dx.doi.org/10.1121/1.4976112.

Verlinden C. M. A., Sarkar J., Hodgkiss W. S., Kuperman W. A., and Sabra K. G.. Passive acoustic tracking using a library of nearby sources of opportunity. The Journal of the Acoustical Society of America. Submitted 06 March, 2017

Kubicko J., Verlinden C., Sarkar J., Fagan, A., Nichols B., Martin J., Sabra K.. A feasibility study for passive acoustic estimation of vertical sound speed structure using sources of opportunity on a drifting volumetric array. The Journal of the Acoustical Society of America. Submitted 06 March, 2017

Tippmann, J., Sarkar, J., Verlinden, C., Hodgkiss, W., Kuperman, W.A.. Toward ocean attenuation tomography: Determining acoustic volume attenuation coefficients in seawater using eigenray amplitudes. The Journal of the Acoustical Society of America, 2016

Thode A., Mathias D., Straley J., Andrews, R. Lunsford C. Moran J., Sarkar J., Verlinden C., Hodgkiss W., Kuperman W.. Exploiting the sound-speed minimum to extend tracking of vertical arrays in deep water environments. The Journal of the Acoustical Society of America, 136, 2091 (2014).

ABSTRACT OF THE DISSERTATION

Acoustic sources of opportunity in the marine environment - applied to source localization and ocean sensing

by

Christopher M. Verlinden

Doctor of Philosophy in Oceanography

University of California, San Diego, 2017

William A. Kuperman, Chair

Controlled acoustic sources have typically been used for imaging the ocean. These sources can either be used to locate objects or characterize the ocean environment. The processing involves signal extraction in the presence of ambient noise, with shipping being a major component of the latter. With the advent of the Automatic Identification System (AIS) which provides accurate locations of all large commercial vessels, these major noise sources can be converted from nuisance to beacons or sources of opportunity for the purpose of studying the ocean. The source localization method presented here is similar to traditional matched field processing, but differs in that libraries of data-derived measured replicas are used in place of modeled replicas. In order to account for differing source spectra between

library and target vessels, cross-correlation functions are compared instead of comparing acoustic signals directly. The library of measured cross-correlation function replicas is extrapolated using waveguide invariant theory to fill gaps between ship tracks, fully populating the search grid with estimated replicas allowing for continuous tracking. In addition to source localization, two ocean sensing techniques are discussed in this dissertation. The feasibility of estimating ocean sound speed and temperature structure, using ship noise across a drifting volumetric array of hydrophones suspended beneath buoys, in a shallow water marine environment is investigated. Using the attenuation of acoustic energy along eigenray paths to invert for ocean properties such as temperature, salinity, and pH is also explored. In each of these cases, the theory is developed, tested using numerical simulations, and validated with data from acoustic field experiments.

Chapter 1

Introduction

This thesis explores the use of noise generated by acoustic sources of opportunity, such as ships, to study the marine environment. This includes applications in acoustic source localization (Chapters 2-4) and characterizing the marine environment (Chapters 5-6).

1.1 Ocean Acoustics

Ocean acoustics is the study the propagation of sound in the marine environment. Acoustics is pertinent to the field of oceanography because acoustic energy can be used to study the ocean. In the atmosphere, electromagnetic radiation is used for communications (radio) and remote sensing (RADAR/LiDAR). In air, electromagnetic radiation is capable of propagating great distances with minimal distortion or lost energy. Conversely, in water, electromagnetic radiation attenuates rapidly; therefore, underwater remote sensing and communication is accomplished by utilizing acoustic energy, as sound is capable of propagating great distances in water.

1.1.1 History

The study of ocean acoustics dates back to 1490 with Leonardo da Vinci, who conducted experiments by inserting a listening tube into the water, and noted

that ships and other activity could be detected from great distances[1]. Colladen and Sturm were the first to make quantitative measurements of acoustic propagation in water, conducting an experiment in 1826 to measure the speed of sound in water to within 0.2% accuracy using a bell and a listening tube–not unlike the one used by da Vinci. Colladen and Sturm took note of the great distances over which relatively low energy sounds could propagate in water. The history of acoustics includes many notable physicists and mathematicians. Pythagoras developed the theory of Western musical scale, while Mersenne added irrationals to the concept, noting that the frequency of a vibrating string was proportional to the square root of its cross-sectional area[1]. Galileo, Newton, Rayleigh, Euler, Lagrange, d'Alembert, and more recently in the study of oceanography, Munk and Wunsch, have all made significant contributions to the study of acoustics[1]. Instrumentation and applications of ocean acoustics have increased in both sophistication and value over the centuries. During the second World War, with the rise of active SONAR, the study of ocean acoustics became paramount for defense applications. This continued over the decades that followed with the Cold War, fueling research interests into increasingly sophisticated active and passive detection methodology. These detection algorithms required extensive knowledge of the marine environment, motivating the development of acoustic ocean sensing technology. After the Cold War, interest in ocean sensing for environmental studies heightened, becoming one of the primary applications of ocean acoustics.

1.1.2 Passive and Active Techniques

In the study of ocean acoustics, techniques are generally classified as either active, or passive. Active techniques involve generating an acoustic signal, and detecting how that signal has been changed by the ocean waveguide in order to gain information about the environment or localize objects. In the case of active SONAR, a sound signal is emitted, and the time it takes for the signal to reflect off an object is used to determine the range to that object. Passive acoustic techniques do not involve producing a sound in order to sense the environment; in other words they involve simply listening to sounds produced by other sources. In the case of

passive SONAR, a series of underwater microphones, or hydrophones, are used to detect the sound made by a target. The direction the sound originates from is determined using the relative time lag across an array of hydrophones.

1.1.3 Applications

Applications of ocean acoustics can generally be grouped into three categories: underwater communications, localization, and ocean sensing.

Communication Sounds propagates great distances with very little loss of energy in water. In air, at 20 degrees C, with 10% relative humidity, a 1000 Hz acoustic signal will attenuate at 14.1 dB/km, which means a 60 dB sound will be detectable at ranges of about 4 km. In seawater, that same 1000 Hz signal will attenuate at about 0.07 dB/km, meaning it could potentially propagate over 850km[2]. The speed of sound in seawater is approximately 1500 m/s, compared to 340 m/s in air, which means acoustic communication can occur more rapidly in water. Acoustic communications methods are currently the most viable way to send information over great distances underwater, quickly and efficiently.

Detection, Classification, and Localization (DCL) One of the primary applications of ocean acoustics is to find objects underwater. This includes depth-finding and probing the seafloor using active fathometers, multi-beam SONARs, and sub-bottom profilers. These instruments rely on the time delay between the transmission of an acoustic signal and the echo of that signal off the bottom, or a layer within the bottom to determine distance. Marine biologists localize marine mammals and other fauna using passive techniques. In defense applications, the Navy uses active and passive acoustics to localize ships and submarines.

Active SONAR functions by broadcasting a pulse of acoustic energy and using the time it takes that signal to reflect off an object, such as a submarine, and return to the receiver to determine the range to that object. Combined with the angle that the returned signal arrived from, this is enough localize the target. Passive SONAR functions by listening to sounds emitted by targets and using

the direction of those incoming signals to determine their position. This can be as simple as triangulation, where at least three hydrophones are used to find an acoustic radiator, using the relative time delay between signal arrivals at each of the hydrophones. When the relative time delay of incoming signals across combinations of many hydrophones is used to determine the direction of an incoming signal, this is known as beam-forming. Beam-forming involves modeling what the arrival structure (relative set of time delays) an incoming signal would have across an array of hydrophones for a source in any direction. The direction that corresponds to the set of arrivals that most closely resembles the arrival structure on the array in the presence of an acoustic radiator is taken to be the direction of that incoming signal. To beam-form, or steer, an acoustic array to listen in just one direction at a time, the signal on each of the elements in the array is summed with the time delay associated with an arrival from that direction. This effectively amplifies signals coming from that direction and suppresses those coming from any other direction.

More sophisticated passive acoustic source localization techniques exist to localize acoustic sources in three dimensions in an ocean acoustic waveguide. Matched field processing (MFP) is a technique that involves modeling the acoustic arrival structure on an array of hydrophones for a source in every possible position in a waveguide, using an acoustic propagation model. The library of modeled replica arrival structures is compared to the arrival structure of an acoustic signal from a source in the waveguide that is being localized, and assigning the location with the modeled arrival structure that most closely resembles the observed structure as the location of the target. There are many different versions of MFP that have been developed over the years[3]. There are a variety of numerical propagation models that can be used to simulate the signals in order to create a library of replica signals including ray tracing, spectral or wavenumber integration techniques, normal mode and parabolic equation based propagation models. There are also a variety of comparison metrics that can be used to compare the data signal (signal from the source being localized) with the library of replica signals (signals simulated using a propagation model for all positions within the waveg-

uide). Traditional Bartlett beam-forming methods can be used, along with more sophisticated adaptive algorithms such as a minimum variance distortion reduction (MVDR) or white noise constraint (WNC) beam-formers[3]. Additionally, sparse processing techniques[4] are available to further enhance MFP as a localization technique. MFP is fundamentally limited by the inability to model the environment with sufficient precision to consistently localize sources. The ocean is a non-stationary and complex media for acoustic propagation, meaning changes from seasonal or diurnal heating/cooling, the passage of internal waves, or even complicated bottom features and compositions, can be difficult to account for in numerical models of sound propagation. For this reason, it is often impossible to generate modeled replicas with sufficient precision to localize contacts in three dimensions using MFP. This motivates the need for the passive acoustic source localization methods which are discussed in the following chapters.

It is important to note that determining the position of sub-surface contacts is not the only topic of interest when it comes to source localization. The United States Coast Guard has interest in localizing loud surface and semi-submersible vessels engaged in smuggling and other nefarious activities, which are not transmitting their location via radio beacon and may not be detectable by RADAR. This motivates the need for the development of localization techniques designed to find loud surface contacts, particularly in coastal environments.

Ocean Sensing For many of the aforementioned acoustic communications and source localization applications, it is beneficial to understand the physical characteristics of the ocean as they pertain to acoustic propagation. The speed of sound in seawater, and as a result the direction sound propagates, is a function of temperature, salinity, and pressure. Movement of water in ocean currents and internal waves can cause distortion, scattering, focusing, and deflection of acoustic waves in seawater. Because the attenuation of sound in seawater is is a function of temperature, salinity, pressure, and even pH, these properties must all be known in order to understand acoustic propagation for source localization and communications purposes. Understanding the distribution and dynamics of ocean properties and features including currents, eddies, and internal waves, are also of interest to

physical oceanographers and are useful for environmental studies.

In the study of climate science and physical oceanography, as well as in ocean acoustic source localization applications, it is beneficial to understand the distribution of ocean properties such as temperature and salinity[5]. For climate studies, knowing the temperature of the ocean to a high degree of accuracy with sufficient temporal and spatial resolution is required to populate climatological models[6]. Currently, ocean temperature is measured through a variety of means including isolated transects taken from research vessels, as well as a worldwide system of autonomous floats (e.g. Argo floats). Argo floats allow oceanographers to resolve coarse climatological variability; however, a gap exists in physical oceanographic data for the Arctic, Antarctic (under sea-ice), and coastal regions, which are among the most important and least understood areas for understanding the global heat budget[7]. Higher spatial and temporal resolution is needed[7] in these regions as well as in the open ocean. Active acoustic methods of measuring ocean temperature for climate change related studies are discussed in the next section of this paper. Developing passive acoustic methods to measure ocean temperature for this purpose is the focus of Chapter 5 of this document.

Global warming of the world's oceans is not the only topic of interest in the climate science community; ocean acidification is also of increasing concern[2]. Increasing levels of anthropogenic carbon dioxide in the atmosphere contributes to CO2 flux into the ocean. CO2 in seawater disassociates into carbonic acid and free hydrogen ions, which drives the carbonate reaction to the left.

$$CO_2 + H_2O \Rightarrow H_2CO_3 \Rightarrow H^+ + HCO_3$$

$$H^+ + CO_3^- \Rightarrow HCO_3^-$$

This reaction decreases pH, which has a harmful impact on biology, especially organisms with calcareous shells or tests[2]. With growing concern for ocean acidification, obtaining accurate and complete pH estimates of the ocean is more important than ever. Unfortunately, pH is difficult to measure in the environment. Most pH probes cannot be used at depth (pressure limitations), so bottle samples must be taken, transported, and processed in a laboratory environment, which is both time consuming and expensive. For this reason, developing an acoustic

method of imaging the ocean for pH is paramount. This motivates the research in Chapter 6 of this thesis.

Ocean currents and seafloor properties are also surveyed using ocean acoustics. Acoustic doppler current profilers (ADCPs) are acoustic instruments that emit high frequency sound and use the doppler shift caused by the sound reflecting and scattering off moving particulates in the water to estimate current velocity. These instruments are crucial to the field of physical oceanography for studying ocean currents and volumetric transport. Developing passive acoustic methods, using sources of opportunity, to make direct measurements of ocean current might be possible and is a subject for future research. Within the field of geoacoustics, bottom properties and sub-bottom structure are studied through the use of active acoustic techniques. Sub-bottom profilers generate an acoustic signal, using the time it takes the signal to travel through the water, and layers of the bottom and reflect back to the receiver to image seafloor properties. Developing passive acoustic methods for accomplishing this is also an area for future research.

1.1.4 ATOC

In the 1990s, Munk et al.[8] proposed to measure large portions of the ocean using acoustic tomography. Acoustic tomography uses the path sound takes through the ocean, which is a function of sound speed and by extension temperature, to 'image' the ocean for environmental properties such as temperature. The 1998 Acoustic Thermometry of Ocean Climate (ATOC) experiment, used time-of-arrival tomography to measure the temperature of the ocean, taking advantage of long-range acoustic propagation through the SOFAR channel[8, 9, 10]. The purpose of the study was to measure the changing temperature of the global ocean in order to better understand climate change. The experiment did not generate the long term records of ocean temperature that were the ultimate goal of the study, due in part to concerns surrounding the required use of a loud active acoustic source[8]. The goal of this research is to replace the active source used in the ATOC experiments with ships, used as acoustic sources of opportunity, to measure the ocean for parameters relevant to climate studies such as temperature, salinity,

and pH.

1.2 Passive acoustic sensing applications

Recently in the field of ocean acoustics there has been a movement to explore the use of passive, rather than active, acoustic techniques for ocean sensing. This is partially driven by environmental regulations prohibiting the use of loud active acoustic sources which were traditionally used in ocean sensing, and partially motivated by cost and energy savings associated with passive acoustic techniques. Passive techniques require only hydrophones and no energetically and monetarily expensive transducers or other acoustic sources. These hydrophones can be deployed for months or years without extensive cabling to provide power. From a tactical perspective, passive acoustic source localization techniques do not produce sound; which means they do not give away the observers position like active techniques do.

1.2.1 Acoustic Daylight

In the 1990s acousticians introduced the concept of "Acoustic Daylight" [11]. Acoustic Daylight refers to the idea that ambient ocean noise can be used to 'image' the marine environment in a way that is analogous to the way that ambient electromagnetic radiation from the sun, or daylight, can be used to image the terrestrial environment. Similar to the manner in which our eyes and brain receive and process the electromagnetic radiation from the sun to form images and gain information about our surroundings, the ambient acoustic waves refracting and reflecting throughout the world ocean can be used to extract information about the environment. In his 1991 paper, Dr Michael Buckingham, of the Marine Physical Laboratory at Scripps Institution of Oceanography, described an experiment in which a metal sphere was imaged in a totally passive manner using an array of hydrophones. The noise was generated largely by snapping shrimp. The experiment is analogous to the way our eyes would detect a plane in the air at night using the backscattering of light from the ground. The concept of acoustic daylight suggests

that many of the active acoustic techniques that are currently used to probe the ocean can, in theory, be accomplished in a totally passive manner, using acoustic energy that already exists in the ocean environment. This is the motivation for developing methods for using ships as acoustic sources of opportunity to study the environment as is the theme of this thesis[11].

1.2.2 Extracting coherent wave fronts from acoustic ambient noise in the ocean

In the past, ambient noise in ocean acoustics has been considered a nuisance parameter and something to be minimized and filtered; however, it carries valuable information [12]. In recent years there has been a paradigm shift in ocean acoustics where ambient noise has become the signal and the subject of study. While ocean noise is uncorrelated by definition, coherent wavefronts can be extracted by measuring space-time correlations of ocean noise across pairs of spatially separated hydrophones. In Roux et al. (2004) the authors demonstrate the ability to extract the coherent wavefronts, and by extension make estimates of the local time dependent Green's function (TDGF) of the media, by cross-correlating ocean noise from ships, as well as ambient volumetric noise sources. The TDGF is the transfer function of the acoustic waveguide. In other words, the signal received on a hydrophone in the marine environment is the source signal convolved with the TDGF, which is a function of the characteristics of the waveguide. As a result, if it is possible to use cross-correlations of ambient noise to extract the TDGF. This provides information about the waveguide, potentially including information about the bottom, and sound speed characteristics of the water; which by extension will provide information about ocean properties such as temperature and salinity. This implies that ambient ocean noise can be used to 'image' large portions of the ocean in a manner similar to the way the Acoustic Daylight experiments demonstrated small scale ambient noise processing for imaging purposes. There are countless applications of this technique of extracting information about the waveguide using cross-correlations of ambient and source of opportunity noise sources, described in Roux et al. (2004). Many such applications are presented in the following sections;

and the methods presented throughout this thesis are all additional applications and extensions of this work.

1.2.3 Passive fathometry

One notable application of using cross-correlations of ambient ocean noise to gain information about the environment is passive fathometry[13, 14, 15]. Most ambient noise in the ocean originates from the surface in the form of breaking waves, bubbles, ships, and biology. Surface noise can be modeled as an infinite screen of point sources, covering the entire surface of the ocean. Most noise originating from the seafloor is actually surface generated noise which has reflected off the bottom. As a result, it is possible to use the time delay between up and down going noise fields to estimate the distance to the bottom, and even sub-bottom layers, in a manner similar to the active bottom profilers described in the previous section. This is accomplished by beam-forming using a vertical array of hydrophones in the vertical direction. The up-going beam is cross-correlated with the down-going beam, to compute the peak lag time between the up and downward propagating acoustic noise fields. Assuming the upward propagating noise has traveled from the surface, through the array, to the seafloor and to any sub-bottom layers, then reflected back to the array, then the lag time between those two beams can be used to estimate the distance to the bottom and sub-bottom layers using the speed of sound. This method has been expanded using adaptive processing methods[15], and even applied towards estimating bottom loss coefficients by comparing energy in upward propagating and downward propagating noise fields[16]. This can provide insight into bottom sediment composition. An extension of this method has been applied using ship noise to estimate bottom loss coefficients [16].

1.2.4 Extracting the local time dependent Green's function from ambient ocean noise

Another notable application of using noise correlations to extract information about the environment was the work of Fried et al. (2008), which used cross-correlations of ambient noise across hydrophone elements on a bottom-mounted horizontal line array (HLA) to extract the local TDGF, and estimate information about the environment. This includes the critical angle at the sediment interface. The critical angle refers to the angle at which incident sound will be almost entirely reflected back into the water, meaning sound propagating below the critical angle will propagate for long distances while sound propagating at steeper angles will be absorbed into the bottom. The critical angle is a function of density and sound speed in the water and sediment, thus it can be used to gain information about the composition of the sediment in the seafloor. The noise used in this study primarily originated from croaker fish [17]. One of the main limitations of this study included the difficulty associated with building up enough coherence in the noise across the array, due to difficulty in predicting when the noise generated by croaker fish would be most coherent. This is where the concept of using sources of opportunity, as is the primary focus of this thesis, is beneficial. Shipping noise can be highly coherent across a horizontal array, especially when the ships generating the noise are crossing the end-fire orientation of the array. These end-fire crossings are easy to pick out because ships can easily be tracked using the Automatic Identification System (AIS).

This is not the first application of marine organisms as sources of opportunity for acoustic research. Marine mammals such as whales can have source levels as high as 180 dB with clearly discernible signals that can propagate for thousands of kilometers [18]. Geoacoustic inversions and analysis of water column structure has been accomplished by way of marine mammal vocalizations.

1.2.5 Sensing deep-ocean temperatures using ambient ocean noise

Tomography for measuring ocean temperature, similar to ATOC, has also been conducted passively [19]. Cross-correlations of ambient ocean noise on horizontally separated hydrophones can be used to estimate temperature structure in the Ocean[20, 21, 22, 23]. In the experiment described in Woolfe et al. (2016), two triangular arrays separated by 130 km, with the leg of each triangle measuring approximately 2 km, are used to estimate the speed of sound, along the deep sound, or Sound Fixing and Ranging (SOFAR) channel. This experiment involved cross-correlating extremely low frequency (˜10 Hz) signals across the two arrays and summing these cross-correlations coherently for approximately one week long periods of time. This was done to increase SNR sufficiently such that lag times between the two arrays could be detected, and those lag times used to estimate the speed of sound between the arrays[22]. While the method was successful, and deep ocean thermometry results gained using this method provided bulk estimate temperatures that are in good agreement with other sampling techniques such as Argo floats (ARGO) for the same period, the method is fundamentally limited by the long integration times, which limits temporal resolution of the resulting temperature estimates. The necessity of using low frequency noise capable of propagating long distances over which this method was applied, results in limited spatial resolution of the inversion, as sound at these frequencies is not sensitive to small scale features of the physical oceanographic environment. Many physical oceanographic features that are of interest to oceanographers, such as major ocean current systems and mesoscale eddies, change on time scales shorter than the one week resolution this method was capable of resolving. Small scale features such as sub-mesoscale eddies are subject of increased attention in climate dynamics research because of the important role they play in ocean mixing. The spatial scales of these features can be missed by the low frequency noise used in this demonstration. Using acoustic sources of opportunity, such as ships, can decrease integration times to seconds, improving the temporal resolution of tomographic output. Ships are loud, broadband acoustic radiators, consistently present in the marine environment, and their

location is well known due to advancements in tracking technology. The subject of this thesis is to explore ways to exploit knowledge of the location of ships to use the noise they generate to improve and supplement passive acoustic sensing techniques such as those explored in[22]. Chapter 5 of this thesis discusses one such approach.

1.3 Sources of Opportunity

Sources of opportunity refer to any source of acoustic energy present in the marine environment not produced for the explicit purpose of ocean sensing. Source of opportunity acoustics can be thought of as a hybrid between active and passive sensing techniques. In active acoustics, the source of noise is well known; both in signal characteristics and location. In purely passive acoustics, the source of noise is completely unknown. In the case of sources of opportunity, something about the source may be known, and exploited to enhance the method. Wave noise and sea ice are examples of acoustic sources of opportunity that have been exploited in the past. In this example, it is known that both of these noise sources occur only at the surface, and this information is used in methods such as passive fathometry[13] and bottom loss estimation. In the case of ships, even more information is known about the source. The subject of this thesis is developing ways to exploit that knowledge to enhance ocean sensing and source localization techniques.

1.3.1 Ships

Ships are loud (100-200 dB) broadband (10-1000 Hz) acoustic radiators that are ubiquitous in the marine environment[24]. In the frequency band between 10-300 Hz, shipping noise tends to be the most dominant source of ocean noise[1]. Ships have relatively consistent, tonal spectral signatures, due to the mechanical nature of the noise source. Due to recent advances in tracking technology, namely the Automatic Identification System (AIS), most large commercial ships are tracked at all times, and this data is available to researchers. As a result, ships represent powerful and potentially underutilized acoustic sources of oppor-

tunity, that can be exploited to gain information about the marine environment and localize acoustic sources.

1.3.2 Automatic Identification System

Most modern commercial vessels regularly transmit their location via VHF radio using the Automatic Identification System (AIS). AIS is an automated system of tracking ships for the purposes of collision avoidance and safety of life at sea. AIS was not designed to function as a global monitoring system or for use in research applications, but the data can be logged and used to track ships for the purposes of using them as acoustic sources of opportunity. AIS utilizes standard Very High Frequency (VHF) radio communications to transmit name, identification number, course, speed, position, and other various data for ships equipped with the system. AIS can be picked up by satellites.

AIS was originally developed in the early 1990s as a short-range identification and tracking system for avoiding vessel collisions. In 2002 the International Maritime Organization (IMO) Safety of Life at Sea (SOLAS) mandated most vessels over 300 gross tons be equipped with AIS. Over the next three years individual nations and the IMO started to implement stricter and more comprehensive mandates requiring vessels be equipped with AIS. In 2005, some government entities and private companies began experimenting with collecting AIS data via satellite, and by 2006 most maritime nations had mandated large commercial vessels on international voyages be equipped with some form of AIS. The United states implemented regulations requiring nearly all commercial vessels operating in major ports, all vessels on international voyages, and vessels over a certain size carry AIS. In 2008, satellite AIS data started to become available for purchase over the internet for sale by private companies operating micro-satellite constellations. By 2010, all commercial vessels in European Internal Waterways were mandated to use AIS. In 2012, over 250,000 vessels worldwide were equipped with AIS, with over one million vessels expected to be outfitted in the next few years. In 2013 and 2014 the United States and Europe (respectively) expanded AIS carriage requirements further and all of the aforementioned requirements became enforceable by

law without exception.

Currently the IMO requires all vessels over 300 gross tons on international voyages, all vessels over 500 gross tons on domestic voyages, and all passenger vessels regardless of size be outfitted with AIS. In the United States, commercial vessels over 65 ft in length, except small passenger vessels and fishing vessels, all tanker vessels, and passenger vessels over 150 GT wishing to travel internationally must transmit AIS. Additionally, most vessels 65 ft in length or more operating in or near a Vessel Traffic System (VTS; present in most major ports), and all towing vessels over 26 ft and more than 600 HP must always transmit AIS. Vessels classified as warships are exempt from this requirement but nearly always transmit when near areas of high vessel traffic for safety purposes. There are additional rules going into effect in the United States and Europe that will require fishing vessels over 15 m in length, and vessels on domestic voyages to carry AIS as well.

All vessels that carry AIS must always be transmitting. This means that any vessel that could potentially operate in a Vessel Traffic System (VTS), travel internationally, or carry passengers must always be transmitting their location via AIS. Nearly all commercial vessels, and pleasure craft of any considerable size are transmitting on AIS, which means the location of nearly all acoustic radiators in the frequency range between about 10 and 300 Hz is known at all times. The potential applications of this knowledge to acoustic sensing techniques is exciting.

AIS uses standard VHF Radio Communications, which means it is limited in range to nearly line of sight communications. For the 12 W class A AIS transmitters that most large vessels are equipped with, this limits the range, under ideal atmospheric conditions, to about 74 km. Under more typical conditions this number is more realistically closer to half of that. This depends on the height and quality of the transmitters and receivers. AIS transmissions are time multiplexed using Self-Organized Time Division Multiple Access (SOTDMA) and there are 4500 time slots per minute, which can be overloaded by 400-500% by sharing time slots between ships. This system of sharing bandwidth amounts to each ship in a crowded port being able transmit their location every 2-4 seconds depending on amount of vessels in the area sharing the time slots. Larger commercial ves-

sels equipped with Class A transmitters transmit their location every few seconds, while smaller vessels equipped with class B transmitters only transmit their location every 30 seconds. Faster moving vessels will automatically transmit their location more often (every 2 seconds) while ships at anchor only transmit every 60 seconds.

Standard AIS integrates the ships' GPS navigation system, electronic charting systems, and VHF radio transceiver. There are 27 possible types of AIS messages. For class A systems, navigational data including vessel name, Maritime Mobile Service Identity (MMSI) number, course, speed, rate of turn, position, and a time stamp in UTC seconds are transmitted every few seconds. The latitude and longitude can be transmitted with up to 0.0001 min precision; but is limited by the accuracy of the GPS which can potentially be accurate to less than a meter when within 370 km of land where the signal can be corrected by a Differential (or Digital) GPS (DGPS) tower, and accurate to within 2-15 m when further offshore. In addition to navigational data transmitted every few seconds, ships equipped with class A AIS units also transmit static reports every 6 minutes, which include type of cargo, type of vessel, dimensions of the ship (to the nearest meter), surveyed location of ship's positioning system antennae (GPS) in meters from bow, stern, and port and starboard sides. Additional information transmitted in the static reports includes the type of positioning system the ship is equipped with, the draft of the ship, destination, ETA, and an optional high precision UTC time stamp. All of this information makes it possible to characterize the ship as an acoustic radiator with great precision. For example, if one was to focus on noise generated by cavitating ship's propellers for a study, it would be simple to localize the propeller to within a few meters of accuracy from the information transmitted via AIS.

AIS data is available anywhere in the world. Between government agencies that log the data from arrays of shore based radio towers, and private companies that record massive databases of satellite derived AIS ship tracking data, one could reasonably obtain AIS data for any experiment conducted from 2009 through the present. In United States' coastal waters, the United Stated Coast Guard

Navigation Center (NAVCEN) Nationwide AIS (NAIS) database uses a network of 200 VHF radio transceiver towers nationwide to record all AIS data within about 100 km of the US coast for the primary purpose of Maritime Domain Awareness. In reality, data is actually available for 500-700 km offshore via the NAIS database because each ship acts as a repeater for every other ship. In other words, with a tower on shore, one could detect every ship within 30 km, and every ship within 30 km of those ships until there is a gap in shipping coverage. Under typical coastal shipping traffic conditions, for most of the western seaboard, there is continuous coverage out to nearly 700 km. NAIS provides historical data upon request to most organizations, and institutions affiliated with the United States Government can request live-feed access to their database for real time coverage. NATO has a similar system which records AIS data along the European coast that is also sometimes available upon request.

Other sources of AIS ship tracking data include NATO's Centre for Maritime Research and Experimentation (CMRE), which records AIS ship tracking for several European and international regions for research purposes and is often willing to share data with outside researchers. Commercial sources of AIS data include the Marine Exchange, a company that manages some Vessel Traffic Systems in the United States, ORBCOMM, ExactEarth, and Spacequest: three companies that have been recording and distributing satellite AIS ship tracking data since 2008. With few exceptions, these companies can provide AIS data anywhere in the world in a variety of formats, and they make specialized products and analysis available to paying customers. There are also open source AIS data providers that have limited coverage and availability including MarineTraffic.com, which even has a cell phone application for tracking ships.

AIS Data is originally transmitted in the standard National Marine Electronics Association (NMEA) format. There are a total of 27 different types of NMEA messages utilized by AIS systems, but we are primarily concerned with message types 1-3 which relay navigational data, and message type 5 which relays static reports including information about the ship.

1.3.3 Summary

Ships can be used as acoustic sources of opportunity to enhance passive ocean acoustic sensing techniques. This includes applications in source localization (Chapters 2-4), and characterizing the marine environment (Chapters 5-6).

A method for passive acoustic source localization using ships as sources of opportunity is explored explored in Chapter 2. The method is applied to localizing acoustic sources in discrete locations where measured replica cross-correlation functions are available. Ship noise is used to characterize the environment by parameterizing the propagation physics of the waveguide using waveguide invariant (WGI) theory (Chapter 3). This increased knowledge of the environment is used to enhance the localization method by extrapolating measured replica cross-correlation functions onto a larger search grid. This augmentation allows the method to be used for continuous tracking (Chapter 4).

The localization technique described in Chapters 2-4 uses fixed hydrophones with known locations. Chapter 5 of this dissertation explores the information content of cross-correlation function waveforms, computed across an array of drifting hydrophones. The feasibility of using ship noise to estimate the temperature of the ocean in shallow water environments, using cross-correlated signals from a drifting volumetric array, is explored through simulation and corroborated using four acoustic field experiments. Attenuation based tomography, which shows promise for measuring ocean properties such as pH is discussed using active techniques in Chapter 6. The method may be applied using sources of opportunity in the future.

Chapter 2

Passive Acoustic Source Localization Using Sources of Opportunity

Authors:
Christopher M. Verlinden
J. Sarkar
W. S. Hodgkiss
W. A. Kuperman
K. G. Sabra

2.1 Abstract

The feasibility of using data derived replicas from ships of opportunity for implementing matched field processing (MFP) is demonstrated. The Automatic Identification System (AIS) is used to provide the library coordinates for the replica library and a correlation based processing procedure is used to overcome the impediment that the replica library is constructed from sources with different spectra and will further be used to locate another source with it own unique spectral structure. The method is illustrated with simulation and then verified using acoustic

data from a 2009 experiment for which AIS information was retrieved from the United States Coast Guard Navigation Center (USCG NAVCEN) Nationwide AIS (NAIS) database.

2.2 Introduction

Recently in the field of Ocean Acoustics there has been a movement towards the use of passive, rather than active, acoustic techniques for ocean sensing. This is partially driven by environmental regulations prohibiting the use of loud potentially disruptive active acoustic sources traditionally used in ocean sensing, and partially motivated by cost and energy savings associated with passive acoustic techniques. Locating acoustic sources in the ocean using methods other than active SONAR systems has been the subject of a great deal of research. Passive source localization methods such as Matched Field Processing (MFP) have been developed since the 1970s[3].

Matched Field Processing [3] (MFP), as a source localization technique is limited by one's ability to model the acoustic environment with sufficient accuracy to create a library of modeled replica signals. An alternative to model based replicas is to build up a library of data derived replicas as was demonstrated using a controlled source [25]. In this letter, rather than use a purposefully deployed source, we demonstrate MFP localization using surface ships as sources of opportunity for the replica library.

In using these sources of opportunity, we have to overcome three immediate difficulties:

1. We have no control of the location of the sources: We use the Automatic Identification System (AIS) to georeference the library sources. AIS is accurate to between 10 cm and 15 m depending on the navigation system of the transmitting vessel.

2. Ships are random radiators with their own inherent spectral characteristics: We use cross-correlations between horizontally separated hydrophones

as replicas and source data to eliminate any specific ship uniqueness in the library and target source. Further, broad-band cross-correlation based MFP [26] [27] ultimately represents time delays which are basically frequency independent. Complex environments enhance the diversity and hence the uniqueness of the replicas in the library.

3. Surface ships do not provide replicas for searching in depth: We use omni-receivers or vertical arrays that have less vertical angular resolution than the vertical propagation cone which is typically twenty degrees or less. Hence, the replicas and subsequent MFP are for range and azimuth localization. The first difference between this method and previous studies is the use of measured replica fields rather than modeled replicas. In other words, the library the data is compared to is made up of correlation values determined from historical data associated with events in which acoustic sources were located in certain grid points [25]. The inclusion of sources of opportunity is also unique. In previous studies that utilized measured replica fields for source localization, towed acoustic sources were used to populate the library. No active sources are used in this study; all acoustic sources are sources of opportunity; in this case ships, tracked using Automatic Identification System (AIS). The final difference between this study and previous studies is that this study utilizes the correlation of the signal received across hydrophones separated horizontally, such as those on two horizontally separated vertical arrays, rather than the signal itself as the library for comparison. The use of correlation vectors in place of the actual acoustic signal for differencing the library of replicas from the data, is due to the fact that ships as sources of opportunity all possess different spectral characteristics, and a comparison of the actual acoustic signal would be meaningless; but the cross-correlation of the signals on two horizontally separated arrays is based on the arrival structure, and is therefore frequency independent, meaning it can be used to compare signals coming from sources with different frequency content.

2.3 Basic Procedure and Illustrative Simulation

This source localization technique is conceptually illustrated in Figure 2.1, which shows a ship, the signal received on two hydrophones on adjacent arrays, and the cross-correlation of the two signals. This cross-correlation vector is saved georeferenced with the latitude and longitude of the acoustic radiator that generated the correlated signals, and is used as the library replica field. Correlation vectors are used for comparison between library replicas and data instead of raw acoustic signals in order to account for the different spectral structures of different ships.

Once a grid of library correlation replicas has been generated, they are compared to the 'data' correlation vectors, referring to the cross-correlation of the acoustic signals on the two hydrophones in the presence of an unknown acoustic radiator, which we will call the 'event' correlation vector. Cross-correlation (or least squares differencing) of the two cross-correlation vectors can be used for comparison of the library replicas to the event data. The process is illustrated in Figure 2.1.

For simplicity of illustration, we use only one element on each of two vertical arrays, at approximately the same depth, separated by approximately 500 meters. We will associate cross-correlations of the acoustic signals across two array elements with the position that a ship was in, when those time series were generated. This will be our library of measured cross-correlation replica fields. We start with the time series on each element, $X_1(t)$ and $X_2(t)$. Each time series is filtered using a standard 4th order digital Butterworth bandpass filter selecting the frequency content between 20 and 300 Hz to focus on the area of the spectrum dominated by shipping noise. Using this low frequency band also mitigates the effect of environmental variability (e.g. internal waves, diurnal heating, etc..) on the acoustic propagation, thus potentially enhancing the long-term stability of the replica vectors. While using low frequencies reduces the impact of these phenomena, more research needs to be conducted in order to determine how sensitive this method is to such perturbations, and consequently how long a library replica can be used to localize a target before the waveguide has changed sufficiently to

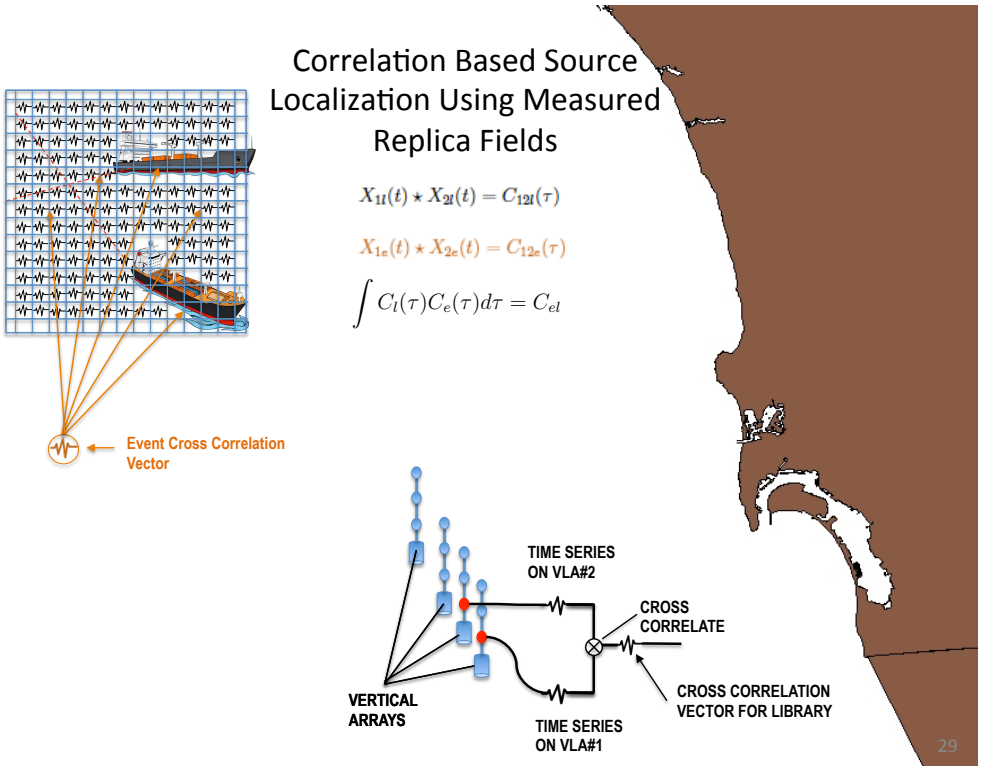

Figure 2.1: (color online) An illustration of the theory behind this source localization method. There are four vertical arrays approximately 15 km offshore of San Diego (as in the Noise 09 Experiment). A grid is constructed; the time signal on each of two hydrophones on adjacent arrays are cross correlated, and the resulting time domain cross-correlation vector is saved associated with the latitude and longitude of the ship that created the signal at the time of recording. Ultimately the goal is to populate the entire grid with correlation vectors (measured replicas) from when ships were in each position in the grid. This library of measured replica correlation vectors is then compared to the cross-correlation of the time signal on the two elements in the presence of an unknown acoustic radiator, and whichever library vector most closely correlated to the event vector must then be the location of the unknown acoustic radiator.

invalidate the replica; in this experiment replicas are used for five days without significant degradation. Time-domain cross-correlations are computed using the filtered time-series from the two selected receivers, and are saved associated with the AIS derived latitude and longitude of the ship that generated the signals. This is our library of replica correlation fields.

The event data were computed using the same method described above. The acoustic signals on the two elements during the event involving the unknown acoustic radiator are cross-correlated and this cross-correlation vector is compared to the library of cross-correlation vectors associated with latitude and longitude using another correlation as stated in equation (2.2).

To summarize, the library and event correlation vectors are generated as below:

$$X_1(t) \star X_2(t) = C_{12e,l}(\tau) \tag{2.1}$$

where the X is the data and subscripts e, l denote event or library quantities. Implementation of the MFP is done by the comparison of library and event data correlations through computing the scalar correlation of the cross-correlations, with approximately zero time-lag.

$$\int C_l(\tau) C_e(\tau) d\tau = C_{el}, \tag{2.2}$$

where the C_{el} is the scalar maximum correlation at zero lag time.

Numerical simulations (using normal-mode formulations in a simple range independent ocean waveguide) were first used to demonstrate the feasibility of this source localization method. To do so, we chose a search grid some distance away from the hydrophone arrays and generated simulated signals from each of the locations in the grid on the array of hydrophones. To emulate the experiment that will be reported below, it was determined that a 100m resolution was appropriate for the grid size based on lobe thickness of the beam directivity pattern for the array geometry, the average speed of vessels, and the approximate azimuth angle of the grid relative to the array orientation. This determination was made so the correlation vectors would sum coherently for a target vessel in a given grid. Calculations were also performed in order to determine appropriate vertical array

aperture, and it was determined that the entire 16 meter array used in the ocean experiment would be appropriate to use since that length is about 3 wavelengths giving a vertical resolution of order 20 degrees thereby covering the full propagation cone. The grid was then populated with simulated replica correlations vectors, that is, each point on the grid was used as the source location for a simulated source, and the cross-correlation of the simulated acoustic signal received on each element in the array was recorded as a library replica value associated with the simulated source location. Many different array geometries, acoustic environments, source and event spectra, and signal to noise ratio environments were tested. For this example only two elements were used, separated horizontally by 500 meters. The source spectra for the library and event simulated signals were different distributions sampled over a band between 0 and 100 Hz. The library source signal had a skewed normally distributed spectrum with a peak in the lower portion of that band and the event signal had a peak in the upper portion of the band as shown in Figure 2.2. These spectra are arbitrary; as long as the spectra were sampled over approximately the same band the localization method was effective. Once the library of simulated correlation vectors had been generated, the same acoustic propagation model was used to generate a simulated 'data' acoustic signal for a simulated event involving an acoustic radiator of unknown origin. The library of correlation values were compared to the value obtained for the event as shown in equation (2.2) using a second correlation. Figure 2.2 shows the source localization results obtained when the library and event ships have different frequency spectra with some white noise added to the simulated data. The simulations were run by adding homogeneous white, gaussian noise to the source signal, in SNR environments ranging from 16 to 1 dB with positive results; this particular example was generated with an SNR of 16 dB.

A library of correlation vectors created using a source with certain spectral characteristics can be used to localize a source with entirely different spectral characteristics. Using simulated acoustic fields generated using a standard normal mode propagation model it has been shown that replica acoustic fields generated by acoustic radiators in different positions can generate correlation values with

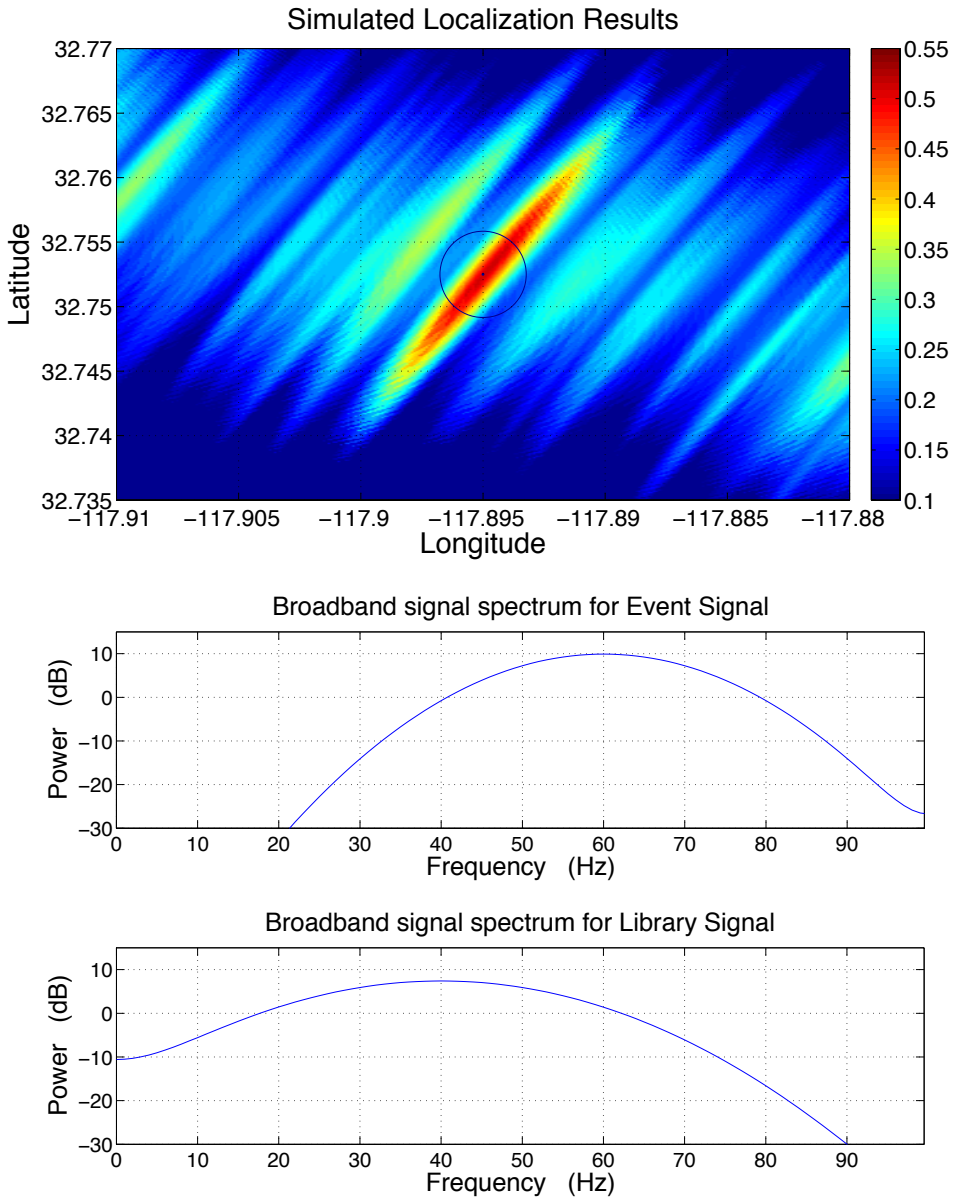

Figure 2.2: (color online) Source localization output for system using different frequencies to create library and event correlation vectors. The source is localized in every case as long as the sampling in frequency space is not too sparse, and the spectra are computed over approximately the same band. The spectrograms of the synthetic source signals used to simulate the library and event ships are included below.

sufficient uniqueness to identify the position of a future unknown acoustic radiator. This suggests that the method of using measured correlation replica fields to localize acoustic sources in the ocean environment may be effective, but testing needs to be done with experimental data in the ocean environment to test the robustness of this system in the marine environment.

2.4 Experiment

2.4.1 Source Localization

Ships, used as sources of opportunity, are tracked using Automatic Identification System (AIS) data obtained from the US Coast Guard Navigation Center Nationwide AIS (NAIS) database. The acoustic data comes from the Office of Naval Research supported field Experiment, Noise 09, a ten day experiment with 4 vertical line arrays (VLAs) of 16 elements, spaced 1m apart, each deployed approximately 15 km offshore of San Diego CA, spaced 500m, 1000m, and 1500m apart respectively. The depth of water in the experiment area was approximately 150m. For the purposes of this demonstration of feasibility, only one element on each of the two closest arrays are used. The 5th element was chosen arbitrarily, approximately 17 meters above the bottom.

The cross-correlations displayed in Figure 2.3 were calculated over intervals of 5 seconds because given the speed of the vessel in question (as determined by AIS), and the grid size calculated based on the beam width and directivity pattern of the array, a ship would remain in the same grid box for at least 5 seconds. For the first trial, we start with building the cross-correlations of "library" ships between single elements of two vertical arrays (VLA1 and VLA2) and assign those correlation vectors to the AIS derived latitude and longitude of the "library" ship at the time that the correlation was computed. Next, cross correlation vectors were computed for the "event" ship. The band between 50 and 300 Hz was used and both library and event vessels generated spectra with dozens of distinct tonals associated with those ships, albeit tonals centered around differing frequencies in each case. The spectrograms for the Event and Library ships are included in Figure

2.3. As with the simulation, replica-event cross-correlation was employed. Several individual ships have been localized using this method at distances ranging from a few hundred meters away from the array to 45 km. Several source differencing methods were used including using only the portion of the cross-correlation vector that can be associated with a contact in the direction of the library vessel based on anticipated arrival time structure of the contact on the array elements used to compute the correlation as shown in Figure 2.3. Note that this source differencing method needs to include the section of the correlation vector associated with the entire complex multi-path arrival structure from the source location to the receiver expressed in the correlation vector.

2.4.2 Multiple Library Vessels

In order for this method to be a useful technique for localizing acoustic sources in the ocean environment there are several additional steps that need to be taken. The method must be demonstrated for multiple shipping events and it must be able to localize sources under a variety of circumstances with varying geometries. It needs to work when the sources are at any angle with respect to the azimuth of the array, and for sources at any range. Figure 2.4 shows the results of the source localization for a series of shipping events within a few hundred meters of the array, with multiple ship tracks used to populate the library. In every event the target ship is localized. Figure 2.4(d) illustrates the tracks of the library ships and event ship. The three subplots (a,b,c) show the value of the correlation of the library and event cross-correlation vectors, as a function of time in the library and time in the event ship track. The color of the subplots represents the correlation between the library and event cross-correlation vector, normalized by the autocorrelation of each; in other words the output of equation (2.2). The x-axis on each subplot is time in the library record, in seconds; and the y-axis is time in the event record. The red circles show the time in both vectors when the event ship and library ship were located in the same place, where one would expect the two cross-correlation vectors to be most closely correlated; and in every case the localization method shows a peak at the proper time in the library and event series.

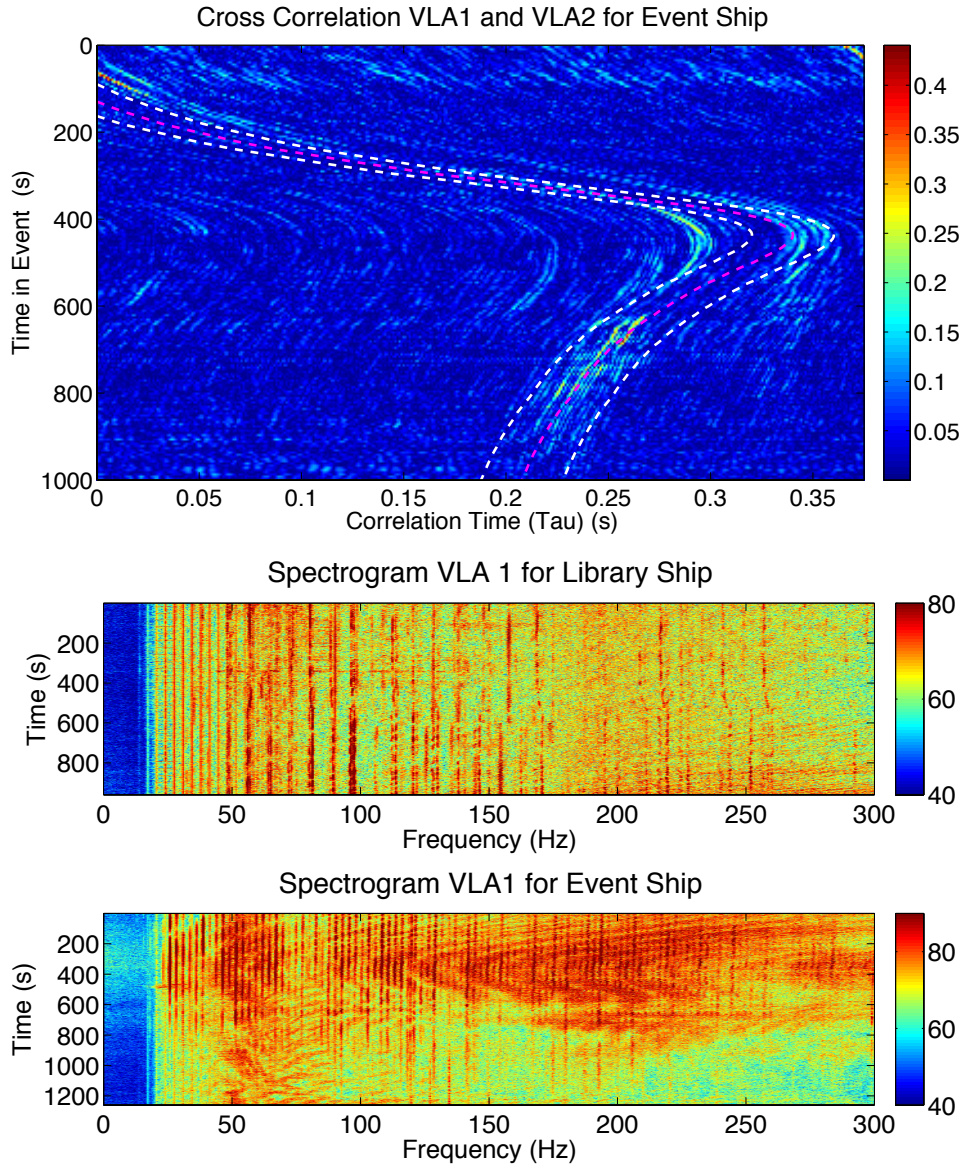

Figure 2.3: (color online) The cross-correlation of the event ship over time is plotted as a colored surface with amplitude of the correlation represented by the color bar, correlation time on the x-axis, and time in the experiment on the y-axis. These event cross-correlation vectors could be used as a library of replicas to localize a different source, in which case one would use only the portion of the cross correlation vector between the two white dotted lines, centered around the theoretical peak correlation time for a ship in that position shown in the dotted magenta line. The spectrograms for both library and event ship are also included.

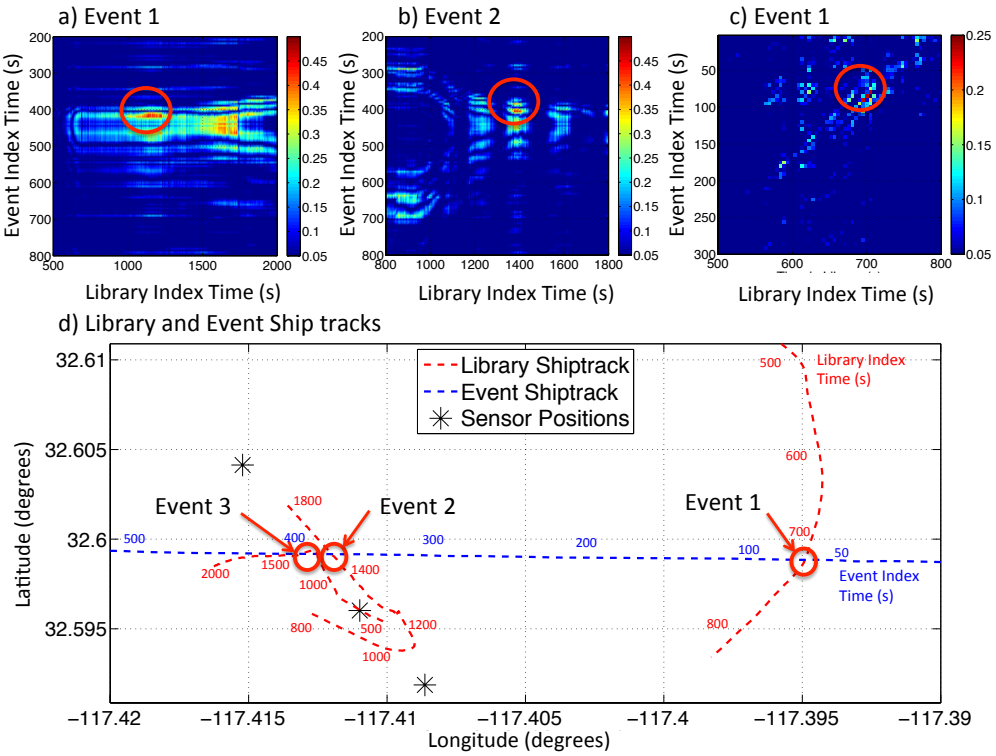

Figure 2.4: (color online) Correlation between multiple libraries' measured replica correlation vectors and the data correlation vectors when the 'event' ship crosses the tracks of the three library vessels. In subplot (d) The stars represent the location of the VLAs, the red lines are the tracks of vessels used to populate the library, and the blue line is the track of the 'event' ship, that the method was able to localize. The red circles show the locations where the 'event' ship crossed the tracks of the library vessels. During each of these three crossings, the results of the localization method are shown in subplots (a), (b), and (c). In every case, the index time in the event track is on the y-axis, and index time in the library is on the x-axis. The colors represent the value of the correlation between the library and event cross-correlation vectors; the output of equation (2.2). The red circles highlight the time when the event ship crosses the track of the library vessel, and in every case the localization method shows a peak during the crossing and nowhere else. It is important to note these subplots are not localization results in space (i.e. latitude and longitude), rather these three plots show localization in time, illustrating the correlation between every 'replica' correlation vector in the library and every 'data' correlation vector in the event dataset, indexed by time in each dataset.

2.5 Conclusion

We have demonstrated the feasibility of using data derived replicas from ships used as sources of opportunity to locate other sources. The technique, similar to matched field processing, compares replica correlation vectors between horizontally separated receivers or receiver arrays to the equivalent correlation vector, respectively, associated with an acoustic radiator in an unknown position. The uniqueness of the correlations, which are related to the multi-path time delays from the sources to the array, is enhanced by the complexity (such as bathymetry), of the environment. The primary difference between traditional matched field processing and this technique, aside from the use of correlation vectors in place of the acoustic signal itself for matching, is the use of measured replica fields, populated using ships as sources of opportunity. The replica vectors are taken from a library of correlation vectors calculated for ships in locations, georeferenced using the Automatic Identification System (AIS). The method overcomes the impediment that the library replica and event data are derived from random sources with different spectral characteristics. For a practical system, libraries would be continuously updated. In this experiment, libraries were used to localize sources up to four days later. More research needs to be done to determine how long a library of correlation vectors may be valid. This feasibility demonstration leads to future work to enhance this methodology, such as developing an interpolation scheme to increase the grid density.

Further work remains to be done in terms of developing a robust source localizing method that can reliably be used in the field. An adaptive processor needs to be developed to adjust the parameters of the correlation computation such as correlation time, and bandwidth based on the geometry and signal characteristics of the problem. An interpolation method needs to be developed to interpolate the library of cross-correlation vectors to regions where no measured replicas exist. Methods utilizing the waveguide invariant, and empirical orthogonal functions have been explored. Finally, a certain degree of track-before-detect needs to be implemented. A method such as this one will always exhibit sidelobes, and in order to localize real contacts one needs to preferentially weight coherent

contacts, as is done in the SONAR and RADAR communities. Similar algorithms needs to be developed and applied to this method. While further work remains to be done before this method can be applied in robust field applications to localize acoustic sources, it has been demonstrated using models, and experimental data from open-ocean experiments, that it can be determined when an unknown acoustic radiator crosses the historical ship path used to build the library of correlation vectors. In conclusion, the Correlation Based Source Localization using Measured Replica Fields technique shows promise but requires more research before it can be implemented in the field.

Acknowledgements

This work is supported by the Office of Naval Research.

Chapter 2, in part has been published in the Journal of the Acoustic Society. Verlinden C. M. A., Sarkar J., Hodgkiss W. S., Kuperman W. A., and Sabra K. G.. Passive acoustic source localization using sources of opportunity. The Journal of the Acoustical Society of America, 138(1):EL54, 13 July, 2015. doi: http://dx.doi.org/10.1121/1.4922763. The dissertation author was a primary investigator and author of this material. Dr. William Kuperman, the chair of the committee, is a co-author.

Chapter 3

Determination of Waveguide Invariant using Ships as Sources of Opportunity

Authors:
Christopher M. Verlinden
J. Sarkar
B. D. Cornuelle
W. A. Kuperman

3.1 Abstract

The waveguide invariant (WGI) is a property that can be used to localize acoustic radiators and extract information about the environment. Here the WGI is determined using ships as sources of opportunity, tracked using the Automatic Identification System (AIS). Using a single hydrophone, the acoustic intensity as a function of range and angle is measured in the presence of ships at a variety of ranges and angles. The relationship between range, intensity, and frequency is used to determine the WGI parameter β. These β values are interpolated and a map of β is created for the environment in question. The method is demonstrated and verified using data collected on a single hydrophone in a shallow water environment off the coast of Southern California.

3.2 Introduction and Background

The waveguide invariant is a property which describes acoustic intensity fluctuations in range and frequency [28, 29, 30, 31]. It is defined as the ratio of the change of the modal group slowness with respect to the change of the phase slowness, and therefore encapsulates the dispersive characteristics of the waveguide into a single scalar parameter [32]. In a range dependent environment, the WGI involves an average change of the group speed over the entire propagation path [33] so that in principle, as per Jensen et al,[28]the WGI in our space involves an inherent physical smoothing process. Many experiments have been performed to

determine or confirm the existence of the WGI [34, 35, 31]. The WGI has applications in underwater communications [36, 37], environmental inversion [38], and source localization [39, 40, 41] including source ranging [42], as well as potentially depth determination based on the depth dependent nature of the WGI explored by Turgut et al [43]. The interference pattern created by constructively and destructively interacting modes creates lines of constant intensity in range-frequency space for a waveguide of given characteristics. The waveguide invariant is a parameter which describes the slope of these lines at given ranges between source and receiver at given frequencies by the relationship defined in Eq. 3.1,

$$\beta = (\frac{r}{\omega})(\frac{\Delta\omega}{\Delta r}) = \frac{d(1/v_m)}{d(1/u_m)}, \tag{3.1}$$

where β represents the waveguide invariant; r is the range from source to receiver; ω is the angular frequency; u_m is the modal group velocity; and v_m is the modal phase velocity. The waveguide invariant is useful because it is a regional characterization that depends on the sound speed profile, bathymetry, and bottom composition. While the waveguide invariant is sensitive to fluctuations in the physical oceanography of the waveguide,[44, 45] this experiment focuses on the simpler lower frequency regime (20-300 Hz). This study primarily focuses on uses of the WGI for source localization[46, 39, 42]. Since the WGI requires extensive knowledge of the ocean environment, using data-derived WGI measurements has been shown to be advantageous [46, 42]. Rakotonarivo et al.[46] demonstrate a single-hydrophone localization method using measurements of the WGI. There have been a number of methods for determining the waveguide invariant experimentally using either fixed or moving active sources [32], and horizontal arrays of hydrophones [47] for both source localization and inversion purposes. Cockrell et al.[48] determine the WGI analytically using the WKB approximation from the phase of the bottom Rayleigh reflection coefficient. Additionally, Harms et al.[49] propose, and demonstrate through simulation, a method of determining the waveguide invariant using tonal sources, such as ships, by comparing the fading characteristics of each tonal.

This experiment represents an alternative method of measuring the waveg-

uide invariant. The waveguide invariant can be mapped by populating a library of measurements using ships as sources of opportunity. Ships are broadband radiators in lower frequency bands between 20 and 300 Hz, and when acoustic intensity on a received hydrophone is plotted as a function of range and frequency, the slope of striations representing lines of constant intensity, when taken in conjunction with the range and frequency being considered, gives an estimate of the waveguide invariant. As the spectral signatures of ships are tonal in a nature, the slope of the striations in range-frequency space are not always possible to discern; this paper makes use of a radon transform filtering technique to accommodate the ships' tonal spectral signatures.

An experiment was conducted in 150m of water, 20km off the coast of San Diego, California. There was a strongly downward refracting sound speed profile as shown in figure 1a, that was fairly stable for the 10 day experiment conducted in January-February of 2009. For the purposes of this demonstration, only a single hydrophone approximately 15m off the bottom was required. Ships in the vicinity of the hydrophone were tracked using the Automatic Identification System (AIS), data for which was obtained from the United States Coast Guard Navigation Center. The ship tracks are shown in white dots in figure 1b.

3.3 Methods and Results

Over the course of 10 days, the acoustic intensity on a hydrophone approximately 135m deep was recorded. When ships which were clearly discernible passed within 20km of the hydrophone the intensity across frequency was plotted as a function of range, as the ship transited through the area. Range-frequency spectrograms like the one shown in figure 2b were created using tracking information derived from AIS. Since ships tend to have tonal spectral signatures that make it difficult to measure the slope of the striations effectively without filtering the range-frequency spectrograms, a Gaussian image filter was applied to the spectrogram and the radon transform of the resulting surface was computed. The tonal signature of the ship dominated the radon transform so the slope of the striations

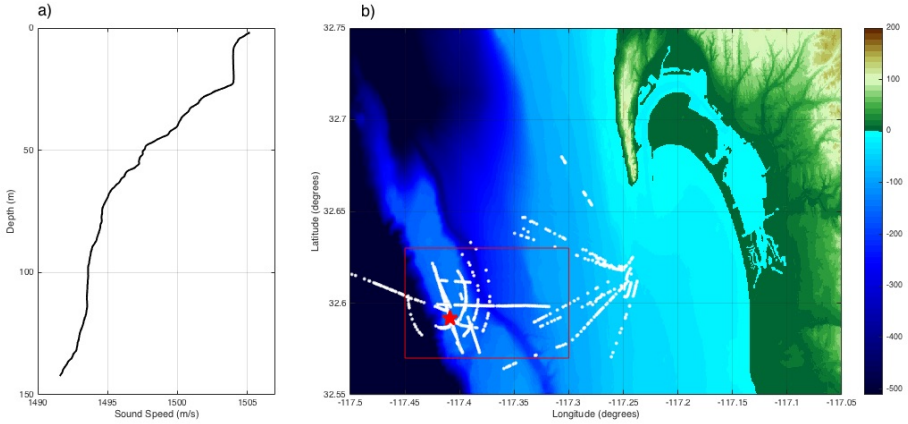

Figure 3.1: (color online) Experiment setup. The experiment was conducted in 150m of water with a strongly downward refracting sound speed profile (figure 1a) approximately 20km off the coast of San Diego, CA. Figure 1b shows the bathymetry in the vicinity of the hydrophone used in this experiment. The white dots represent locations of ship tracks used to create the library of waveguide invariant values that were included in the WGI map shown in figure 3a. The red star indicates the location of the hydrophone which was used for the experiment. The red box represents the area for which the map of WGI values was generated and the area shown in figure 3a.

were not discernible. The 90 degree angle (vertical) components of the image were removed, and the inverse radon transform of the resulting surface was computed. The result was a range-frequency spectrogram with the vertical tonal striations removed. These spectrograms were normalized across frequency (whitened) and the resulting image made striations in range-frequency space easier to recognize. The slope of these striations were measured and the waveguide invariant was computed using Eq. 3.1 for every point along the vessel's track as shown in figure 2b. The measurements were binned into 75% overlapping, 200m bins and the average β was computed for each bin, for each vessel track.

When enough tracks are considered together (roughly 50, each with approximately 50 measurements of the waveguide invariant) it is possible to fully populate a library or map of the WGI for a given hydrophone location by computing an inverse distance weighted average (IDW) interpolation of the measured values. This surface is shown in figure 3a with white markers representing the positions of sample estimates of the WGI along along one particular track. When values taken from this map are compared to the WGI computed along the track of an additional vessel not contained in the library which transits the region at a future time, the results compare favorably. Figure 3b shows the value of the library WGI values taken from the surface along the track of a vessel in a solid gray line with the value of the WGI computed using that vessel's acoustic intensity as a function of range and frequency at the same points shown in black stars. Other measurements of the WGI that were used in the creation of the library are depicted as gray stars in the background. The standard deviation for each of the 75% overlapping, 200m bins, computed using the standard form of variance for a weighted average is shown bracketing the value of the WGI on the surface in thin gray lines. Given the sparsity of measurements that went into generating this surface, and the fact that a priori estimation statistics are highly speculative, using a standard error calculation carried through the inverse distance weighting used to generate the WGI surface omits some of the representational uncertainty of the WGI values in the surface. In addition, it gives zero error when no duplicate measurements are available, so it is a lower bound on the error of the WGI estimate. It is clear that

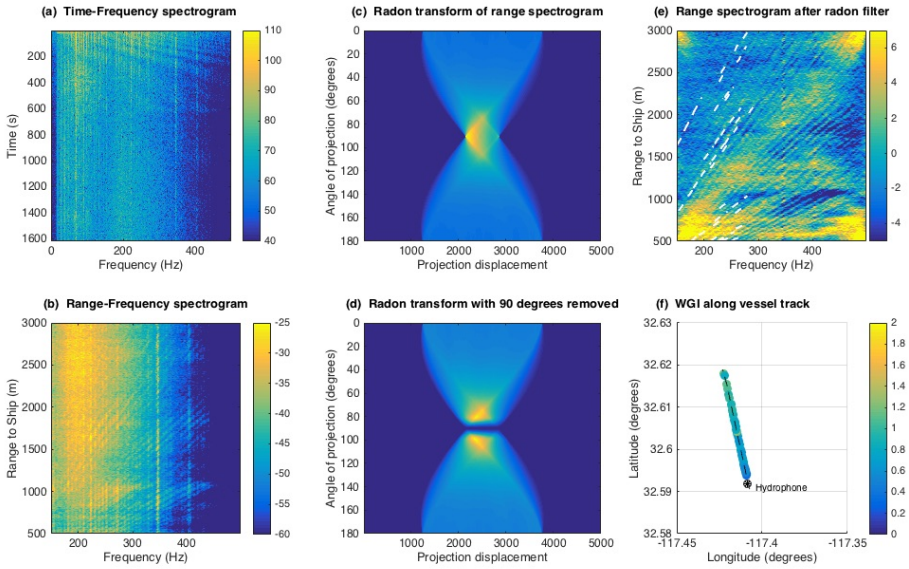

Figure 3.2: (color online) Figure 2a is an example spectrogram of acoustic intensity as a function of frequency, as it changes in time during the passage of a vessel in the vicinity of the hydrophone. The spectrogram is sorted by source-receiver range using AIS ship tracking data to generate a plot of intensity as a function of frequency and range, as shown in figure 2b. Lines of constant intensity in range-frequency space are indicative of the WGI; unfortunately the slope of these lines is not distinguishable because the spectrogram is dominated by vertical tonal striations, characteristic of shipping noise. To de-emphasize the tonal structure, a radon-transform based filter was implemented: the spectrogram is first smoothed using a Gaussian image filter, and the radon transform of the result is computed, as shown in figure 2c. The 90° components of this transform represent the vertical patterns in the spectrogram, which dominate the image, and are removed using a Gaussian window, as shown in figure 2d. The inverse radon transform is then employed to recreate the spectrogram with diminished tonal emphasis, and is normalized across frequency to produce the filtered plot shown in figure 2e, where the lines of constant intensity in range-frequency space are now clearly discernible. These striations are traced (indicated by the white dashed lines on the spectrogram), and the slope of these traces used to calculate β. Figure 2f shows the values of β (given by the color of the points) computed with this method.

the values of the WGI measured along the track of the vessel are consistent with the library, demonstrating that this is a stable parameter that can be applied to future experiments and applications.

3.4 Conclusion

The waveguide invariant is mapped using ships as sources of opportunity. A single hydrophone combined with AIS ship tracking data can calibrate a region. Maps of WGI, constructed using sources of opportunity, can be used for robust geo-acoustic environmental inversions as in Gervaise et al.[38] and Turgut et al.. [47]. Time varying physical oceanographic tomography using WGI measured using ships may also be possible when the dependency of the WGI on ocean structure, as described in Rouseff et al.,[45, 44] is considered. These data-derived libraries can also be used for source localization[46, 39, 42, 41, 47]and in acoustical communications applications[37]. Additional applications of creating data-derived libraries or maps of the waveguide invariant using ships as sources of opportunity include other potentially novel source localization techniques. One such technique involves using the WGI to interpolate the data-derived correlation function replicas used for source localization [50] to positions where data derived replicas are not available. Additionally maps of the waveguide invariant across multiple microphones can be used to localize contacts through other means. For example, as a vessel of unknown position transits across a region where the waveguide invariant across multiple spatially separated hydrophones is well known, the changing slope of the striations in the spectrograms will represent a track across the continuously changing WGI surfaces for each microphone. Depth discrimination of contacts may also be possible when libraries of WGI populated using surface vessels are combined with the work of Turgut et al.[51, 43]. It may be possible to estimate the WGI of sub-surface vessels using the relationships explored by Turgut et al.[51, 43] applied to a library created using surface vessels, but additional experimental verification will be required.

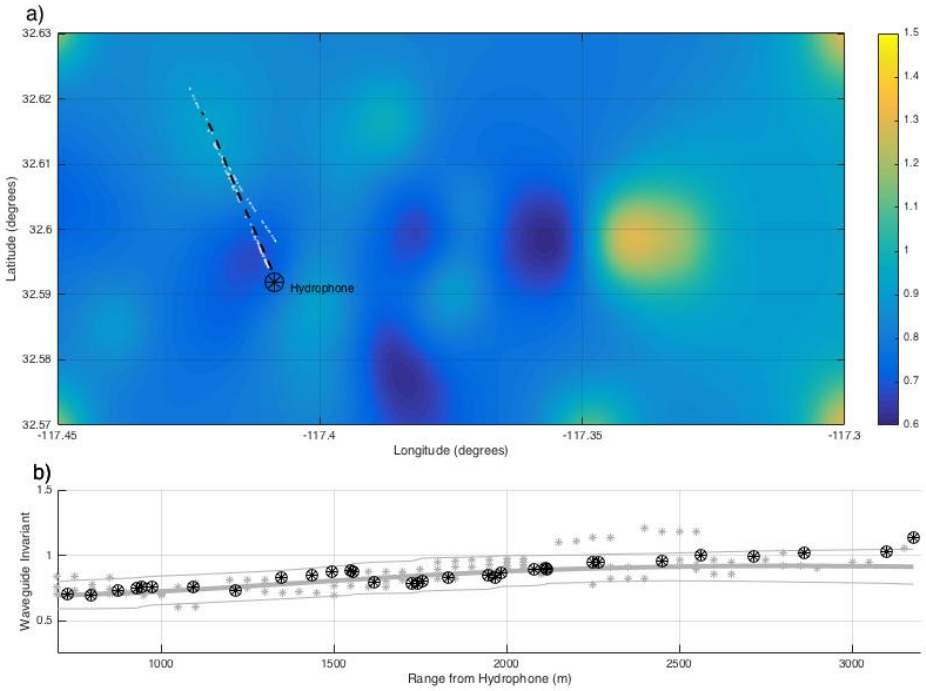

Figure 3.3: (color online) Figure 3a shows a map of the WGI for the hydrophone used in this experiment. The color represents the value of the WGI. The black dashed line represents the track of a vessel that is not included in the library used to generate the surface. Figure 3b is a plot of the WGI as a function of range from the hydrophone along that vessel track. The values of the WGI for that vessel, measured along the track are plotted as black stars. The values of the WGI surface, generated using the library, along the same vessel track is plotted as a thick gray line in the background. The standard deviation of the inverse distance weighted average used to compute the surface WGI value is plotted in thin gray lines, bracketing the thick gray line. There are a number of gray stars in the background which represent values of the WGI taken from other vessel tracks that were included in the library in the vicinity of the track (defined as within 200m of the original vessel track) to show the distribution of values that went into creating the surface. The locations where these measurements were made are plotted in figure 3a as white dots.

Acknowledgements

This work is supported by the Office of Naval Research.

Chapter 3, in part has been published in the Journal of the Acoustic Society. Verlinden C. M. A., Sarkar J., Cornuelle B.D., Kuperman W. A.. Determination of acoustic waveguide invariant using ships as sources of opportunity in a shallow water marine environment. The Journal of the Acoustical Society of America, 141, EL102, (2017). doi: http://dx.doi.org/10.1121/1.4976112. The dissertation author was a primary investigator and author of this material. Dr. William Kuperman, the chair of the committee, is a co-author.

Chapter 4

Passive acoustic tracking using a library of nearby sources of opportunity

Authors:
Christopher M. Verlinden
J. Sarkar
W. S. Hodgkiss
W. A. Kuperman
K. G. Sabra

4.1 Abstract

A method of localizing unknown acoustic sources using data derived replicas from ships of opportunity has been reported previously (Verlinden et al., 2015). The method is similar to traditional matched field processing, but differs in that data-derived measured replicas are used in place of modeled replicas and, in order to account for differing source spectra between library and target vessels, cross-correlation functions are compared instead of comparing acoustic signals directly. The method is capable of localizing sources in positions where data derived replicas are available, such as locations previously transited by ships tracked using the Automatic Identification System (AIS), but is limited by the sparsity of ships of opportunity. Here we present an extension of this localization method to regions where data derived replicas are not available by extrapolating the measured cross-correlation function replicas onto a larger search grid using waveguide invariant theory. This new augmentation provides a method for continuous tracking.

4.2 Introduction

Passive acoustic source localization methods, such as matched field processing (MFP)[3] break down because of the difficulty in modeling the acoustic environment in the ocean with sufficient precision to generate modeled replicas accurate enough to consistently localize targets[3]. The method presented in Ver-

linden et al., 2015[50] addresses this issue by using measured replica fields, rather than modeled replica fields, in a localization scheme[50] similar to MFP. This type of measured replica field matched field processing had been demonstrated previously using an active acoustic source of known characteristics by Fialkowski et al [25]. In Verlinden et al., 2015[50], the library is instead populated using replicas generated by ships, used as acoustic sources of opportunity, and the difference in source spectra between different ships is overcome by using the cross-correlation of the acoustic signal on two arbitrarily horizontally separated hydrophones, rather than the signal itself. The cross-correlation is dependent on the arrival structure of the incoming signal, and is therefore a function of the position of the radiator and characteristics of the waveguide, and is independent of source spectra[12].

The theory developed by Verlinden et al., 2015[50] was demonstrated using numerical simulations for the case of a fully populated library, and validated using experimental data for discrete locations populated with measured replicas. A grid is populated with measured replica cross-correlation functions computed across two horizontally separated hydrophones using the acoustic signals from ships tracked using the Automatic Identification System (AIS)[50]. Contacts are localized by comparing the library of measured replica cross-correlation functions to the cross-correlation function computed across the same two hydrophones, in the presence of an acoustic radiator in an unknown position, and assigning the location corresponding to the closest match between replica and data to the target vessel[50]. This method is necessarily limited by the inherent sparsity of ship traffic, in that replicas will only exist in areas transited by vessels. This motivates the need for an interpolation scheme designed to fill in the gaps between existing measured library replicas, in order to positively localize contacts in all locations, and continuously track moving targets.

This paper describes the environmental acoustic formulation for such an interpolation scheme, demonstrates the theory using numerical simulations, and validates those simulations using data gathered from an acoustic field experiment conducted off the coast of San Diego, California. The method presented here allows for continuous tracking of contacts in the experiment area. The experiment was

conducted in 150m of water, 20km off the coast of San Diego, California. There was a strongly downward refracting sound speed profile as shown in Figure 1a that was fairly stable for the 10 day experiment conducted in January-February of 2009. For the purposes of this demonstration, only a single hydrophone from each of two 16-element vertical line arrays (VLAs) were required. The VLAs were horizontally separated by 511m and located 18m off the bottom. The method requires only two individual hydrophones, but arrays of hydrophones can be combined to improve SNR and enhance the method, provided the aperture of the array is such that the entire propagation cone, meaning sound propagating at angles less than the critical angle, is included in the broadside beam. It may be possible to extend this method to localize sub-surface sources using libraries derived from surface sources, but this demonstration focuses on the localization of surface sources in a high signal to noise ratio (SNR) environment. Localizing surface and semi-submersible acoustic targets at or near the surface is of interest to the Navy and Coast Guard for defense and law enforcement applications. Ships in the vicinity of the hydrophones were tracked using Automatic Identification System (AIS) data obtained from the United States Coast Guard Navigation Center (USCG NAVCEN).

In the previously reported literature[50] it is possible to detect target vessels only in discrete locations where they cross the tracks of library vessels. In order to continuously track a target acoustic radiator, it is necessary to fully-populate a grid with measured replicas. Populating the region between measured replica functions requires extrapolation of the time-domain cross-correlation functions in the library to different locations in range and azimuth distributed in the horizontal plane. To do so, replica cross-correlation functions at known bearing and ranges can be modified to estimate the cross-correlation function at a different bearing and range using the formulation described next.

4.3 Theory

In the scenario of interest, when a vessel transits through the search grid, the acoustic signal on two horizontally separated hydrophones is recorded and

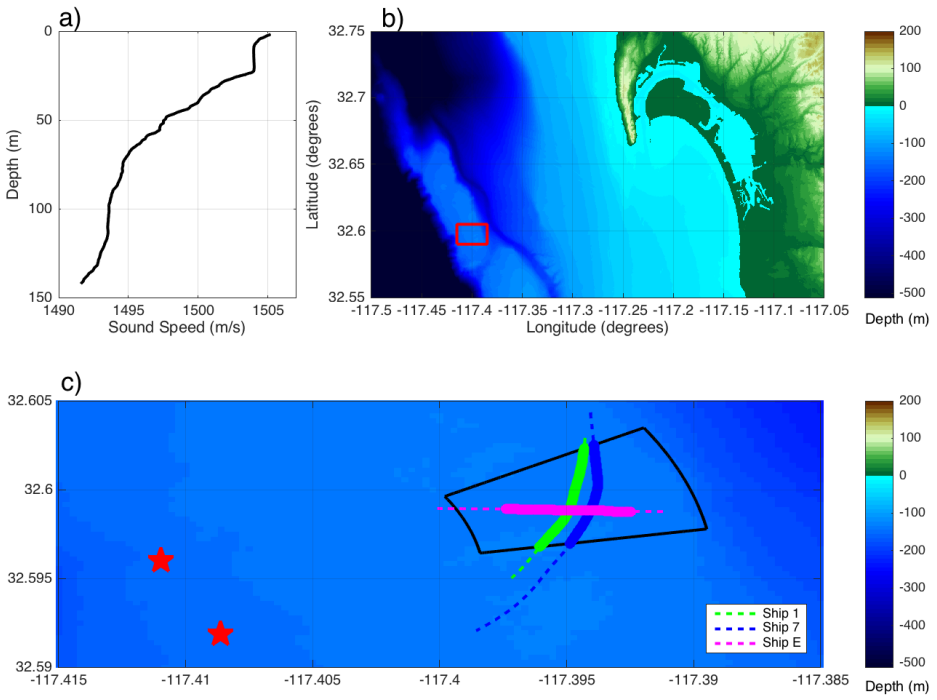

Figure 4.1: (color online) Experiment setup. The experiment was conducted in 150m of water with a strongly downward refracting sound speed profile (Figure 1a) approximately 20km off the coast of San Diego, California. Figure 1b shows the bathymetry in the vicinity of the hydrophones used in this experiment with a red box indicating the experiment site. The blue and green colored lines in Figure 1c indicate ship tracks used to create the library of cross-correlation functions used to localize the target vessel plotted in magenta. The red stars indicate the location of the hydrophones which were used for the experiment. The black box represents the grid for which the library of replica cross-correlation functions was created and is the area shown in the localization ambiguity surfaces in Figure 6.

cross-correlated. These time domain cross-correlation functions are saved as 'measured replicas' for the location of the library vessel, as determined by AIS, at the time the cross-cross correlation function is computed. In the future when an unknown 'target' acoustic source transits the experiment site, it is possible to determine when and where it crosses the paths of all previously recorded library vessels by comparing the envelope of the cross-correlation function computed during the transit of the target vessel with the envelopes of all the measured replica cross-correlation functions in the library[50]. The location with the replica that most closely resembles the cross-correlation function recorded during the transit of the target vessel, determined using the correlation coefficient between target and library cross-correlation function envelopes, is the location of the target vessel. The library cross-correlation functions must be extrapolated in order to fill in the gaps in coverage of measured replicas in order to allow for continuous tracking.

4.3.1 Formulation for fully populated library of replicas

The algorithm for extrapolating the cross-correlation functions is described schematically in Figure 4.2. The blue 'x' represents a location where a measured replica exists, computed by cross-correlating the acoustic signal on two horizontally separated hydrophones or arrays of hydrophones. The orange 'x' represents a point in the search grid that needs to be populated by extrapolating the library cross-correlation function from the known location at angle θ, relative to the array azimuth and range R to the array center to some new angle $\theta + \Delta\theta$ and new range $R + \Delta r$. The array spacing is $2d$, the range to each hydrophone is r_1 and r_2. Measured cross-correlation replica functions exist in all discrete locations that have been populated by a ship as a source of opportunity; the goal is to populate the entire search region with estimated replica cross-correlation functions that have been extrapolated from the measured replicas. This is similar to shifting the focal range of a time reversal mirror by shifting signals in frequency as discussed in Kim et al. 2003[35] and is related to the source ranging methods discussed in Thode, 2000[42].

Extrapolation of measured cross-correlation functions is accomplished by

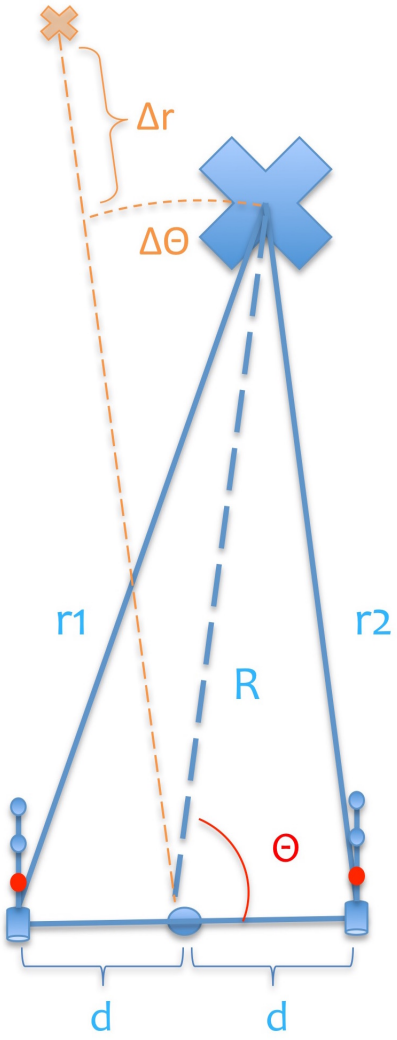

Figure 4.2: (color online) Schematic of extrapolation method with variables from Eq. (1) - (6) labeled. The hydrophones (or arrays of hydrophones) are depicted as strings of dots with a cylindrical base. The distance between the hydrophones is $2d$; in this experiment 511m. An existing measured cross-correlation function exists at the location depicted by the large blue 'x' which is a distance of r_1 meters from hydrophone 1, r_2 meters from hydrophone 2, R meters from the array center position, and angle θ relative to the array azimuth. The goal is to extrapolate the measured replica to the location shown by the small orange 'x' at angle $\theta + \Delta\theta$, and range $R + \Delta r$, with the ultimate goal being to extrapolate the measured replica cross-correlation function at the blue 'x' to all locations in the search grid.

frequency shifting the waveform by some value ($\Delta\omega$) determined using the waveguide invariant, and multiplying the frequency shifted correlation function by a complex exponential, derived in Appendix A, as shown in Eq. (1) and (4),

$$C(R + \Delta r, \theta + \Delta\theta, \omega) \approx C(R, \theta, \omega + \Delta\omega) \cdot \mathbf{F}(\boldsymbol{\Delta}\theta, \boldsymbol{\Delta}\omega), \tag{4.1}$$

where C represents the frequency domain cross-correlation function (i.e. cross spectra), R represents the range to the array center, Δr represents the difference in range to the new point in the library grid, θ represents the angle from the array azimuth to the location of the measured replica, $\Delta\theta$ represents the angle to be shifted or extrapolated, ω is the angular frequency of the cross spectra, and $\Delta\omega$ is the frequency shift needed to approximate the acoustic intensity of a signal at the range $R + \Delta r$ as defined by the waveguide invariant (β) in Eq. (4.2), and $\mathbf{F}$ represents the complex exponential used to modify the correlation function in range and angle, which will be defined in this section and derived in Appendix A.

The waveguide invariant (WGI) is a property which describes acoustic intensity fluctuations in range and frequency [29, 30, 31, 1]. It is defined as the ratio of the change in the modal group slowness with respect to the change in the modal phase slowness, and therefore encapsulates the dispersive characteristics of the waveguide into a single scalar parameter [32]. The interference pattern created by constructively and destructively interacting modes creates lines of constant intensity in range-frequency space for a waveguide of given characteristics. The waveguide invariant is a parameter which describes the slope of these lines at given ranges between source and receiver at given frequencies by the relationship defined in Eq. (4.2),

$$\beta = (\frac{r}{\omega})(\frac{\Delta\omega}{\Delta r}) = -\frac{d(1/v_m)}{d(1/u_m)}, \tag{4.2}$$

$$\Delta\omega = \beta\frac{\omega}{r}\Delta r \tag{4.3}$$

where β represents the waveguide invariant; r is the range from source to receiver; ω is the angular frequency; u_m is the modal group velocity; and v_m is the modal phase velocity. In many applications the WGI is assumed to be one for a shallow water downward refracting environment such as the one used in this demonstration, illustrated in Figure 1. That was not sufficient for the purposes of this localization method; the spatial variations in the WGI had to be accounted for[52]. For the purposes of this experiment the WGI was measured experimentally, using ships as sources of opportunity, for each hydrophone, using the methods from Verlinden et al., 2017[52] to create a map of β for the study area. Each grid point in the experiment area was assigned a β value for each hydrophone, which accounts for the propagation physics between that point and the hydrophone. This value was determined by measuring the slope of intensity striations in range-frequency space as described in Verlinden et al., 2017[52]. A map of β values for this experiment area on one of the hydrophones used in this demonstration are published in Verlinden et al., 2017[52].

Eq. (4.4) is the formulation for F in the frequency domain,

$$\mathbf{F}(\mathbf{\Delta}\theta, \mathbf{\Delta}\omega) = e^{-2i\bar{s}d\Delta\omega cos(\theta+\Delta\theta)} e^{-2i\bar{k}d\Delta\theta sin(\theta)} \tag{4.4}$$

where $\bar{k}$ represents the average horizontal modal wavenumber, and $\bar{s}$ represents the average modal group slowness or the reciprocal of modal group speed. In simulations $\bar{k}$ and $\bar{s}$ can be modeled; in practice these parameters are estimated using ships as sources of opportunity. Initial estimates of $\bar{k}$ and $\bar{s}$ are made using a standard normal mode propagation model for the acoustic environment used for the experiment, then these estimates are used to constrain a simple inversion for $\bar{k}$ and $\bar{s}$ using the localization formulation described in Eq. (4.7), and a library vessel in a known location transiting across the experiment area; adjusting $\bar{k}$ and $\bar{s}$ until the ship is localized in the proper location. The $\bar{k}$ and $\bar{s}$ values obtained using this method appear to be stable parameters of the waveguide, independent of source spectra. The derivation for Eq. (4.8) and 4.4 is included in Appendix A.

As an aside, there are two special cases of this formulation. If sufficient library vessel tracks are available and measured replicas exist at all ranges, then

the measured replica cross-correlation functions need only be extrapolated in angle and the formulation simplifies to:

$$C(R, \theta + \Delta\theta) = C(R, \theta) e^{-2i\bar{k}d\Delta\theta sin\theta} \tag{4.5}$$

at the limit where Δr approaches zero in Eq. (4.8) and the WGI is no longer required.

A variation of this formulation also exists where library cross-correlation functions at all ranges and angles can be estimated using a single measurement of acoustic intensity on a single hydrophone recorded from a library vessel in a known position. The intensity function is modified in range using the waveguide invariant, and the cross-correlation function across the pair of phones is estimated by multiplying the frequency-shifted intensity function by a complex exponential:

$$C(R + \Delta R, \theta) = I(R, \omega + \Delta\omega) e^{2i\bar{k}dcos(\theta)} \tag{4.6}$$

where $I(R, \omega + \Delta\omega)$ is the intensity function, frequency shifted by some $\Delta\omega$ as determined using the waveguide invariant for the desired range shift Δr. The derivation of this variation to the formulation is also included in the appendix. This method is advantageous because a single hydrophone can calibrate a region, and populate the full grid with measured cross-correlation replica functions. It is often the case that, in the presence of a potential library vessel, only one hydrophone records a good signal with sufficient SNR and as a result the library cross-correlation function can not be computed. When this is the case, the formulation in Eq. (4.6) can be used to estimate a library cross-correlation function and create a more densely populated library.

4.3.2 Generating the localization ambiguity surface

Once the library of measured replicas is fully populated, an ambiguity surface is generated to show the results of the localization method. The ambiguity surface is generated by computing the correlation coefficient (C_{el}) between the

envelope of the normalized time domain library cross-correlation function at every point in the grid (C_l) computed by taking the absolute value of the Hilbert transform of the cross-correlation function; and the envelope of the normalized cross-correlation function computed during the passage of the 'target' or 'event' vessel (C_e).

$$\int C_l(\tau)C_e(\tau)d\tau = C_{el}, \tag{4.7}$$

where τ is correlation lag time in seconds.

The envelope, or absolute value of the Hilbert transform of the cross-correlation waveforms, is used for comparison instead of the cross-correlation waveforms themselves because the differing spectral content of the library and event vessels can cause minor differences in the structure of the cross-correlation waveform which is smoothed over in the Hilbert transform. Different methods of pre-whitening the signals could be used in place of the Hilbert transform to account for this, without sacrificing the precision in the localization results that is a consequence of using a Hilbert transform, but here the Hilbert transform is employed for robustness. The cross-correlation functions are normalized by the autocorrelation of the signals on each hydrophone. The magnitude of the correlation coefficient between the two envelopes is the value plotted in the ambiguity surface. There are a number of methods that may be used to compare the data and replica cross-correlation functions; the correlation coefficient is the comparison metric presented here.

Each library vessel position with a corresponding measured cross-correlation replica function can be used to fully populate a grid with extrapolated cross-correlation functions. In the example in Section 4, seven individual libraries are used, which means there are seven completely populated grids, and the ambiguity surface described above is computed for each of these grids. These ambiguity surfaces are then combined with an inverse distance weighted (IDW) average based on the how far each of the original library cross-correlation functions had to be extrapolated in range. The final ambiguity surface used for localization is:

$$C_{eL} = \frac{1}{N} \sum C_{el_n} W_n \tag{4.8}$$

where C_{eL} is the final summed ambiguity surface, N is the number of libraries that are being averaged, C_{el_n} represents each of the library grids or surfaces being summed, and W_n is a Gaussian weighting matrix for the n^{th} library,

$$W_n = e^{-\Delta r_n^2 / 2\sigma^2} \tag{4.9}$$

where Δr is the difference in range between the grid point in the ambiguity surface and the original library, and σ is the standard deviation of a Gaussian-like curve that describes the inverse distance weighting surface. In other words, each library grid has an influence on the final ambiguity surface that is weighted based on the inverse-distance the library was extrapolated to each point in the grid. The closest library has the greatest influence on the final result.

4.4 Simulations

Simulations are first used to test the localization method by using the normal mode propagation model formulation described in Jensen et al. 2011[1] with an input environment very similar to the acoustic environment off the coast of southern California. A grid was selected approximately 10-15 km away from a simulated array in a 150m deep, downward refracting, range independent acoustic environment. The two hydrophones were spaced 511m apart. The parameters were chosen to mimic that of the acoustic experiment described in Section 4.

In order to test the method using a simulation, a fully populated library was simulated using a broadband acoustic radiator at every position in the grid shown in Figure 3a, then cross-correlating those signals and saving the cross-correlation function with the associated latitude and longitude of the simulated contact. The library used to generate the localization results shown in Figure 3b was populated using the extrapolation method described in Section 2.1, Eq. (4.2). The black 'x' represents the location of a ship simulated using the normal mode propagation model. The remainder of the library, 7 degrees to the left and right of the ship's

position, and 1.5 km radially closer to the array and further from the array, was populated by modifying the frequency-domain cross-correlation function using the formulation described in Section 2.1, and Eq. (4.2). Figure 3c is very similar but the library is populated using the acoustic intensity on a single hydrophone for a source in a given location, extrapolated in range and angle according the formulation in Eq. (4.6).

The ambiguity surfaces shown in Figure 3 were generated (fully populated and extrapolated libraries) by comparing all of the envelopes of the library cross-correlation functions to the envelopes of the cross-correlations computed for a simulated source in a certain location plotted as the red '+', using a correlation coefficient. The color that is plotted in the ambiguity surfaces in Figure 3 is the correlation coefficient for the envelope of each replica correlation function and the 'data' correlation function. In other source localization literature, ambiguity surfaces such as those shown in Figure 3 are often plotted in dB, with a significant dynamic range; whereas these surfaces are plotted on a linear scale from -1 to 1 because they represent the normalized correlation coefficient. This is necessarily a relatively small dynamic range compared to many localization methods but the relative peaks are discernible and allow for continuous tracking. There is some ambiguity; however, this can be reduced with averaging the ambiguity surfaces of multiple libraries, or using multiple combinations of hydrophones. Each case (fully populated and extrapolated libraries) performs nearly identically in this simplified simulated environment, with approximately equal dynamic ranges on the ambiguity surfaces. It is important to note that these simulations were conducted in range independent environments, with no bathymetry. More unique environments yield more complex acoustic propagation, leading to arrival structures on the hydrophones with more geographic uniqueness. In other words, the method works better in range dependent environments and results from field experiments often outperform simulations conducted in simple range independent environments as long as the variability of the waveguide invariant values over the search grid can be estimated a-priori. In these more complex environments the extrapolated cross-correlation function libraries shown in Figure 3b start to outperform the

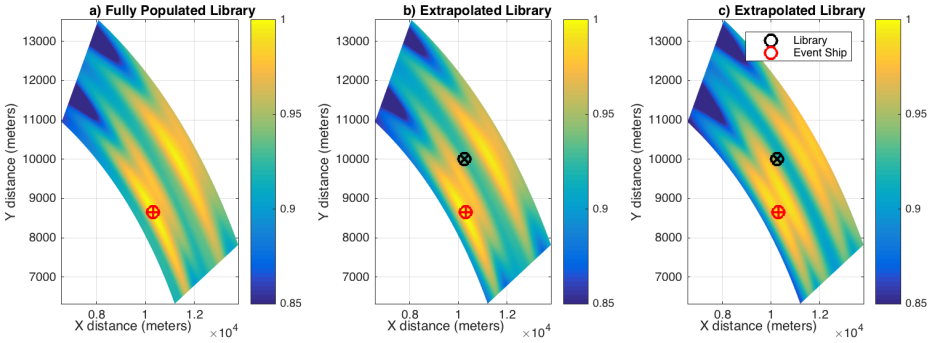

Figure 4.3: (color online) Modeled localization results. Figure 3a is the ambiguity surface generated using a fully populated library of measured replica cross-correlation functions, simulated for every point in the grid and compared to the cross-correlation function of a simulated contact in the position represented by the red '+'. The color in the ambiguity surface represents the correlation coefficient between the envelope of each library cross-correlation function and the envelope of the 'event' cross-correlation function. Figure 3b is a similar ambiguity surface, but the library of replica cross-correlation functions was populated using the formulation in Section 2.1, Eq. (4.2), extrapolating a single measured cross-correlation function in range and angle. A measured (simulated) cross-correlation function at the position indicated by the black 'x' was extrapolated to every point in the grid and those extrapolated cross-correlation functions were compared to the 'event' function. The library of replica functions used to generate the ambiguity surface in Figure 3c was populated using the formulation in Eq. (4.6); estimating the cross-correlation functions for every point in the grid using the acoustic intensity on a single phone computed for a source at the position indicated by the black 'x'.

extrapolated intensity function libraries shown in Figure 3c.

4.5 Experimental Results

After exploring the method using numerical simulations, it was tested using data from a field experiment conducted in 2009. The experiment involved a 10-day deployment of four vertical line arrays (VLAs) approximately 20 km off the coast of San Diego, California, USA. The VLA's each consisted of 16 elements regularly spaced one meter apart, starting approximately 7 meters off the bottom. They were deployed in water approximately 155 meters deep, and were spaced approximately 500, 1000, and 1500 meters apart. One element from each of two

VLAs spaced 511 meters apart and positioned approximately 18 meters off the bottom, were selected for this demonstration. The VLAs sampled at 25 kHz, but the data was down-sampled to 1 kHz, and bandpass filtered between 20 and 300 Hz. Ships were tracked during the entire 10-day experiment using the Automatic Identification System (AIS); the tracking data was obtained upon request from the United States Coast Guard Navigation Center (USCG NAVCEN) Nationwide AIS (NAIS) database.

Figure 1 shows a plot of the geometry of the experiment. There are three ship tracks transecting the localization grid outlined in black lines in Figure 1c. Ship 1 and Ship 2 plotted in green and blue respectively in Figure 1c, were used to construct the library of measured replicas. The magenta line represents the target ship, not contained in the library data, to be localized using the method. The library ships and event ship have different spectral signatures as can be seen from the spectrograms in Figure 4d, 4e, and 4f. For each of these vessel tracks, cross-correlations are computed using 0.5 s long snapshots of the data recorded on each of the receivers, at every point along the vessels track. These time varying cross-correlation functions are plotted in Figures 4a, 4b, and 4c. While consistent peaks are present where one would expect for a ship along the track of each vessel, in Figures 4a and 4b the peaks are not as easy to discern as in Figure 4c. Figure 4c represents a better, more strongly correlated ship track; the method performs best when the signals are strongly correlated so this demonstration is less than ideal. Nevertheless, the method functions. Library ship 1 and 2, were both the R/V NEW HORIZON moving from north to south across the grid, on two different days, five days apart. The 'event' ship was a tug and tow that transited from east to west across the experiment site on a day in the middle of this time period.

When the library cross-correlation functions created using the extrapolation method described in Section 2.1 are plotted for every point along the event ship track alongside the actual measured cross-correlation function computed along the event ship track as in Figure 4.5, it is clear that the extrapolation method is capturing the structure of the cross-correlation function in all locations. Seven discrete locations along the path of two library vessels were selected as 'library'

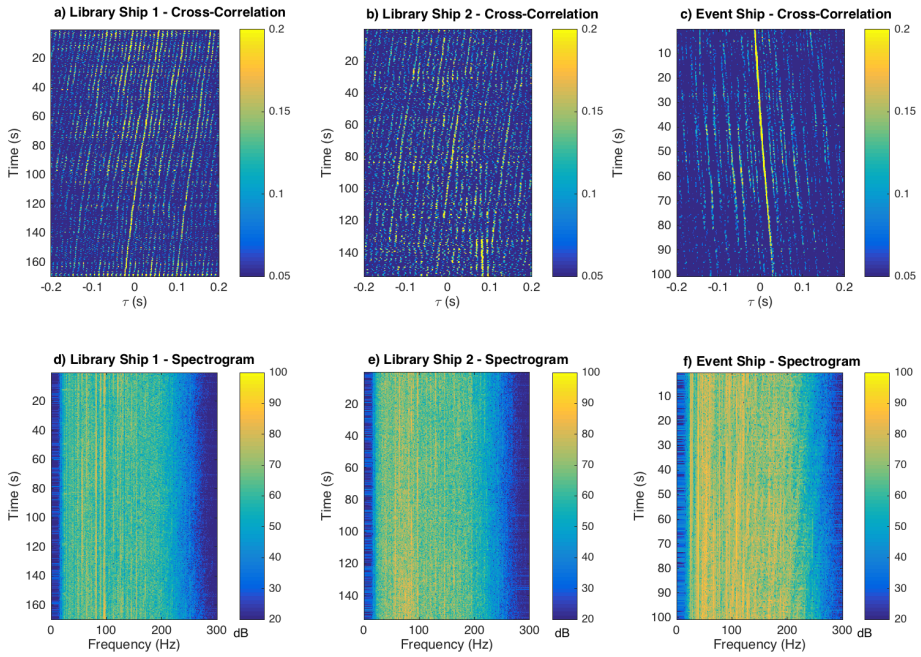

Figure 4.4: (color online) Figure 4a shows the time varying cross-correlation function, normalized by the autocorrelations between the two hydrophones, computed along the track of Library Vessel 1 (the green track in Figure 1c). Correlation time, τ is plotted on the x-axis and time along the vessels track is plotted on the y-axis. For the purposes of this demonstration, the signals were band-pass filtered between 20 and 300 Hz, and cross-correlations were computed using 0.5 s long snapshots of the data recorded on each of the receivers. Similarly, Figure 4b and 4c show the same information but for Library Vessel 2 and the "event" vessel (the target vessel to be localized). Figures 4d, 4e, and 4f are the spectrograms for each of these vessels at the time the cross-correlations were computed with frequency on the x-axis and time along the vessel track on the y-axis.

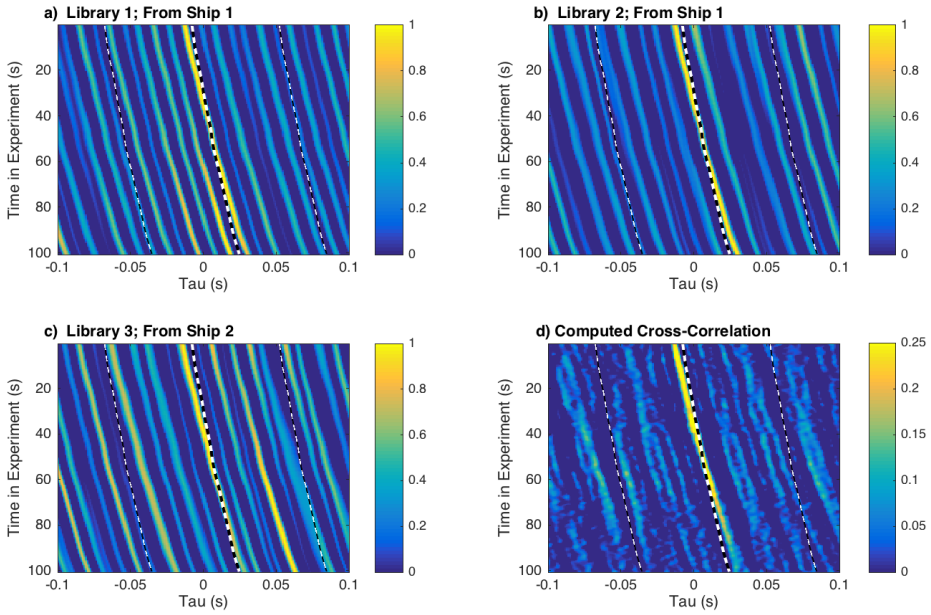

Figure 4.5: (color online) Figure 5a, 5b, and 5c are the extrapolated time-varying cross-correlation functions taken from the same three libraries used for the experimental localization results. Correlation time, τ is plotted on the x-axis and time along the vessel's track is plotted on the y-axis. The actual cross-correlation function along the 'event' vessel track is plotted in Figure 6d. The functions plotted in Figure 5a, 5b, and 5c are similar to the measured function plotted in Figure 5d, which means the extrapolation formulation is doing a reasonable job approximating the cross-correlation at these positions. The black and white lines in each plot represent the theoretical peak lag time across the two phones, and the window of the correlation function used for the comparison.

cross-correlation functions. These 'library' functions were extrapolated to every point in the search grid; and the time varying cross-correlation functions from every point along the track of the 'event' vessel are extracted from that grid and are plotted for three of these libraries in Figure 5 alongside the computed cross-correlation function along the track of the 'event' vessel.

Several discrete locations along the tracks of the library vessels, represented by the black x's in Figure 6d are selected as library points. The cross-correlation functions computed when the vessel was in that location, horizontal slices through Figure 4a and 4b, are extrapolated to all the points within the grid using the formulation in Eq. (4.2). Then, each of those points are used to generate a fully

populated library of estimated replica cross-correlation functions. The envelopes of each of these extrapolated cross-correlation functions are correlated with the envelope of the event cross-correlation function and the correlation coefficient at every point in the grid is plotted in Figures 6a, 6b, and 6c, representing the ambiguity surfaces for three of the seven libraries generated for this demonstration of the method. These surfaces are combined using an inverse distance weighted (IDW) average, preferentially weighting the libraries that have been extrapolated the least distance using the formulation in Section 2.2. This surface is plotted in Figure 6d. The locations of the local maxima, defined as points with a correlation coefficient within 1% of the global maximum of the surface, are plotted as red dots. There is some ambiguity in range, but the method does accurately localize the target vessel at all points along the vessel's track. The ambiguity in range decreases when the method is applied at greater ranges in simulation, but the data was limited in this implementation to close ranges. Interestingly, the localization results from experimental data often outperform the modeled results owing to the environmental complexity of the range dependent geometry of the waveguide creating a more diverse set of unique replica cross-correlation functions.

As with any localization method, side lobes and ambiguity can lead false detections. One of the benefits to this method over the work of Verlinden et al., 2015[50] is the fully populated libraries allow for continuous tracking. If the ambiguity surfaces are generated for every point along the event ship track, and the local maxima (plotted as red dots in Figure 6) are plotted on the x-y plane with the color of the points representing the time along the track as in Figure 7a it is clear that, while there are outliers, there is a discernible path. The standard error of all the detections, defined as points in the ambiguity surface having a correlation coefficient within 1% of the global maximum of the ambiguity surface in Figure 6d was 175.1 m. When a simple 3D, iterative, regression-based tracking algorithm is applied to the dataset the precision of the localization result improves dramatically to a standard error of 24.7 m. The tracking algorithm is not the focus of this study and any number of tracking algorithms such as a Kalman filter, could be applied. In this demonstration the tracking algorithm used involved calculating a best fit

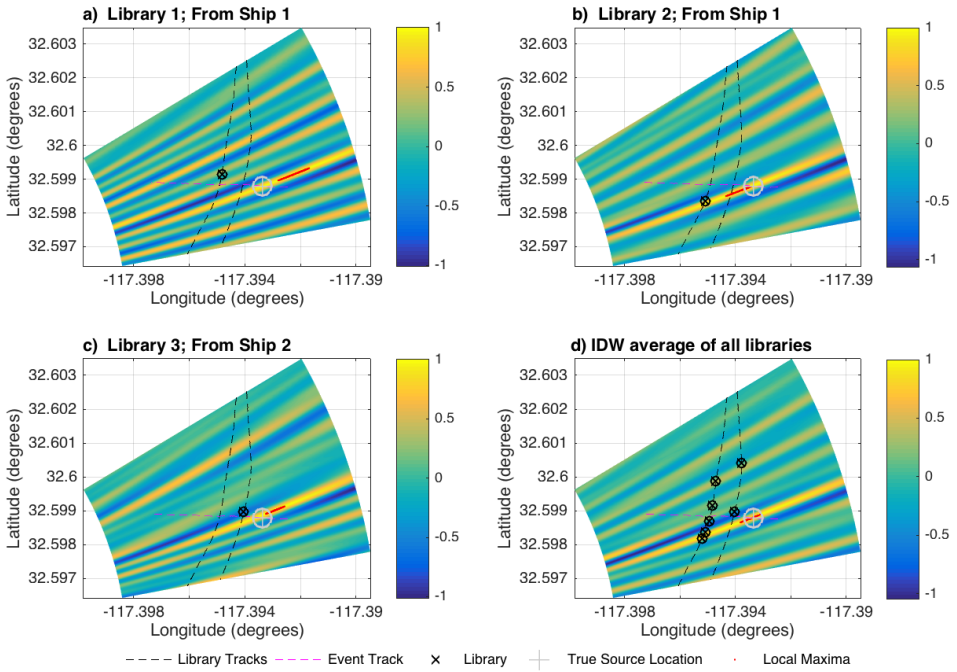

Figure 4.6: (color online) Localization Results. Figure 6a, 6b, and 6c show the ambiguity surface for three library points shown as black 'x's generated using the formulation in Section 2.2. Figure 6d is the inverse distance weighted (IDW) average ambiguity surface computed using the formulation in Section 2.2 for the seven library points plotted as black 'x's. While in every snap shot the averaged surface does not necessarily look better, the results are more consistent and the track that is derived from this surface is far better than from any single library. In each plot the red dots represent the locations of the local maxima, defined as values in the ambiguity surface within 1% of the value of the global maximum of the surface, and can be thought of as positive 'detections'. The grey crosshairs show the 'true' position of the target vessel.

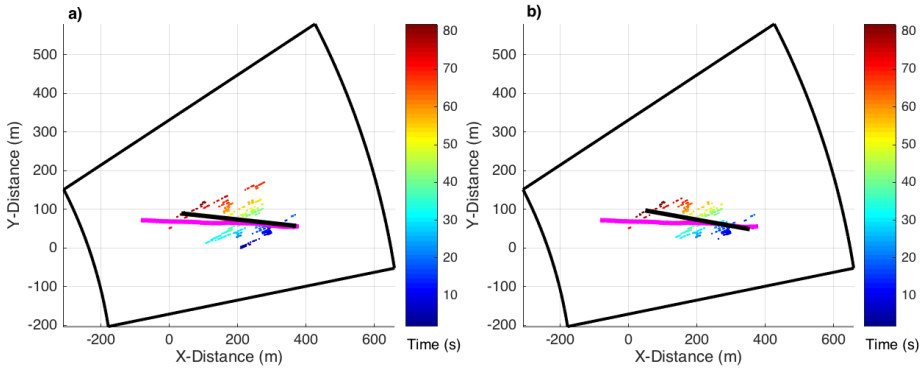

Figure 4.7: (color online) Figure 7a shows all of the 'detections' from the ambiguity surface shown in Figure 6d along the track of the 'event' vessel plotted on the x-y plane with the color of the dot representing the time along the track in seconds. The true track of the vessel is shown in magenta, while the detected track is shown in black. It is clear that there is a track that follows along the points but there are outliers. Figure 7b shows the detections once the tracking algorithm had been applied and all points along the track that deviated from a 3D regressive best fit line to the data points in Figure 7a are removed. The standard error of the resulting track in Figure 7b is 24.65 m, which represents a considerable improvement over the track in Figure 7a which has a standard error of 175.1 m, for contacts approximately 2 km from the array.

line through the detections in x-y-t space, eliminating detections that fell outside a certain threshold from that line; recomputing a best fit line, and repeating this process until the standard error is no longer reduced. Figure 7b shows the results of the tracking algorithm. The actual path that the event ship took is plotted as a magenta line, the locations of each detection are plotted as colored dots, with the color corresponding to time along the vessel's track, and the black line shows the best fit track resulting from the tracking algorithm. There is good agreement between the vessel track and results of the localization method.

While the method performs well in this demonstration, it is sensitive to mismatch in the parameters used in the extrapolation, β, $\bar{k}$, and $\bar{s}$. Small changes in these three parameters can lead to error in the resulting localization method in angle and range, depending on the geometry of the experiment. This sensitivity was modeled for the geometry of the simulated localization results shown in Figure 4, for a contact approximately 12 km away, 45 degrees from array end fire, for hy-

drophones spaced 500 m apart. The simulated contact is localized using a library extrapolated 750 m in range, and 5 degrees in angle. Small errors in β result in significant errors in range localization. For example, introducing 1% error in β results in a 10 m error in source range, or approximately 1.3% of the extrapolated range; and virtually no error in source azimuth. A 10% mismatch in β yields 75 m error in source range or approximately 10% the extrapolated range; and approximately 0.2 degrees error in source azimuth or 4% of the extrapolated angle. Introducing an error in $\bar{k}$ has very little impact on source range, but a significant impact on angle. A 1% error in $\bar{k}$ gives virtually no error in range, but approximately 0.1 degrees error in angle or 2% of the extrapolated angle. A 10% error in $\bar{k}$ yields 10 m error in range or approximately 1.3%, and approximately 0.5 degrees error in angle or 10% of the extrapolated angle. The method is comparatively less sensitive to mismatch in $\bar{s}$ with 10% error in $\bar{s}$ yielding virtually no error in range, and only about 0.1 degrees error in angle or 2% of the extrapolated angle. It is important to correctly estimate β and $\bar{k}$ in order to achieve accurate localization results using this method.

In Section 2.1, Eq. (4.6) an alternative method of estimating library cross-correlation functions is derived, that involved using the acoustic intensity function on a single phone to approximate the cross-correlation function across a pair of hydrophones. The results of this method are simulated in Figure 3c; performance in field experiments is as predicted.

4.6 Environmental Robustness

The cross-correlation functions that are used in this method to localize contacts derive their uniqueness from the geoacoustic and physical oceanographic environment. The physical oceanographic environment is non-stationary, and changes with seasonal and diurnal heating-cooling as well as with the passage of internal waves. If the waveguide changes sufficiently between when the library cross-correlation function was computed and the passage of the ship one is attempting to localize, it stands to reason that the library cross-correlation function will no

longer be representative of a particular location within the waveguide and the method could break down. In areas with heavy ship traffic libraries can be constantly renewed with up to date measured replicas, but it is valuable to know how often this must be done. In deep water, and at high frequencies where the acoustic propagation is strongly dependent on water properties, this is a concern. This experiment was conducted in sufficiently shallow water and at frequencies low enough that the arrival structure was primarily a function of the geoacoustic environment (i.e. bottom properties and bathymetry), so this was not a concern. During the experiment, measured replicas were used to localize contacts up to seven days later at any time of day and during different stages in the tidal cycle.

In order to demonstrate this principle, an average climatological sound speed profile for the region during the winter taken from the World Ocean Atlas (WOA)[53] was used to create a library of replicas using a standard normal mode propagation model, and this library was then used to localize a contact with a signal that was simulated using the same propagation model but using an average climatological summer sound speed profile. This was designed to show how the method would behave under the most different of possible physical oceanographic environments for the region. Figure 8a shows the two sound speed profiles; winter (blue) used to generate the library of replicas; summer (red) used to generate the source signal of the contact to be localized. Figure 8b shows the localization result when the two profiles are the same, both winter; and Figure 8c shows the results when the winter library is used to localize the summer target. Performance of the method degrades, but does not entirely break down. This means that the library cross-correlation functions do not have an expiration date in this environment, but this will not be true in all environments. For example, in the Bering Sea, a region of comparable depth, the sound speed profile changes more dramatically from strongly downward refracting in the summer to isovelocity or even upward refracting in the winter. A standard summer and winter sound speed profile are taken from the WOA and are plotted in Figure 8d. The localization method works when the sound speed profile from the library matches the event as is the case in Figure 8e, but when a winter sound speed profile is used to generate the library, and that

library is used to localize an event simulated using a summer profile the method does not perform as well as shown in Figure 8f. There is still a large peak in the correlation coefficient ambiguity surface, but it is offset significantly in range, and slightly offset in azimuth. This is consistent with errors in β, $\bar{k}$, and $\bar{s}$ values used to extrapolate the library, which is expected given the change in surface sound speed. It is likely that this change can be accounted for by modifying the β, $\bar{k}$, and $\bar{s}$ values used to construct the extrapolated cross-correlation function library as is sometimes done in MFP[3]. Additionally, by nature of the library being populated with sources of opportunity, it will necessarily be continually refreshed as ships continue to transit the region, eliminating the issue of seasonal expiration of measured replicas in certain areas, and diminishing the need to modify existing libraries of measured replicas.

4.7 Conclusion

It is possible to localize an acoustic radiator at any position in the marine environment using a library of replica cross-correlation functions, estimated by extrapolating existing measured cross-correlation functions to different angles and ranges, using waveguide invariant theory. The spatial uniqueness of the library is enhanced in complex, range dependent marine environments. The fully populated library allows for continuous tracking which improves localization results.

There are a number of signal processing techniques that could be used to optimize and improve the results of this localization method. Various methods of pre-whitening and normalizing replica cross-correlation functions including the use of a SCOT transform[54] and cross-coherence functions[55] will likely improve performance in localizing sources that have vastly different source spectra than those used to construct the library.

Areas for future research include employing combinations of hydrophones or arrays of hydrophones in constructing the correlation libraries, along with experimenting with different array geometries may optimize results. Cross-correlating beams taken from vertical arrays will improve the uniqueness of the cross-correlation

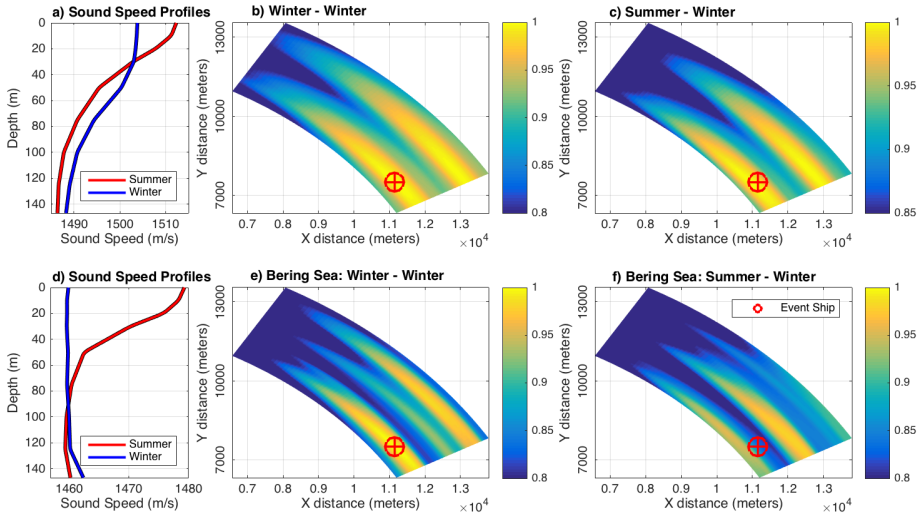

Figure 4.8: (color online) Figure 8a shows a typical sound speed profile for the experiment site taken from the WOA for summer (red) and winter (blue). When a winter profile is used to generate the simulated cross-correlation functions used to create the library and the event cross-correlation functions, the method works as before, as shown in Figure 8b. When a winter profile is used to simulate the library replicas, but a summer profile is used to simulate the event cross-correlation function, the method still performs acceptably well in this environment, as shown in Figure 8c. Figure 8d shows typical summer and winter sound speed profiles taken from WOA for the Bering Sea. Figure 8e shows the results of the localization method when the library and event correlation functions are both generated with the winter profile, while Figure 8f shows the results of the method when a winter library is used to localize a summer event ship. Here the method does not perform well due to the significant difference between the summer and winter sound speed profiles.

functions used for localization. Cross-correlating broadside beams on horizontally separated VLAs will likely emphasize mode one arrivals and make it possible to localize a sub-surface contact with a surface derived library. It is possible that this method could be expanded to localize subsurface sources using a library derived from surface sources, by modifying β, $\bar{k}$, and $\bar{s}$ values used to construct the extrapolated libraries. Library cross-correlation functions can also likely be modified to account for seasonal changes in the sound speed profiles.

Additional experimental verification is required in different marine environments. Further study may include an experiment in deeper water (500-700 m) with longer propagation paths to investigate how robust the method is to physical oceanographic complexity. Ideally, an experiment site with high vessel traffic density will be selected so the library of measured replicas can be more densely populated than in this demonstration, allowing for the exploration of different methods for combining multiple libraries for a single localization result.

4.8 Acknowledgements

This work was supported by the Office of Naval Research.

Chapter 4, in part has been submitted for publication in the Journal of the Acoustic Society. Verlinden C. M. A., Sarkar J., Hodgkiss W. S., Kuperman W. A., and Sabra K. G.. Passive acoustic tracking using a library of nearby sources of opportunity. The Journal of the Acoustical Society of America. Submitted 06 March, 2017. The dissertation author was a primary investigator and author of this material. Dr. William Kuperman, the chair of the committee, is a co-author.

4.9 Appendix

4.9.1 Extrapolation Derivation

Measured library replica cross-correlation functions can be modified in range and angle to fully populate a search grid allowing for continuous tracking by

frequency-shifting the cross-correlation function according to WGI theory, and multiplying it by a complex exponential term derived here.

It is helpful to start from the standard normal mode approximation for the cross-correlation function across two hydrophones.

$$C_{12}(R,\theta) = (P(r_1)P^*(r_2))_\theta = \sum a_{nm} e^{i(k_n - k_m)R} e^{i(k_n + k_m)dcos\theta} \tag{A1}$$

To extend this in both angle and range an approximation for $C_{12}(R+\Delta r, \theta+\Delta\theta)$ must be derived so R is replaced with $R+\Delta r$, and θ is replaced with $\theta+\Delta\theta$.

$$C_{12}(R+\Delta r, \theta+\Delta\theta) = \sum a_{nm} e^{i(k_n - k_m)(R+\Delta r)} e^{i(k_n + k_m)dcos(\theta+\Delta\theta)}$$

First the $(R+\Delta r)$ in the first exponential can be accounted for with standard waveguide invariant theory where

$$(k'_n - k'_m)(R) = (k_n - k_m)(R+\Delta r)$$

and k'_n and k'_m are the horizontal modal wavenumbers shifted by some frequency $\Delta\omega$ corresponding to the Δr in accordance with WGI theory.

$$k'_n = k_n(\omega + \Delta\omega)$$
$$k'_m = k_m(\omega + \Delta\omega)$$

So the $e^{(i(k_n - k_m)(R+\Delta r))}$ term becomes $e^{(i(k'_n - k'_m)R}$. Expanding k'_n about k_n yields:

$$k'_n = k_n(\omega + \Delta\omega) = k_n(\omega) + \frac{dk}{d\omega}\Delta\omega)$$

which means that

$$(k'_n + k'_m)dcos(\theta+\Delta\theta) = ((k_n(\omega) + \frac{dk_n}{d\omega}\Delta\omega) + (k_m(\omega) + \frac{dk_m}{d\omega}\Delta\omega))dcos(\theta+\Delta\theta)$$

which with some rearranging becomes:

$$(k_n + k_m)dcos(\theta+\Delta\theta) = (k'_n + k'_m)dcos(\theta+\Delta\theta) - (\frac{dk_n}{d\omega} + \frac{dk_m}{d\omega})\Delta\omega dcos(\theta+\Delta\theta)$$

So the $e^{i(k_n + k_m)dcos(\theta+\Delta\theta)}$ term becomes:
$e^{i(k'_n + k'_m)dcos(\theta+\Delta\theta)} e^{-i(\frac{dk_n}{d\omega} + \frac{dk_m}{d\omega})\Delta\omega dcos(\theta+\Delta\theta)}$

And

$$C_{12}(R+\Delta r, \theta+\Delta\theta) =$$
$$\sum a_{nm} e^{i(k'_n - k'_m)R} e^{i(k'_n + k'_m)dcos(\theta+\Delta\theta)} e^{-i(\frac{dk_n}{d\omega} + \frac{dk_m}{d\omega})\Delta\omega dcos(\theta+\Delta\theta)}$$

Now using trigonometric identities,

$cos(\theta + \Delta\theta) = cos(\theta)cos(\Delta\theta) - sin(\theta)sin(\Delta\theta)$

And for small $\Delta\theta$'s, $cos(\Delta\theta) \rightarrow 1$ and $sin(\Delta\theta) \rightarrow \Delta\theta$, so the expression becomes

$cos(\theta + \Delta\theta) = cos(\theta) - sin(\theta)\Delta\theta$

So the $e^{i(k'_n+k'_m)dcos(\theta+\Delta\theta)}$ term becomes $e^{i(k'_n+k'_m)d(cos(\theta)-\Delta\theta sin(\theta))}$, and the entire expression simplifies to

$C_{12}(R + \Delta r, \theta + \Delta\theta) =$
$\sum a_{nm} e^{i(k'_n-k'_m)R} e^{i(k'_n+k'_m)d(cos(\theta)-\Delta\theta sin(\theta))} e^{-i(\frac{dk_n}{d\omega}+\frac{dk_m}{d\omega})\Delta\omega dcos(\theta+\Delta\theta)}$

which with some rearranging becomes

$$C_{12}(R + \Delta r, \theta + \Delta\theta) = \sum a_{nm} e^{i(k'_n-k'_m)R} \; e^{i(k'_n+k'_m)dcos(\theta)} \; e^{-i(k'_n+k'_m)\Delta\theta sin(\theta)} \; e^{-(\frac{dk_n}{d\omega}+\frac{dk_m}{d\omega})\Delta\omega dcos(\theta+\Delta\theta)}$$

According to waveguide invariant theory, $\sum a_{nm} e^{i(k'_n-k'_m)R} e^{i(k'_n+k'_m)dcos(\theta)} = C_{12}(R, \theta, \omega + \Delta\omega)$; in other words the original cross-correlation function frequency shifted by some $\Delta\omega$ corresponding the the Δr you desire to range shift the function. Then we introduce the average wavenumber term $\bar{k}$ where $\bar{k} = \frac{1}{2}(k_n + k_m)$; as well as an average modal group slowness term $\bar{s}$. Since modal group speed $u_n = \frac{d\omega}{dk_n}$,

$\frac{dk_n}{d\omega} + \frac{dk_m}{d\omega} \approx 2\bar{s}$

where $\bar{s}$ is the average modal group slowness or the reciprocal of modal group speed. Substituting $\bar{k}$ and $\bar{s}$ into the expression for the extrapolated cross-correlation function, the expression for $C_{12}(R + \Delta r, \theta + \Delta\theta)$ becomes:

$$C_{12}(R+\Delta r, \theta+\Delta\theta) = C_{12}(R, \theta, \omega+\Delta\omega) e^{-i2\bar{k}\Delta\theta sin(\theta)} e^{-2\bar{s}\Delta\omega dcos(\theta+\Delta\theta)} \qquad \text{(A2)}$$

which is the formulation from Eq. (4.2). It is important to note that if the change in range is set equal to zero, then $\Delta\omega$ is zero and the formulation becomes an angle-only extrapolation as in Eq. (4.5). In other words if measured

replicas exist at all desired ranges (for example from a radial ship track) then it may only be necessary to extrapolate the measured replicas to other angles. Using this formulation it is possible to extrapolate a cross-correlation function measured when a ship was in one position to a different range and bearing; which makes it possible to fully populate a region with extrapolated measured cross-correlation replica functions which can be used for localization and continuous tracking. In simulations this method was effective up to about 7 degrees. The angle over which the replicas can be extrapolated is limited by the law of cosines approximation in the first section of this derivation and is therefor a function of range from the receivers. It is also limited by the changing bathymetry in the region.

4.9.2 Estimating cross-correlation functions from intensity

There is a variation of this formulation that can be used to construct a library of estimated cross-correlation functions from the recorded acoustic intensity on a single hydrophone. This formulation is useful in circumstances where, for whatever reason, measured cross-correlation replica functions do not exist in all desired places, but intensity has been recorded on at least one hydrophone. If for example there is only one functional hydrophone in the region, or one of the phones in the array did not receive a clear signal from the library vessel it is still possible to estimate cross-correlation functions for the library. In many instances during the experiment, this method was useful for creating a more densely sampled search grid of replica cross-correlation functions which can improve localization results; but the experimental results are not presented here. It is important to note that, while the library cross-correlation functions are estimated using the following formulation, the data from the target vessel to be localized is still the measured cross-correlation across the two hydrophones in the array. Beginning with the same normal-mode based expression for the cross-correlation function from before,

$$C(\theta, R) = (P(r_1)P^*(r_2))_\theta = \sum a_{nm} e^{i(k_n - k_m)R} e^{2i\bar{k}dcos\theta} \tag{A3}$$

and the formulation for the acoustic intensity on a single phone at a range R,

$$I(R) = P(R)P^*(R) = \sum a_{nm} e^{i(k_n - k_m)R} \tag{A4}$$

where I is the acoustic intensity, it is possible to write the expression for a cross-correlation function at a given range R from the array center position and bearing θ off the array azimuth in terms from the intensity of a source at the same range.

$$C(R,\theta) = I(R)e^{2i\bar{k}dcos(\theta)} \tag{A5}$$

This means that the cross-correlation function at a certain angle θ and a range where measured replicas do not exist $R+\Delta r$, can be estimated by frequency shifting the intensity function recorded from a source at a known range, by some $\Delta\omega$ associated with the proper shift in range Δr according the waveguide invariant (4.3).

$$C(R+\Delta R,\theta) = I(R,\omega+\Delta\omega)e^{2i\bar{k}dcos(\theta)} \tag{A6}$$

Using this formulation, it is possible to fully populate a library of estimated cross-correlation functions for all ranges and bearings, using intensity from a single hydrophone, frequency shifted using the WGI, and modified using a complex exponential term.

No matter which method is used for fully populating a spatial library with cross-correlation replica functions, once the entire study is populated it is possible to localize contacts using the methods from Verlinden et al., 2015[50] in all locations and do continuous tracking.

Chapter 5

A feasibility study for passive acoustic estimation of vertical sound speed structure using sources of opportunity on a drifting volumetric array

Authors:
Jacquelyn S. Kubicko
Christopher M. Verlinden
J. Sarkar
K. G. Sabra
B. V. Nichols
J. Martin
A. I. Fagan

5.1 Abstract

This study investigates the practical feasibility of using a drifting volumetric array, such as a series of free-floating buoys with suspended hydrophones, which record ships as acoustic sources of opportunity, for performing ocean acoustic thermometry or other environmental inversions, in near-shore environments in a totally passive manner, using correlation processing. Ships are tracked using the Automatic Identification System (AIS). Numerical simulations using a standard normal mode propagation model are used to test limitations of the proposed approach with respect to frequency band, drifting receiver configuration, precision and accuracy of the inversion results, along with sensitivity to environmental and position mismatch. Performance predictions using this model are compared with results from a field experiment using at-sea data collected off the coast of New London, CT in Long Island Sound.

5.2 Introduction

In the study of climate science and physical oceanography, as well as in ocean acoustic source localization applications, it is beneficial to understand the distribution of ocean properties such as temperature and salinity[5]. For studying

climate change, knowing the temperature of the ocean to a high degree of accuracy (1-2 degrees C at all depths), with sufficient temporal and spatial resolution, is required to populate climatological models[6]. Currently, ocean temperature is measured through a variety of means, including isolated transects taken from research vessels, as well as a worldwide system of autonomous floats (e.g. Argo floats). Argo floats allow oceanographers to resolve coarse climatological variability; however, a gap exists in the availability of physical oceanographic data under sea-ice (Arctic and Antarctic), and coastal regions, which are among the most important and least resolved areas for understanding the global heat budget[7]. Higher spatial and temporal resolution is needed in these regions, in addition to the open ocean.

In the 1990s, it was proposed to measure large portions of the ocean using acoustic thermometry. Acoustic thermometry uses the path sound takes through the ocean, which is a function of sound speed, to invert for ocean environmental properties, such as temperature distributions. The 1998 Acoustic Thermometry of Ocean Climate (ATOC) experiment, used time-of-arrival tomography to measure the temperature of the ocean, taking advantage of long-range acoustic propagation through the Sound Fixing and Ranging (SOFAR) channel[8, 9, 10]. The purpose of the study was to measure the changing temperature of the global ocean in order to better understand climate change. However, the need of maintaining a (potentially loud) active acoustic source[8], that requires complex hardware deployment, caused a significant increase in operating costs and limited the scope and duration of the study. Concerns about ocean noise pollution—in particular, its effects on marine mammals—have also proven to be a constraint on experiments.

Similar to ATOC, ocean acoustic thermometry has been proposed with a focus on the use of passive acoustic methods. An implementation of passive acoustic thermometry has been demonstrated using ambient noise in deep-water environments, with long integration times[23, 22, 5]. In this approach, the cross-correlation of ambient noise was computed across two spatially separated hydrophones to estimate the arrival structure of the Green's function between these two receivers, without the use of controlled active sources. Passive acoustic tomography may also

be done using sources of opportunity such as ships, using short-term correlation processing, a method that can make use of significantly shorter integration times, allowing for greater temporal resolution of the resulting measurements. When using sources of opportunity for tomography, the cross-correlation of the signal received on spatially separated hydrophones is still necessary, as in the ambient noise case, because the source signal is unknown, as discussed hereafter. These cross-correlation waveforms, computed between all pairwise combinations of receivers, are sensitive to local environmental parameters, and thus can be used to locally invert for such parameters, provided the ship position is known with some level of accuracy. Ships are examples of ubiquitous acoustic sources of opportunity, that are well suited for applications in source localization and tomography. Ships are typically broadband radiators with energy between 20 and 1000 Hz, characterized by tonal spectral signatures[1]. Moreover, surface vessels can be tracked using the Automatic Identification System (AIS), with relatively high-precision, thus allowing for sufficient approximation of the spatial origin of the ship radiating noise. All commercial vessels over 300 Gross Tons, commercial vessels which embark on international voyages or operate within vessel traffic systems in U.S. waters, and all passenger vessels are equipped with AIS transponders. These devices broadcast information about course, speed, and position every 2-10 seconds depending on the signal multiplexing, as well as ancillary information about the vessels' characteristics, such as draft, and position of the Global Positioning System (GPS) antennae every few minutes[56]. If the ship is equipped with Differential GPS (DGPS), it may be possible to fix the ship's propeller to within a few meters using AIS, or 10-15 meters if the ship is equipped with standard GPS. As such, surface ships represent powerful and underutilized potential sources of opportunity that can be used for tomography,[57] and source localization/target detection[50].

Large-scale acoustic tomography using drifting volumetric arrays, such as hydrophones on free-floating buoys or profiling floats, can provide a cost-effective means of imaging ocean environmental characteristics, improving both temporal and spatial resolution, while increasing the coverage in areas under sea-ice and near coastal regions, to better populate climatological models. Traditionally, tomogra-

phy on an array made up of moving hydrophones, particularly in shallow water, is considered difficult, because the inversion process requires adequate knowledge of the geoacoustic environment and hydrophone locations, in order to obtain precise sound speed measurements[58, 59, 60, 61]. Measurements of sound speed are made by comparing the arrival structure of acoustic signals generated by sources of opportunity on two spatially separated hydrophones. The differences in arrival times are determined using the cross-correlation of the signals on the two hydrophones, which is necessary for passive acoustic tomography because the source signal is unknown. This is different from active tomography, where the source signal is known, and traditional time of arrival tomography may be used. The direct arrival lag times determined using the cross-correlation function are compared to modeled direct arrival lag times with varying input environments, in order to estimate the sound speed and by extension the temperature and salinity of the water column.

The goal of this study is to explore the feasibility of estimating the vertical sound speed structure using ships as sources of opportunity on a drifting volumetric array of hydrophones suspended from free-floating buoys in a shallow water marine environment. The demonstration of this technique in shallow water could be expanded to long range propagation experiments in deepwater, and is valuable in itself, due to the importance of coastal environments for the global ocean heat budget. The challenges associated with such a method are quantified through an examination of the sensitivity of the cross-correlation function to changes in the physical oceanographic environment, compared to the uncertainty in knowledge of the geoacoustic environment (bathymetry and bottom properties) and receiver positions. This provides insight into how well source and receiver positions must be fixed and how accurately the geoacoustic environment must be known for a variety of sensor configurations and potential experimental designs[12], in order to conduct passive acoustic thermometry. The performance parameters of the inversion process are explored using numerical simulations, along with a field experiment conducted in Long Island Sound, off the coast of New London, CT, in order to validate the results of the simulations.

5.3 Experimental Setup

A field experiment was conducted off the coast of New London, CT in Long Island Sound, in August 2015, from the R/V Michael Greeley. An experiment site adjacent to a shipping lane was selected, as shown in Fig. 1b, to ensure ship noise was abundant and that there was a sufficient quantity of shipping 'events' in which a vessel, tracked using AIS, would transit in the vicinity of the instrumented buoys, yielding well-correlated acoustic signals across all hydrophones[12]. The experiment took place in approximately 50 m of water, deep enough for the arrival structure to have some dependence on the physical oceanographic properties of the area (i.e. sound speed profile). Four hydrophones, suspended 20-30 m below the surface expressions of the free-floating buoys, were deployed. Different hydrophone depths were used to obtain a variety of ray paths, sampling the entire water column. Deeper hydrophones would make it possible to sample more of the water column, but were not used in order to avoid the receiver hitting potential bathymetric features (e.g. protruding rocks or debris) on the seafloor, while drifting in shallow water; the shallower hydrophones did not receive direct arrivals at longer propagation ranges, and were difficult to decouple from the movement of the surface floats. Measurements of the environment, (Conductivity, Temperature, Depth (CTD) casts), were taken during the experiment over a 12-hour period, spanning a full tidal cycle, and spread out over a distance of approximately 25 km. The sound speed profiles, shown in Fig. 1a, were spatially consistent over the 50 km^2 surveyed area; therefore, a range-independent environment was assumed, in order to focus on the local vertical sound speed profile structure. A geometry representative of the experiment was modeled using ray theory and a standard normal mode propagation model. The ray trace took into account the bathymetry and a range-independent sound speed profile. In the case of short-range propagation (under 750 m), direct arrivals were present for a shallow source (i.e. random ship radiator), shown in Fig. 1c. The simulated acoustic signals, which were cross-correlated and used for the analysis in the subsequent sections, were generated using a standard normal mode propagation model.

The R/V Michael Greeley was driven in such a pattern as to attain a ge-

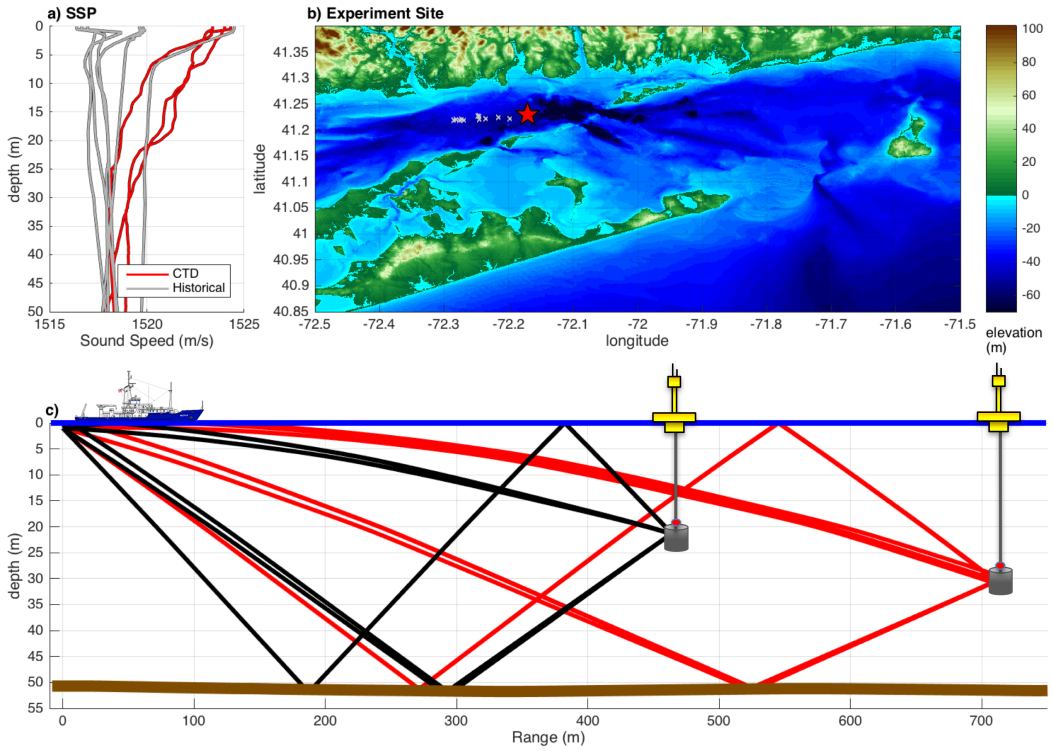

Figure 5.1: a) is a plot of the sound speed profiles with depth in meters on the y-axis and sound speed in meters/second on the x-axis for the August 2015 field experiment, along with historical profiles available for that area for the same time period. b) shows the bathymetry for the area with a red star in the location of the experiment site and elevation in meters shown on the colorbar axis. Smaller gray stars represent locations where individual CTD casts were taken. c) shows a schematic illustrating ray paths from source (ship) to two of the receivers (buoys) used in this experiment given the physical oceanographic environment. Direct arrivals are prevalent out to a range of about 750 m.

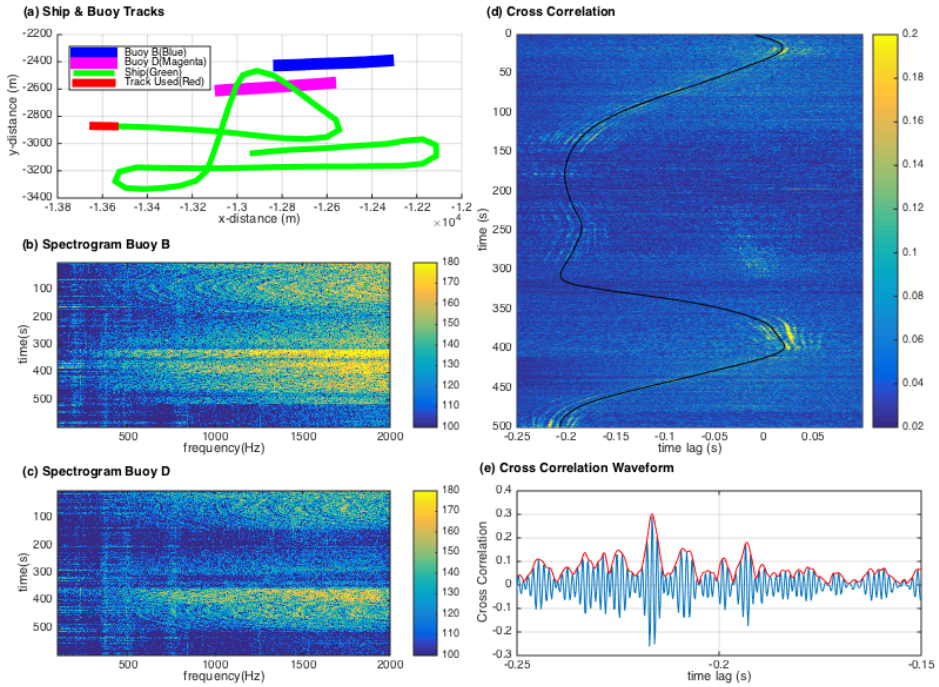

Figure 5.2: a) shows the path of the ship (source of opportunity) and two of the buoys. b) and c) show the spectrograms for two of the four buoys used to form the adaptive volumetric array. d) shows the time-varying cross-correlation between the same two buoys from b) and c). The y-axis is the time in seconds in the experiment and the x-axis is τ in seconds (time lag). The black line represents the theoretical lag time between direct arrivals on each of the buoys for a source with the same horizontal location as the ship GPS position. e) is a sample cross-correlation waveform, which represents a horizontal slice through d) at approximately 500 seconds into the ship track.

ometry that would yield a sufficient sampling of the entire experiment site, with its path shown in Fig.2a. This ship track provided situations where the ship was at broadside, end-fire, and other angles relative to the buoys. Fig. 2b and 2c show the spectrograms for two of the four buoys used to form the drifting volumetric array, showing sufficient energy throughout the band such that acoustic data exists within this frequency regime. The cross-correlations for the buoys were computed using an adaptive correlation (integration) time, with longer integration times (i.e. 1.0 second) at end-fire, and shorter integration times (i.e. 0.25 seconds) at broadside based on the directivity pattern of a 2 element array, which has wider angular beam pattern in the end-fire direction, when compared to the broadside direction[Roux2004]. The final twenty-three seconds, or fifty-five snap shots where the ship was at end-fire to the examined buoys, are used for the final inversion presented in Fig. 9.

5.4 Simulations

5.4.1 Feasibility Analysis

The first inversion method, (akin to a form of matched-field processing), compares the full estimated (i.e. replica) and actual time-domain cross-correlation waveforms across pairs of buoys, in order to determine the physical oceanographic environment; therefore, it is necessary to determine the dependence of the waveforms on various parameters that could hinder sensitivity to the sound speed profile. Three parameters are examined hereafter: position mismatch, bottom depth uncertainty, and bottom sound speed uncertainty.

Exhaustively quantifying the influence of these parameters is not simple, due to the variety of ways the vertical structure of sound speed can vary in a typical marine environment. The ocean may warm or cool due to seasonal variations, experience changes in mixing due to wind/wave surface action, as well as tidal changes, or the thermocline may change depth due to internal waves[62]. For the purposes of this paper, the sound speed profiles were varied in only two distinct ways: using standard deviations from a mean to represent longer-term seasonal

variation, and using internal wave modes indicative of short timescale variability. Supported modes of internal waves were calculated from the buoyancy profile, then varied manually to produce the desired vertical shifts in the thermocline, without any specific empirical model (e.g. Garrett-Munk model[63]) being employed. The modeled cross-correlation functions across the buoy pairs were computed by independently varying the vertical structure of the sound speed profile and each of the three parameters. A downward refracting, range independent water column was used with a flat bottom at 50 m water depth. The modeled sources were flat, broadband acoustic radiators between 20-1000 Hz. Horizontal variability from phenomena such as internal waves and tides is not discussed here. The correlation coefficient of the resulting cross-correlation functions with the reference cross-correlation function generated using the unperturbed environment/geometry, was computed in order to quantify the similarity between the two correlation waveforms. The decorrelation of these two waveforms as a function of the different parameter values is represented in plots such as those in Fig. 3. The color in the plot is the value of the correlation coefficient between the cross-correlation functions generated using the true and perturbed environments, and is indicative of the extent to which each of the parameters impacted the structure of the cross-correlation function waveform. The shapes of the high correlation regions (shown in yellow in the plots in Fig. 3) are representative of the dependence of the cross-correlation function on the parameters being mapped. In this case an environment and geometry representative of the field experiments conducted were used in the simulations. Four buoys were modeled, spaced in a random configuration 100-300 meters apart, as illustrated in Fig. 5a. Each of the ambiguity surfaces shown in Fig. 3 is the average of 1000 random iterations of the simulation, as using greater than 1000 iterations did not significantly affect the resulting ambiguity surface.

The decorrelation coefficient ambiguity surfaces generated for various inversion parameters are plotted in Fig. 3. Sound speed profiles are varied by adding or subtracting some number of standard deviations from the mean profile at all depths for the simulated experiment site, to replicate how the sound speed profile varies based on diurnal or seasonal heating, shown in Fig. 3a. All subplots in the

left column have sound speed varying in this manner. Fig. 3e shows sound speed profiles varied based on the first internal wave mode, adding some percentage of the total variance of the first wave mode to the mean profile. This is designed to simulate how the sound speed profile varies on an hourly timescale, due to internal waves. All subplots in the right column have sound speed varying in this manner. Fig. 3b focuses on the position parameter. The color bar represents the correlation coefficient between two cross-correlation functions, one generated using a normal mode propagation model with the unperturbed mean sound speed profile input and no position uncertainty, the other with the model input sound speed adjusted by adding or subtracting the number of standard deviations on the x-axis and a position error introduced equal to the value on the y-axis. Adding position uncertainty means offsetting the position of the source input into the model in a random direction and random distance, with the standard deviation of the number plotted on the y-axis. In Fig. 3f, the cross-correlation functions across the hydrophones are less sensitive to this type of variation, as shown by the horizontally broader shape of the high correlation region on the Fig. 3f plot. Figs. 3c and 3g provide insight into how well the bathymetry must be known in order to be able to gain information about the physical oceanography (water column properties) using the cross-correlation of acoustic signals across hydrophones. Fig. 3g shows the cross-correlation functions are again less sensitive to this type of variability, thus this type of tomography would likely do a poor job in resolving internal wave variability. Figs. 3d and 3h show bottom sound speed mismatch. These figures suggest that the cross-correlation function is more dependent on the sound speed in the bottom than the sound speed in the water column at these frequencies; as a result, using the correlation coefficient between cross-correlation functions is likely not a viable inversion parameter, for the purpose of inverting for ocean sound speed changes in the presence of large uncertainties of the local geoacoustic parameters, such as bottom sound speed.

In Fig. 3b, using the specific geometry and modeled source characteristics (4 buoys, spaced randomly 100-300 meters at all angles surrounding the simulated source (as shown in Fig. 5a), 50 m of water, flat bottom, flat broadband acoustic

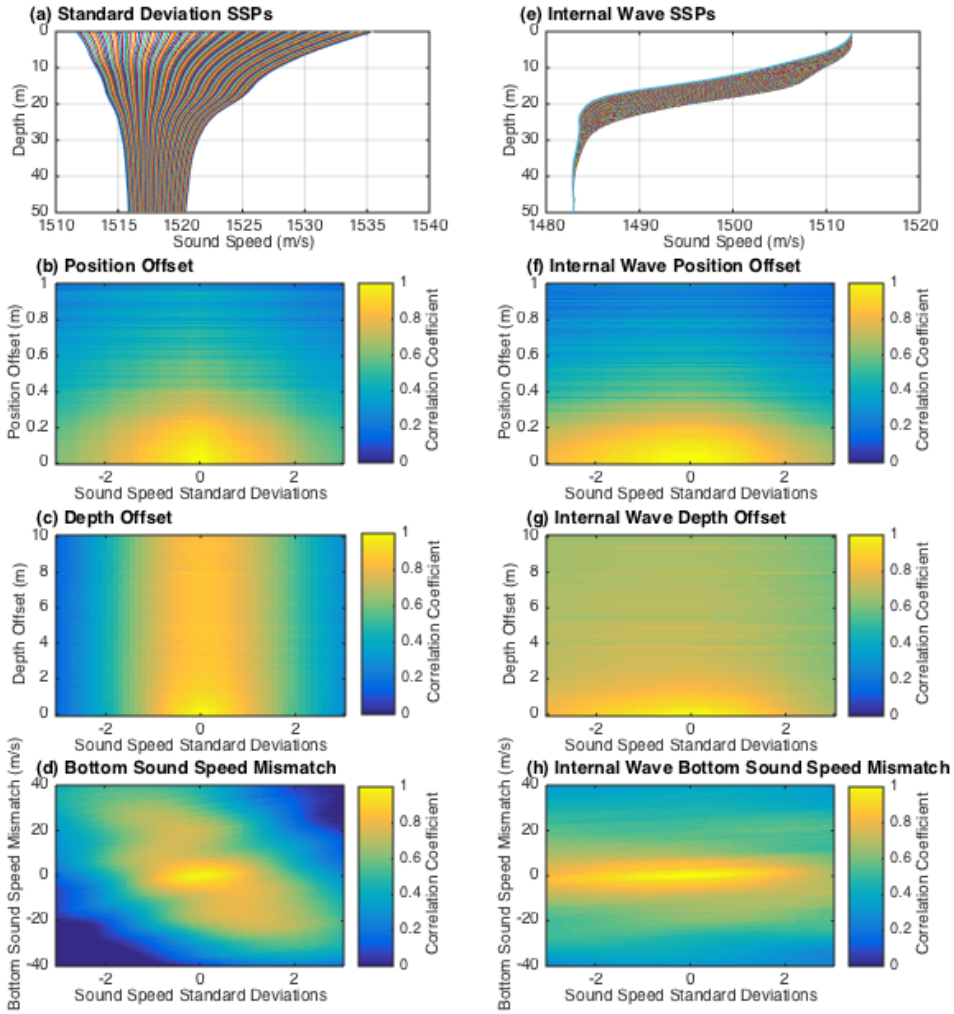

Figure 5.3: a) and e) show plots of the sound speed profiles varied by adding or subtracting standard deviations from the mean profile at all depths or based on adding some percentage of the total variance of the first internal wave mode to the mean profile for the simulated experiment site. b), c), d), f), g), and h) show ambiguity surfaces representing the decorrelation of cross-correlation functions with changing sound speed compared to position mismatch, bottom depth uncertainty, or bottom sound speed mismatch for both methods of varying sound speed, using a frequency band of 100-1000 Hz.

radiators between 20-1000 Hz), sensors would need to be fixed to within approximately 20 cm, in order to resolve the sound speed changes to within approximately one half a standard deviation of the mean sound speed. In order to achieve comparable results, the depth must be known within approximately one meter (Fig. 3c), and the bottom sound speed must be known to within 5 m/s (Fig. 3d). Hence, in order to invert for the changes in sound speed profile only, an accurate geoacoustic inversion must be done prior to making measurements of the physical oceanography, or the portion of the correlation waveform which is dependent only on the water column properties (i.e. direct arrivals) must be isolated.

Fig. 4 displays decorrelation coefficient ambiguity surfaces for bottom sound speed, similar to the panel in Fig. 3d, but for four different frequency regimes. Fig. 4a shows the decorrelation ambiguity surface for bottom sound speed for a low frequency regime (100-200 Hz), for buoys spaced approximately 150-300 m apart. Lower frequencies are able to resolve less information about the water column than higher frequencies at the same range from source to receiver. For this reason there is more ambiguity in Fig. 4a, the lower frequency regime, than in Fig. 4c, the higher frequency regime. Fig. 4b is over a 500-600 Hz band; therefore, it is slightly less ambiguous than the low frequency 100-200 Hz band of Fig. 4a. The broadband approach of Fig. 4d spans 100-1000 Hz, and falls between the higher and lower frequency regimes of Fig. 4a and Fig. 4c in the shape of the ambiguity surface. Overall, the structure of cross-correlation functions generated from signals with higher frequency content is more sensitive to the characteristics of the water column, while lower frequency cross-correlation functions are more influenced by the bottom characteristics.

When the buoys are positioned randomly, as in Fig. 5a, the shape of the high-value region on the position mismatch decorrelation ambiguity surfaces depends on the relative spacing and configuration of the buoys. As the distance between buoys is increased, the cross-correlation function across the two buoys becomes more sensitive to changes in the physical oceanography (i.e. sound speed). For shorter ranges (30-60 m), the region of higher values on the ambiguity surface would be wider, meaning the correlation coefficient between unperturbed and

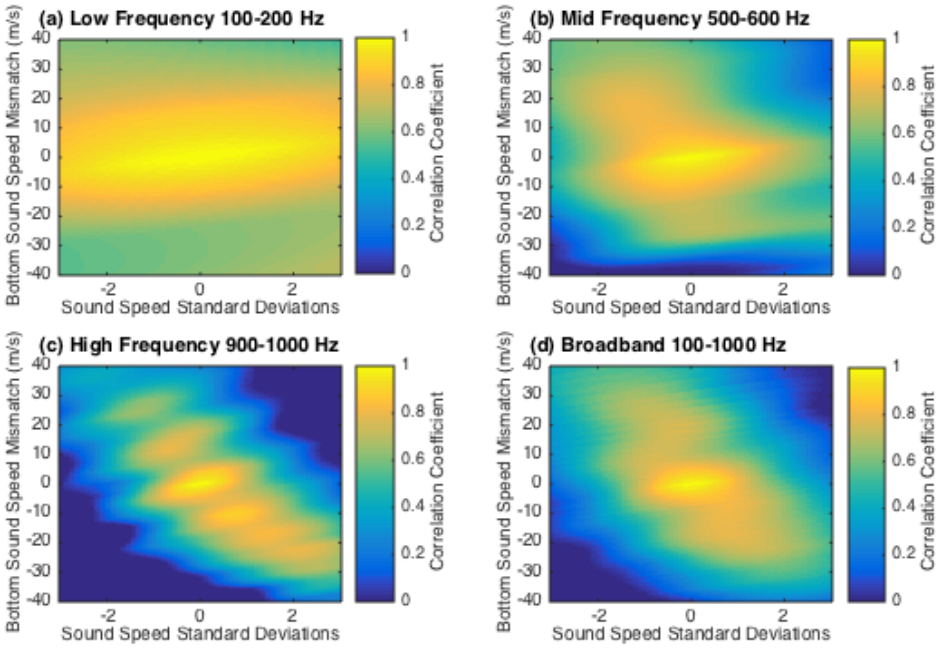

Figure 5.4: a) shows the decorrelation ambiguity surface for bottom sound speed for a low frequency regime, 100-200 Hz. b) is from a 500-600 Hz band. c) represents a higher frequency regime, between 900-1000 Hz. d) is a broadband approach over a 100-1000 Hz band.

perturbed environment cross-correlation functions would decorrelate faster with movement along the y-axis than along the x-axis. The ambiguity surfaces for position mismatch may be thought of in terms of a percentage, rather than as an absolute accuracy (i.e. GPS accuracy where there are fixed variables without dependence on source range). Longer propagation paths will lead to arrival times (lag times) that are relatively more dependent on the sound speed in the water, while shorter propagation paths will be more sensitive to position mismatch of the source/receiver, because the associated timing error will be a greater percentage of the whole (lag time). Fig. 6a shows position offset in meters on the y-axis and standard deviations from mean sound speed on the x-axis. The color bar runs from 0 (blue) to 1 (yellow) with 1 indicating a perfect match. At a short range (randomly distributed buoys approximately 30-60 m apart), the high correlation coefficient region (yellow) on the plot is broader in the x-dimension, indicating that the cross-correlation functions decorrelate more rapidly as source position changes, than for small changes in ocean sound speed. This indicates that it will be difficult to resolve ocean sound speed using buoys that are close together. Fig. 6b shows the same ambiguity surface computed for larger source and receiver ranges (random spacing between 1 and 3 km). The cross-correlation functions decorrelate rapidly with small changes in ocean sound speed, meaning an inversion conducted with buoys spaced further apart will be more sensitive to the physical oceanographic environment and less sensitive to position mismatch.

Fig. 6 also shows the impact of changing the array shape/configuration. When the source is broadside to the receivers, as is the case in Fig. 6c, large changes in the sound speed in the water column correspond to virtually no change in arrival time on the two buoys, meaning the cross-correlation functions will be very similar despite large changes in the water properties. Broadside cross-correlations are less useful for tomography than end-fire cross-correlations because the two arrivals have sampled nearly identical slices of the environment. Fig. 6d shows the same ambiguity surface for end-fire buoy configuration, as shown in Fig. 5b, and it is clear the cross-correlation functions decorrelate far more rapidly with changing sound speed than with position mismatch. For a source located at broadside to

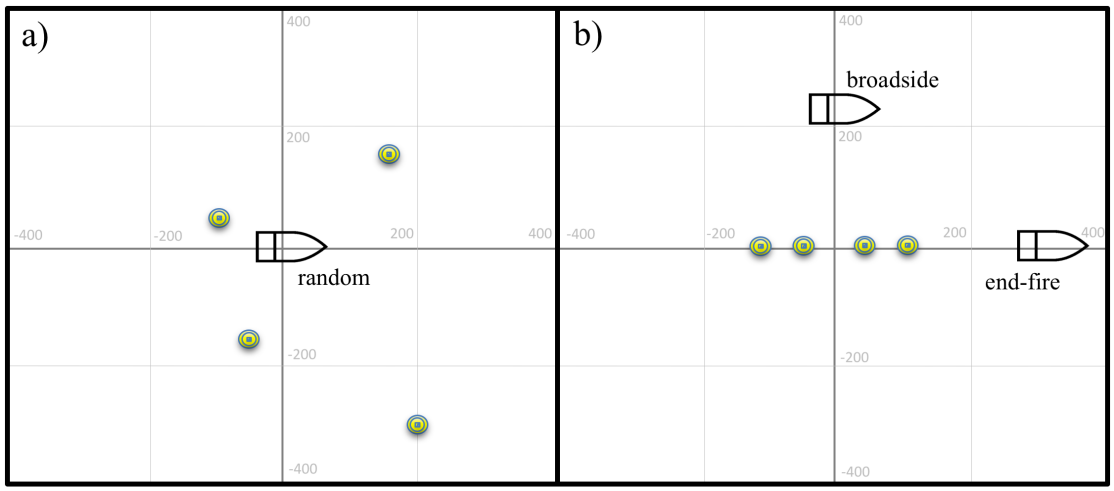

Figure 5.5: Illustrates the changing array configuration used in the model, with buoys offset 100-300 m from the source. a) depicts a randomly-spaced buoy configuration, as modeled in the ambiguity surfaces in Figs. 3, 4, 6a and 6b. b) depicts broadside and end-fire buoy configurations, as modeled in the ambiguity surfaces in Fig. 6c and 6d.

a line of hydrophones, as shown in Fig. 5b, small changes in position lead to large changes in the location of the peak in the cross-correlation function, while for a source located at end-fire to the line of buoys, large changes in position have very little impact on the shape of the cross-correlation function. In other words, sources at end-fire are more sensitive to the physical oceanography than to position mismatch, and should be preferentially chosen or weighted over sources at broadside in an inversion method. Given that ships are tracked using AIS, this is easily accomplished.

In this numerical study, it was determined that receiver position mismatch will always be an issue[64] when performing passive acoustic thermometry. Additionally, the geoacoustic environment (bathymetry and bottom sound speed) must be known to a high degree of fidelity, in order to make meaningful measurements of seawater sound speed, using a full-field inversion technique, such as those based on matched-field processing[65]. This could be achieved by conducting an accurate geoacoustic inversion. Furthermore, it is possible that geoacoustic parameters could be inverted for simultaneously with solving for source position and the physical oceanographic parameters, but this is likely to be an ill-posed problem. If an

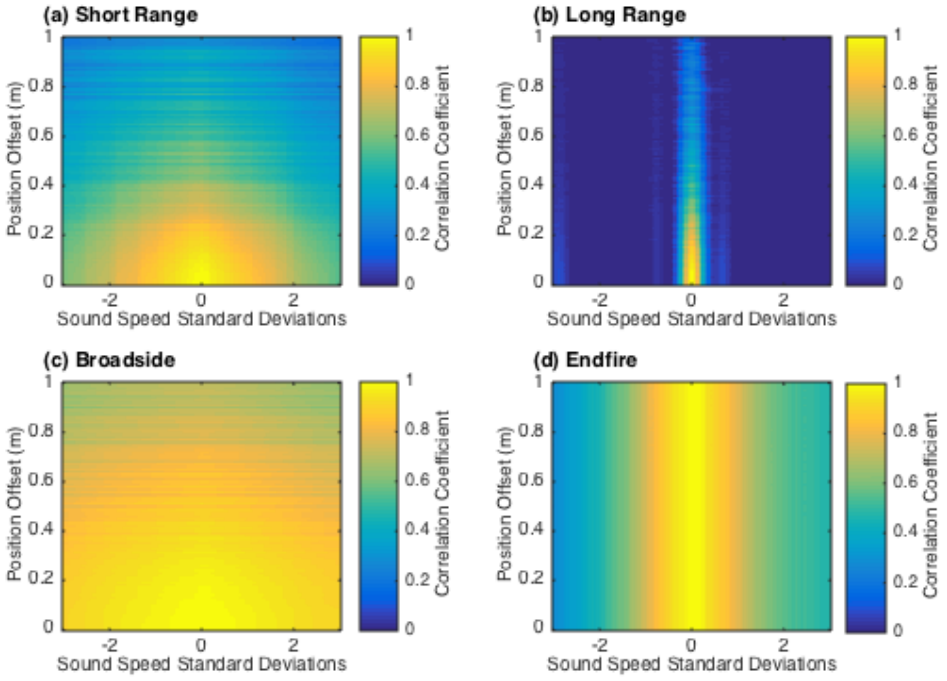

Figure 5.6: Shows the decorrelation ambiguity surfaces for four different array geometries: a) short range buoy spacing (30-60m) random orientation; b) long range buoy spacing (1-3km) random orientation; c) middle range buoy spacing (150-300m) with broadside orientation; and d) middle range buoy spacing (150-300m) with end-fire orientation.

accurate geoacoustic inversion for the environment is not attainable, other methods where only the times of the direct arrivals are considered should be used, in order to mitigate the dependence of the selected arrival-structure on bottom characteristics. Direct arrival-only thermometry is less sensitive to mismatch in the geoacoustic environment, but still approximately equally sensitive to position mismatch as shown in Fig. 7. Fig. 7 is constructed using the Bellhop acoustic ray trace program[60] to estimate arrival times on the same spatially separated hydrophones modeled in Fig. 3. The color of the ambiguity surface in Fig. 7 is the average of the difference in direct arrival lag times that results by changing the position uncertainty on the y-axis and sound speed profile on the x-axis, over 1000 iterations. Similar figures constructed using this approach that vary bottom depth error or bottom sound speed on the y-axis as in Fig. 3c, and 3d would not be meaningful as the direct arrival lag times would not be impacted by changing these parameters. The direct arrivals are not dependent on the bottom, because there is no interaction with the bottom between source and receiver; however, direct arrivals drop off at longer ranges. This is fundamentally at odds with the results shown in Fig. 6, where longer propagation paths are beneficial, because the cross-correlations are more dependent on the sound speed in the water column and less sensitive to position mismatch. This suggests for a given water depth and waveguide characteristics, there is an optimum receiver configuration where receiver spacing is maximized, while maintaining direct arrivals on both hydrophones from the same source; in this case around 750 m. In this instance, the source can be sufficiently close to one of the receivers such that the signal on that receiver could actually characterize the source, making techniques to increase signal to noise ratio as are often employed in active tomography (i.e. time gating or pulse compression) possible.

5.4.2 Inversion Process

There are numerous ways this inversion can be accomplished. In traditional active source time-of-arrival tomography[6], a system of linear equations is constructed where the ocean is separated into layers (in the one-dimensional case), or voxels (in the three-dimensional case). The sound speed in every voxel is an

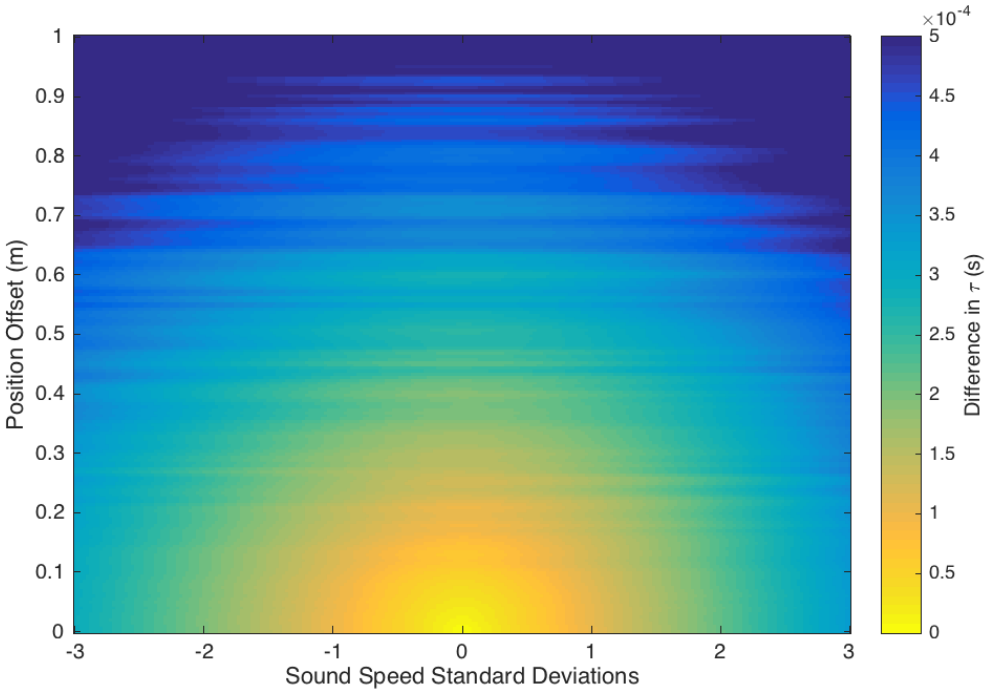

Figure 5.7: An ambiguity surface which depicts the difference in direct arrival lag time (τ) between the sensors in seconds of the simulated cross-correlation function given the unperturbed mean sound speed profile and perfectly known source positions and cross-correlation function generated with the same model but adjusting the input sound speed by adding some number of standard deviations on the x-axis and adding a position error on the y-axis.

unknown, while the arrival time of the source signal on each hydrophone or array of hydrophones, is known. The arrival time along a given ray path is a sum of slowness ($\frac{1}{c}$) in each layer/voxel, multiplied by the distance that ray traveled through that layer/voxel. Since the ray path can be modeled to some degree of accuracy[66], and generally varies fairly little with small changes in the environment, a set of linear equations can be generated to solve for the sound speed in each layer/voxel, provided a sufficient quantity and variety of ray paths are present for the problem to be well determined and the environment to be well-sampled. In the underdetermined case where sufficient rays are not present, a pseudo-inverse or least-squares differencing approach may be used.

Alternative matched-field processing based inversion techniques exist[65], in which the acoustic signal on an array of hydrophones is modeled using a standard propagation model, such as a normal mode or parabolic equation model, and the resulting modeled signal is compared to the received signal for a source in a known position. The environment input into the propagation model is varied, and each resulting replica is compared to the data recorded across the array of hydrophones using a Bartlett-style comparison. The environment that generates the simulated replica with the best match is then selected as the estimate of the true environment. Other methods of conducting environmental inversion include source deconvolution[67], used to obtain the impulse response of the channel. For this demonstration, traditional time-of-arrival tomography using only direct arrivals is used, rather than a full-field or matched-field processing based approach, in order to eliminate the need to obtain a high fidelity model of the local geoacoustics to construct representative replica signals.

In many of these inversion methods, it is necessary to vary the environment and model the resulting signal across a series of hydrophone configurations. It is not feasible to model every possible sound speed in every possible layer/voxel, due to computational limitations, so it becomes necessary to parameterize the environment. Often, empirical orthogonal functions (EOFs), constructed using historical sound speed profiles or a good physical oceanographic model, are used to constrain the vertical variation in sound speed, and a series of cosine functions, constrained

using dominant internal wave modes, are used to parameterize the horizontal variance in the environment[65, 62]. In the simplest one-dimensional case using a singular-value decomposition, the vast majority of the vertical variability of the sound speed in most shallow water environments can be characterized using 5-10 EOFs. The coefficients are varied for each of these 5-10 EOFs, and representative sound speed profiles can be constructed. Alternative methods for parameterizing vertical variation in sound speed include machine-learning based libraries[68], where the variance of the sound speed profile can be accounted for with just one or two library functions, provided sufficient data is available to teach the system. Regardless of which type of function is used to parameterize the environment, it is often still impossible to conduct an exhaustive search through every possible sound speed profile constructed using each of the EOFs or machine-learned functions. In this case, a global optimization tool such as a simulated annealing or genetic algorithm can be used[69] to optimize the search.

There are numerous ways to conduct environmental inversions using active or passive acoustics; however, the inversion itself is not the focus of this investigation. Rather the inversion is included as part of the feasibility study to demonstrate the limitations of conducting environmental inversions in shallow water with ship noise across an array of drifting hydrophones using experimental and/or simulated data. Thus, the method of inversion for the subsequent analysis, may be considered arbitrary.

In this study the inversion was conducted using two of the four drifting buoys from the aforementioned experiment, spaced 100-1000 m apart, with hydrophones suspended 20-30 m below, tracked using Wide Area Augmentation System (WAAS)-enabled GPS, with a standard error of 1.6 meters. Ships, tracked using AIS data obtained from the United States Coast Guard Navigation Center (USCG NAVCEN) Nationwide AIS database (NAIS), were used as the acoustic sources of opportunity. The inversion shown here is a one-dimensional inversion for an assumed range-independent environment. Horizontal variability from internal waves and other phenomena is neglected, given the small area over which the study was conducted. The environment was parameterized using EOF's constructed us-

ing a combination of historical CTD casts taken from previous experiments, and CTD casts collected during the experiment as shown in Fig. 1a. Over 99% of the variance was accounted for in the first five EOFs, with 89% in just the first two. Data was collected as a vessel transited past the drifting array. The data across each of the drifting hydrophones was cross-correlated. The peaks associated with the direct arrival lag times were selected in these cross-correlation function waveforms, with the assistance of ray tracing, to select that peak a-priori. The direct arrival lag times for each cross-correlation function were recorded for every position along the vessel's track. The acoustic signal on each of the hydrophones was then modeled, using a representative environment constructed using EOFs, for a source in the position of the vessel, and those simulated signals were cross-correlated. The modeled 'replica' set of direct arrival lag times across the hydrophones were then compared to the 'data' arrival times using a Bartlett-style comparison,

$$K = d \cdot d^{\dagger}$$

$$B = w^{\dagger} \cdot K \cdot w$$

where K is the outer product of the values for the measured 'data' lag times as in traditional beam-forming applications, d is composed of the direct arrival lag times from the data, w is the set of replica direct arrival lag times from the model, and B is the output of the Bartlett comparison. The environment was varied by changing the coefficients associated with each of the EOF's, and the environment that yielded the closest match, as determined by the highest value for B in the Bartlett comparison, for the direct arrival lag times across each pair of hydrophones, over the entire track of the vessel, was then selected as the estimate of the true (and stationary assumed) environment. To optimize the search through possible replica environments, a simulated annealing algorithm was used with the coefficients of the EOFs as parameters. Position mismatch derived from GPS uncertainty, or potential horizontal displacement of the submerged hydrophone beneath the GPS antennae of the floating buoy, was accounted for by adding horizontal displacement of the source in x and y directions as parameters in the

simulated annealing algorithm. It has been debated whether position mismatch can best be accounted for in a two-step inversion process, where position is found prior to the environmental inversion being conducted, or by including it as a parameter in the inversion, and solving for the position and environment in a single step[64]. Again, exploring the finer points of the inversion method itself is not the purpose of this study, and the position mismatch was accounted for by localizing the acoustic source in a single step, while varying the environment for this case.

In order to test the machinery of the inversion process, the method was simulated using a standard normal mode propagation model for a geoacoustic environment similar to the one used in the previous section of this article, which is representative of the August, 2015 field experiment. For the modeled inversion process, a total of five EOFs were used, along with four acoustic buoys, allowing for six possible combinations of cross-correlation functions between buoy pairs. A ship track was simulated such that the ship passed between the buoys spaced approximately 300 m apart; eleven snapshots in time, each with six combinations of cross-correlation functions, were used along that path. The simulated acoustic signals on each of the four buoys were cross-correlated and the direct arrival lag time was recorded from each of these cross-correlation functions. As described above, the environment was varied and replica cross-correlation functions were generated, with the direct arrival lag times from each of the replica cross-correlation functions extracted. The environment that resulted in the most similar set of direct arrival lag times was selected as the estimate of the true environment. The first five EOFs accounted for over 99% of the vertical variance of the sound speed. A simulated annealing algorithm was used to optimize the search through the coefficients for each of those EOFs. For the purposes of the simulation, the locations of the source and each receiver were taken to be known without mismatch. Fig. 8 shows the sound speed profile that resulted from the modeled inversion. The sound speed profile was further parameterized using EOFs of temperature and salinity, constructed using libraries of historical profiles, and the resulting temperature and salinity profiles are plotted in Fig. 8b and Fig. 8c. Temperature and salinity covary due to similar physical oceanographic phenomena, so the method of parameterizing the

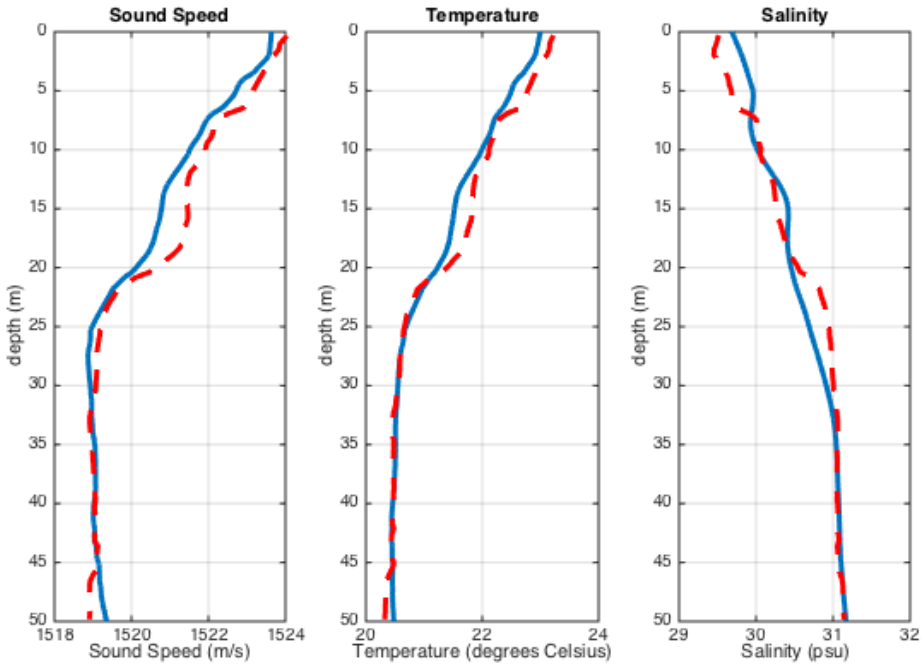

Figure 5.8: a) shows the sound speed profile resulting from the modeled inversion method. A five EOF parametrization was used in combination with a simulated annealing algorithm, with the environment that yielded the closest set of modeled direct arrival lag times to those generated using the true environment (dashed line) selected as the estimate (solid line). b) and c) show the resulting temperature and salinity profiles.

variability of sound speed using EOFs constructed from temperature and salinity was effective in this case, but there are a variety of other methods that could have been used to determine temperature once sound speed has been estimated. It is important to note that the dependence of sound speed on salinity is not strong, thus the method does not resolve salinity very well, and the structure of the salinity profile that results is largely a function of the covariance of temperature and salinity.

5.5 Experimental Results

A field experiment was conducted in Long Island Sound in the vicinity of New London, CT in August of 2015, as described in Section 2. Four buoys were

deployed; each buoy was tracked using a WAAS-enabled GPS, with absolute accuracy of 1.6 m (the relative accuracy being significantly better), with hydrophones suspended below at depths varying between 20-30 m. The GPS tracked position of the buoys was not sufficiently precise to use in the inversion, thus the instruments needed to be localized, within the 1.6 meter area, as part of the joint inversion process. Data was recorded at a sampling rate of 40 kHz, and filtered to 20-1000 Hz, to focus on the portion of the spectrum dominated by shipping noise. A research vessel was piloted in the vicinity of the sensors, as shown in Fig. 2a. During the experiment, numerous CTD casts were taken, to measure the acoustic environment to understand the natural spatial and temporal variability of sound speed in the area, in order to constrain the inversion problem.

When conducting the inversion using experimental data, only direct arrival lag times were used, as in the modeled results. In contrast with the modeled inversion where source and receiver positions were assumed to be perfectly known, source and receiver position mismatch had to be accounted for. To accomplish this, two parameters were added to the simulated annealing algorithm, to account for x and y source offset. Receiver position was not allowed to vary as part of the inversion. In other words, the relative spacing of the buoy constellation was assumed to be perfectly known, due to the high fidelity of the relative positioning from the WAAS-enabled GPS; and only the absolute uncertainty was accounted for by moving the source position within the 1.6 m radius circle, constrained by the GPS fix. A single pair of buoys was selected, rather than using all six buoy-pair combinations, in order to simplify the method for this first demonstration. Fifty-five separate half-second snapshots in time were used. These fifty-five snapshots are the last twenty-three seconds of the time-varying cross-correlation functions plotted in Fig. 2d; and were computed using the signals with the respective spectrograms plotted in the last twenty-three seconds of Fig. 2b and 2c. The portion of the ship track used for the inversion is plotted in red in Fig. 2a. This portion of the track was selected because of the near-end-fire orientation to the drifting buoys. This maximized the dependence of the cross-correlation functions on the sound speed in the water column, as demonstrated in Fig. 6. Inversions using broadside

orientation were less successful.

Sound speed was parameterized in terms of EOFs. Because resolving fine detail in the sound speed profiles was not the objective for this inversion, only two EOFs were used rather than the five EOFs that were used in the modeled demonstration. The first two EOFs accounted for approximately 89% of the variance of the system. The position of the source and the sound speed profile were determined in a single combined inversion. This involved a four-parameter search, optimized using a simulated annealing algorithm, with two position parameters, and two sound speed parameters. The environment that resulted in the direct arrival cross-correlation lag times that most closely resembled those recorded across the hydrophones was selected as the estimate of the true environment. As shown in Fig. 9, the inverted sound speed profile using acoustic data was consistent with the measured sound speed profile. The standard error of the sound speed profile when compared to the true profile is less than 1 m/s, translating to approximately 1 degree C precision for temperature. Fig. 9b and 9c show profiles for both temperature and salinity, generated using the method described in the previous section. The inversion appears to underestimate the sound speed at all depths, which suggests either the need for a constant offset parameter in the inversion in addition to the EOFs or the presence of a relative position error causing the distance between hydrophones to be incorrect. Adding a constant offset parameter was explored and the results were not improved; therefore, a relative hydrophone spacing error is most likely responsible. This could be improved by adding additional position parameters into the inversion for every hydrophone in addition to the position terms which currently exist for the x and y source position error. Additionally, a tracking algorithm can be employed to improve localization results.

5.6 Conclusion

Under the right circumstances, passive ocean acoustic thermometry using ships as sources of opportunity on an a drifting volumetric array could be possible. An accurate geoacoustic inversion is necessary in order to conduct full-field or

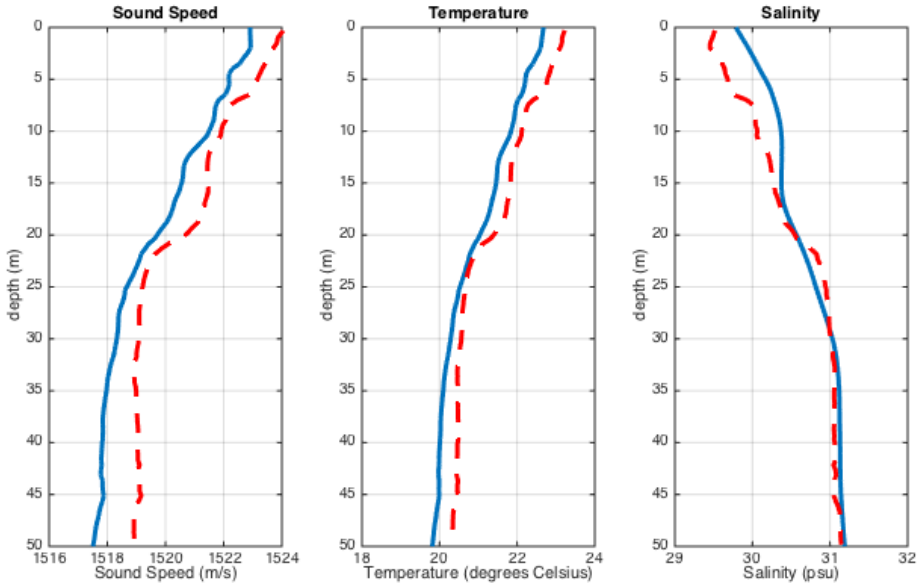

Figure 5.9: a) shows the true environment measured using a CTD (dashed line), and the sound speed profile estimated using the acoustic data (solid line). A similar inversion is used to show temperature (b) and salinity (c).

matched-field processing based inversion techniques. If utilizing traditional time-of-arrival tomography for this type of analysis, only the direct arrivals should be considered. Fixing the sensor positions to a high degree of accuracy is necessary, as demonstrated in Fig. 3. Implementing a tracking algorithm by using more snapshots in time to correct suspected position mismatch, in addition to fixing the positions of each buoy to a greater degree of accuracy, will likely improve the results of this method. Acquiring additional sound speed profiles for the experimental area would better constrain the variability of the physical oceanographic environment. A deep-water experiment with buoys at varying ranges may yield better inversion results, because it would increase the range over which direct arrivals are present. While no pre-processing on the acoustic signals was done for this analysis, pre-whitening of the data is likely to help this method to mitigate the influence of any eventual spectral lines (or tones) in the recorded shipping noise, which could affect the temporal resolution of the measured time-lags from the correlation waveform. Vector sensors may also be utilized in the future to determine signal directional-

ity. For this experiment, range-independence was assumed, and a one-dimensional sound speed profile was measured. Future analysis will include a more traditional three-dimensional inversion, using a time-of-arrival based tomographic approach. This will involve parameterizing the vertical variability in sound speed using EOFs, as in this demonstration, and parameterizing the horizontal variability using internal wave modes or cosine functions[62]. Three additional field experiments have been conducted in different environments using a variety of array configurations. Analysis of these field experiments will include utilizing longer time series, more sensors, and conducting a three-dimensional time-dependent environmental inversion for ocean temperature.

While this method is far from fully developed, this initial feasibility study demonstrates the potential for conducting high-fidelity ocean acoustic thermometry, using ships as sources of opportunity, across a drifting volumetric array, such as hydrophones suspended beneath drifting buoys, or fixed to profiling floats in shallow-water marine environments. Ultimately, this method is aimed at the implementation of a large-scale coastal, Arctic, and open ocean passive acoustic temperature monitoring system, for the purposes of resolving critical temperature measurements to populate climatological models, contributing to the understanding of the ocean heat budget. This work may also be applied towards monitoring the temperature, and by extension transport, of major ocean currents such as the Gulf Stream and Antarctic Circumpolar Current, in addition to monitoring mesoscale features within the open ocean.

5.7 Acknowledgements

This work is supported by the Office of Naval Research.

Chapter 5, in part is currently being prepared for submission for publication of the material. Kubicko J., Verlinden C., Sarkar J., Fagan, A., Nichols B., Martin J., Sabra K.. A feasibility study for passive acoustic estimation of vertical sound speed structure using sources of opportunity on a drifting volumetric array. The Journal of the Acoustical Society of America. Submitted 06 March, 2017. The

dissertation author was a primary investigator and author of this material.

Chapter 6

Toward ocean attenuation tomography: Determining acoustic volume attenuation coefficients in seawater using eigenray amplitudes

Authors:
J.D. Tippmann
J. Sarkar
C. M. A. Verlinden
W.S. Hodgkiss
W.A. Kuperman

6.1 Abstract

A deep-water experiment in the Pacific made *in situ* measurements of the volume attenuation coefficients of sea water in the mid-frequency range. The frequency, temperature, salinity, pH, and pressure dependent seawater attenuation coefficients were determined using a vertical line array that received and identified over 2000 unique paths from 1200 mid-frequency 3-9 kHz LFM source transmissions at a convergence zone range and depth up to 400m. The results show no change in attenuation coefficients in this band compared to estimates from 30-year-old models previously determined from a combination of long-range ocean acoustic and laboratory experiments. The inversion also explores the feasibility of ocean acoustic attenuation tomography to further separate the depth-dependent chemical components responsible for the total attenuation loss through by isolating a group of deep-water refracting acoustic paths.

6.2 Introduction

Jin and Worcester (1989)[70] and, more recently, Duda (2009)[71] suggest that it is possible to determine a depth-dependent ocean property such as ocean acidity through the link with the seawater attenuation coefficient. Ocean properties such as temperature, salinity, pH, and pressure are known to impact attenuation differently in certain frequency bands [72], a result of chemical relaxation effects

[73]. Within the last decade there has been a significant interest in measuring ocean pH due to anthropogenic emissions causing ocean acidification and whether it will increase the ocean noise levels significantly [74, 75, 76]. Regardless of ocean acidification's affect on ocean noise, measuring ocean acidity is important for understanding the global carbon cycle [77]. Additionally, measuring attenuation over long-range transmissions can provide more insight into large-scale ocean acidity levels than from point measurements. Attenuation-based tomography brings the capability to measure depth-dependent ocean acidity not available through time of flight tomography, in addition to the other depth-dependent ocean variables, salinity and temperature, thereby enhancing the accuracy of propagation modeling.

Here, an experiment was conducted in the Northeast Pacific to measure the attenuation coefficients of sound in seawater *in situ* and to further explore the potential for attenuation tomography by identifying individual eigenray transmissions. The experiment involved acquiring underwater acoustic data with a known active source in the mid-frequency band (3 to 9 kHz) and then comparing the results to attenuation coefficients produced from equations established by Francois and Garrison [73], and simplified by Ainslie and McColm[78]. Received acoustic levels from multiple acoustic ray paths for a given source transmission were measured at a range of one convergence zone (approximately 50 km) with a high resolution, 127-element vertical line array (VLA). At this range for sources between 3 and 9 kHz, the predicted total attenuation loss is approximately 7 - 38 dB, respectively. An ocean average attenuation at one convergence zone was estimated for each frequency in this band by using a least-squares solution to a system of linear equations. Attenuation coefficients for a group of very similar ray paths were also estimated.

6.3 Experimental Setup

The experiment was conducted in deep water located off the coast of Oregon, USA, where the depth was approximately 2820 m. A representative sound-speed profile (Fig. 6.1a) has an upper sound channel near the surface in addition

to the standard deep water sound-speed profile [24]. The Scripps Institution of Oceanography's *R/V Melville* deployed a drifting VLA neutrally buoyant at approximately 300 meter depth and then deployed a source approximately 50 km away from the VLA and within the first convergence zone. The source and receiver locations are shown in Fig. 6.1b. For the data analyzed in this paper, the source emitted 2 s, 3 - 9 kHz linear frequency modulated (LFM) chirps continuously as it was lowered from the surface to a depth of 400 meters at a rate of 11 meters per minute over a duration of 37 minutes. The source was then maintained at a constant depth of 400 m for over 10 minutes.

The acoustic data was recorded at a sampling rate of 25 kHz on a 127-element VLA with 10cm element spacing ($\lambda/2$ at 7.5 kHz). The dense sampling of the array and pulse compression of the received signals allowed for high resolution eigenray detection of multiple rays per source event. The array provided a beam width of approximately one degree.

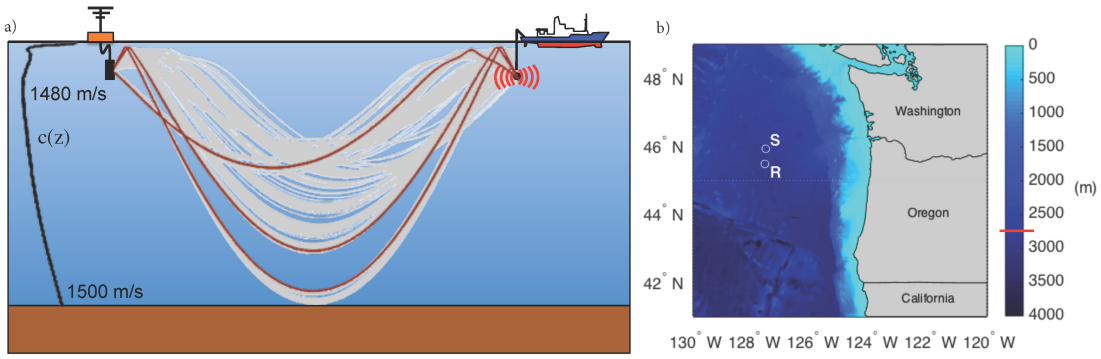

Figure 6.1: (Color Online) (a) The illustration shows the experimental setup with the source and receiver located in deep water. A representative sound-speed profile is plotted for reference. The light shaded eigenrays represent the regions sampled during the source deployment. The dark set of three eigenrays represent paths unique to one source position at 400 m depth. (b) Locations of the source (S) and receiver (R) in deep water (2820 m marked in red on the color bar) located off the coast of Oregon, USA.

6.4 Ray Identification and Transmission Loss

A set of approximate eigenrays between the source and receiver were produced by matching a BELLHOP[60] propagation simulation ray to the experimental received angle of arrival and time of arrival for each individual ray by adjusting the range. An example set of eigenrays for one source event are shown as three highlighted eigenrays in Fig. 6.1a. The eigenrays matched between simulation and experiment are shown in the background in Fig. 6.1a and represent the sampled region of the ocean waveguide during the entire source deployment.

The accumulation of all the best fits between the simulation and data are shown in Fig. 6.2 where simulation and experimentally observed rays are plotted as points in received angle versus time of arrival.

The experimental transmission loss (TL) of each ray was then determined from the subtraction of the power-spectral density (PSD) of the pulse-compressed signal received level (RL) from the calibrated source level (SL) at each frequency, as simply expressed in Eq 6.1:

$$TL = SL - RL. \tag{6.1}$$

The source levels were determined through short-range source-array calibration transmissions. Because a roll off near 3 and 9 kHz in the source level resulted in larger errors towards the boundary of the LFM bandwidth, only spectral levels between 3.5 and 8.5 kHz were used.

The transmission loss at each frequency of each identified ray is a combination of geometric spreading loss (GL(b) where b is for each ray) and the frequency-dependent attenuation loss (AL(b,f)) as expressed in equation 6.2:

$$TL(b, f) = GL(b) + AL(b, f). \tag{6.2}$$

The geometric spreading loss for the observed rays sampled was estimated from a parabolic equation propagation simulation. Perturbations in the sound speed profile, however, cause scintillation that vary the observed levels around the mean geometric spreading loss, as discussed by Jin and Worcester [70] and Duda

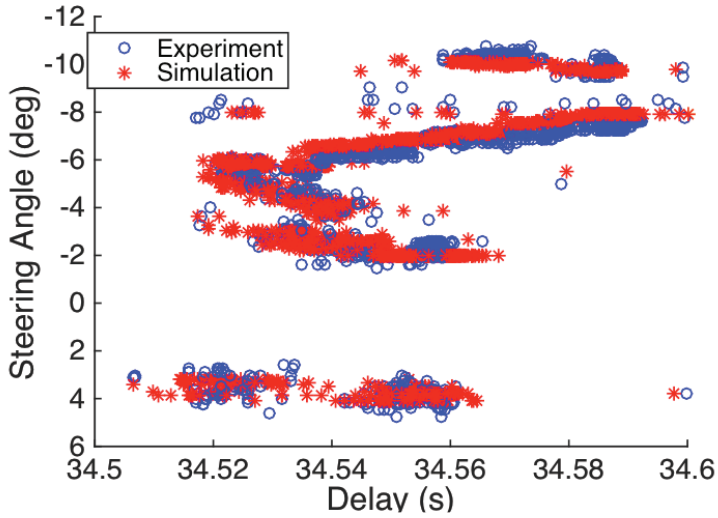

Figure 6.2: (Color Online) The arrival time of each ray is plotted against its beam steering angle (negative angle are upward looking beams) for both the experiment and the simulation. The experimentally observed rays include only those that were within 0.5° in angle and 0.01 s in time of a simulation ray for a given depth and range. Over 1800 rays were matched.

[71]. This was clearly evident in the TL data, demonstrating the requirement for treating the observed levels as a statistical distribution from multiple measurements rather than a single measurement.

6.5 Inverting for attenuation coefficients

We used the experimental TL observations matched to the simulations to solve for the attenuation through a least-squares solution to a system of linear equations. The attenuation loss component in Eq. 6.2 can be expanded as the product of a frequency-dependent sound absorption coefficient $\alpha(f)$ and ray path length $s(b)$, resulting in a TL expression in Eq. 6.3 that can be solved for $\alpha(f)$ and geometric loss $GL(b)$:

$$TL(b, f) = GL(b) + s(b) \cdot \alpha(f). \tag{6.3}$$

The unknowns can be further expanded as perturbations about mean values

(Eq. 6.4). Expected values of the GL and AL are taken from the simulation TL estimates and the attenuation equation estimates, respectively.

$$TL(b,f) = \left(E\left[\bar{GL}\right] + \Delta GL(b)\right) + s(b)\cdot\left(E\left[\bar{\alpha}(f)\right] + \Delta\alpha(f)\right), \qquad (6.4)$$

The resulting least-squares estimates of the frequency-dependent attenuation coefficient, shown in Figure 6.3 as the thick solid lines with error bars for of an average of all ray groups and of a group of very similar ray paths, are compared to both the Thorp [79] equations (dashed) and the ray-integrated average using the Ainslie and McColm simplified version of the Francois and Garrison equation[73, 78] (thin solid line). The error bars represent the combination of two errors: 1) the error of the least squares fit and 2) the error in the source level from the source-array calibration transmissions.

The group of very similar paths occurred when the source was stationary at a constant depth for 10 minutes. The two results are different in that one shows an average frequency dependent ocean attenuation estimate for the ocean highlighted by all gray ray paths in Fig. 6.1a and the other shows the attenuation estimate along of the ray paths shown in red in Fig. 6.1a.

From the 1934 TL observations, only 327 independent observations exist assuming a correlation time of 30 seconds. The correlation time of 30 seconds was a worst case estimate calculated from the temporal auto-correlation of the TL for a group of very similar rays. When considering 410 transmission loss observations from a group of very similar rays, only 37 independent measurements exist using the same correlation time of 30 seconds.

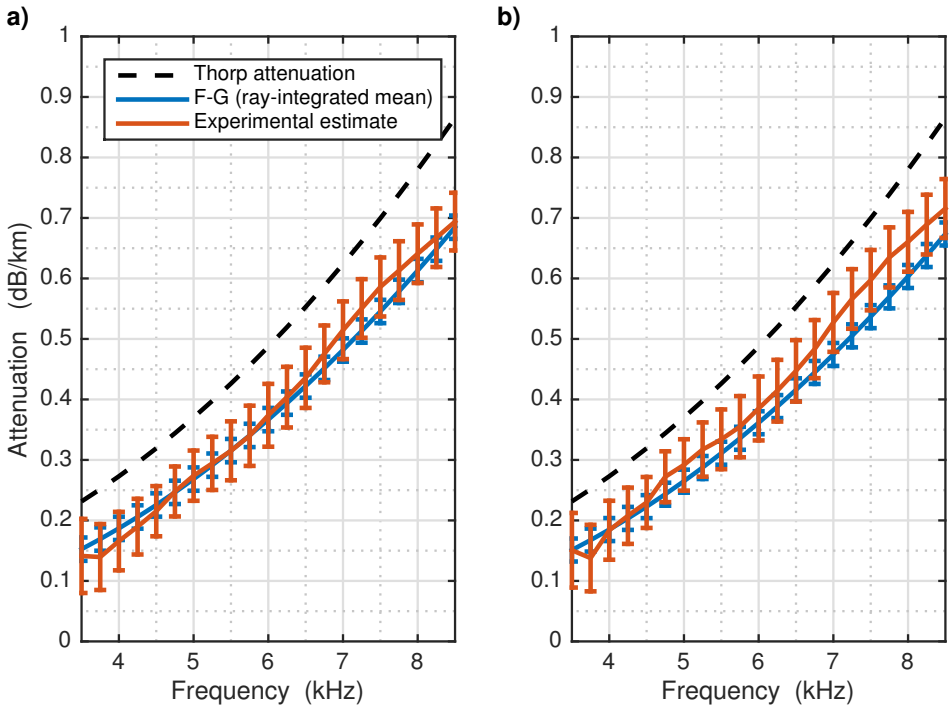

Figure 6.3: (Color Online) Experimental estimates with error bars of the frequency-dependent attenuation constant $\alpha(f)$ for 28 frequencies between 3.5 and 8.5 kHz are plotted against the empirical equation estimates developed by Thorp [79] and Francois and Garrison [73] for the two cases: a) when all rays are included and b) when only a group of very similar rays is included. The FG estimate for all rays is an average of all rays integrated through the experimental environmental profiles, where the FG estimate a for group of very similar rays is integration of only those rays.

6.6 Discussion and Conclusion

The frequency-dependent attenuation coefficients found here from experimental data agree well with those calculated using Francois and Garrison [80], showing the attenuation coefficients in the 3.5-8.5 kHz band have not changed over the past 30 years. More important than agreeing with a model based on data more than 40 years old is the result that climate related ocean change in the same time did not result in a significant change of the equations in this frequency range. It is important to note that this agreement is only in the region of the Northeast Pacific. Future experiments will focus on additional sites in the Pacific

and Atlantic, where attenuation is often assumed to be higher than the Pacific.

Furthermore, these results show that *in situ* broadband measurements of attenuation in the mid-frequency range are possible with this experimental arrangement. The results demonstrate the challenge in having enough independent observations to reduce the error on the estimate of the attenuation as discussed by Duda (2009) [71]. Understanding the fluctuations further for reducing the error on the attenuation coefficients is critical for future work to estimate ocean properties such as pH.

6.7 Acknowledgements

The authors would like to acknowledge Bruce Cornuelle, Andrew Dickson, and Dave Ensberg at the Scripps Institution of Oceanography (SIO) for their guidance and time for very useful discussions on this work.

This research was supported by the Office of Naval Research.

Chapter 6, has been published in the Journal of the Acoustic Society. Tippmann, J., Sarkar, J., Verlinden, C., Hodgkiss, W., Kuperman, W.A.. Toward ocean attenuation tomography: Determining acoustic volume attenuation coefficients in seawater using eigenray amplitudes. The Journal of the Acoustical Society of America, 2016. The dissertation author was a primary investigator and author of this material. Dr. William Kuperman, the chair of the committee, is a co-author.

Chapter 7

Conclusion

7.1 Summary

Ships can be used as acoustic sources of opportunity to localize targets and extract information about the environment. Continuous tracking of acoustic radiators with a MFP-like approach, using ships as sources of opportunity to populate libraries of measured replicas, has been demonstrated. The feasibility of measuring ocean temperature using ship noise detected on a drifting array of sensors has been explored, and initial results are promising enough to warrant additional research. The concept of attenuation based ocean acoustic tomography has been examined, and it may be possible to use the attenuation of sound in seawater to estimate ocean properties such as temperature, salinity, and pH.

7.1.1 Source Localization

Passive acoustic source localization techniques such as MFP break down because of the difficulty associated with modeling acoustic arrivals on arrays of hydrophones with sufficient accuracy to successfully localize acoustic sources, due to the complex and non-stationary nature of the marine environment. The method presented in Chapters 2, 3, and 4 of this dissertation, addresses this issue by eliminating the need to model the arrivals by replacing the library of modeled replicas with measured replicas populated using ships, as acoustic sources of op-

portunity. The difference in spectral content of the signals generated by the library and target vessel, which would normally be a problem in MFP, is addressed by comparing cross-correlation functions of acoustic signals on horizontally separated hydrophones. In order to fill in gaps between where measured replicas exist (i.e. areas not previously transited by ships), an extrapolation method was developed to estimate replica cross-correlation functions in the entire search area, allowing for continuous tracking. In order for the extrapolation method to work, ships of opportunity were used to study the propagation physics of the waveguide parameterized using the WGI. This information was used to estimate correlation functions at different ranges and angles. The theory was developed, validity tested using numerical simulations, and the practicality and operational feasibility was explored using data gathered during an acoustic field experiment. The method has been successfully demonstrated under environmental conditions of the field experiment, but requires additional experimental verification. The performance of the method with regards to precision, SNR, and environmental robustness has been evaluated and found to be acceptable. The method has not yet been demonstrated experimentally for localizing sub-surface sources, which is of interest to the Navy.

The source localization method demonstrated in chapters 2-4 is functional; however, additional experimentation is required in different acoustic environments. The Santa Barbara Channel experiment conducted using the R/V Sally Ride for the Information Content of Ocean Noise Multi-disciplinary University Research Initiative (MURI) is an excellent data set for this application. The water is deeper, approximately 600 m, and the environment is well characterized. There are four large vertical arrays spaced approximately 1 km apart, and ships pass through the experiment site every few hours. The R/V Sally Ride navigated a grid pattern through the experiment site several times during the experiment. Initial examination of the data shows coherent, well-correlated arrivals across the VLAs. The well characterized environment, combined with the use of towed and vertically lowered active acoustic sources at depth, will make it possible to test the concept of modifying cross-correlation function replicas for changing environments, and for localizing sub-surface sources using libraries derived from surface sources. This

could be done by changing the β, $\bar{k}$, and $\bar{s}$ used to extrapolate the libraries. For localizing sub-surface sources using surface derived libraries it may also be possible to sum the entire vertical array, or subarrays, to form a broadside beam to focus on the mode one arrivals, in order to minimize the difference in the arrival structure between surface and subsurface sources.

In addition to expanding the method to potentially locate subsurface sources, the Santa Barbara Channel experiment will also make it possible to explore different ways to combine multiple libraries to create one localization. Currently, each measured library cross-correlation function is extrapolated to populate the entire search grid, and each of these populated search grids is used to localize the source. The resulting ambiguity surfaces are averaged using an inverse distance weighted average. Developing a way to combine the cross-correlation functions themselves may enhance the robustness of this method. In the Noise 09 experiment, there were not enough measured replica functions to accomplish this. In Santa Barbara there are hundreds. It could be possible to average or sum the extrapolated library cross-correlation functions using a method similar to the estimator correlator [81] or by cross-correlating the estimated cross-correlation functions and summing them with a small optimized offset to allow for timing mismatch between the estimated replicas[23]. These are methods used in the active and passive acoustic tomography communities for increasing integration time; essentially sacrificing some level of precision for SNR. This would greatly enhance the method. Additional areas for improvement include various methods of source deconvolution, source separation, pre-whitening of the source signals, combining multiple combinations of hydrophones, cross-correlating beams from VLAs to enhance the spatial uniqueness of the libraries, improved tracking algorithms, and potentially using the SCOT transform in place of the Hilbert transform for making comparisons between replica and event cross-correlation function waveforms[54].

As part of the source localization method, maps of β have been created for two hydrophones in the Noise 09 experiment using ships as sources of opportunity. These same maps should be created for the hydrophones in the Santa Barbara Channel experiment in order for the localization method to be applied there. This

experiment will also allow for a robust examination of the stability of these β maps to changes in the waveguide from the passage of ocean fronts and internal waves as well as to different sources with different spectral content. With the abundance of ships present in this dataset, the stability of β can be examined in a statistically significant way. Additionally, maps of average modal horizontal wavenumber $\bar{k}$, and average modal group slowness $\bar{s}$ can be generated. If the dependence on changes in physical oceanography of these properties is well understood, it may be possible to use the variability of these parameters to conduct environmental inversions. Finally, if these maps are sufficiently stable, it may be possible to develop a localization scheme based on maps of β, $\bar{k}$, and $\bar{s}$. As a vessel moves through a region where β is well known, the changing slopes in the striations of the spectrogram should represent a unique track through space. By optimizing a search through all possible tracks through the area using a genetic or simulated annealing algorithm, or a dictionary or machine learned library of possible changing striation slopes it should be possible to estimate the track of a vessel.

7.1.2 Environmental Characterization

In the study of climate science and physical oceanography, there is need for higher resolution, and denser sampling of the ocean for the purposes of understanding the coupled ocean-atmosphere system. Acoustic tomography represents a way to fill the gaps in data, particularly in regions where other sampling methods such as profiling floats are less effective, such as in polar regions where sea ice limits access, along with in coastal regions. Active tomography using fixed sources has been been accomplished, but concerns surrounding the use of an active acoustic source can limit the method's potential. Experiments have been conducted using moving source active tomography; however, successful demonstrations are difficult to find in the literature. Tomography using moving sources and receivers, such as hydrophones fixed to profiling floats or suspended beneath buoys has been proposed many times, but again, successful demonstrations are not readily found in literature. Shallow water tomography is generally considered difficult, owing to the dependence of the arrival structure on the bottom composition, which may

not be well characterized. Additionally, the necessarily short propagation distances require fixing sensor positions to a very high degree of precision. Using ships, as acoustic sources of opportunity, to conduct ocean sensing is a new and promising area of study. Chapter 5 of this dissertation is designed to contribute to this up and coming field, supplementing the research being done in this area.

In Chapter 5, the feasibility of estimating one dimensional sound speed structure, using ships as acoustic sources of opportunity in shallow water, on an adaptive volumetric array of hydrophones suspended beneath moving buoys, was explored. The sensitivity of the arrival structure on the drifting array to parameters including source-receiver position mismatch, depth uncertainty, and bottom sound speed uncertainty was examined. A simple inversion was conducted using traditional time-of-arrival differencing, using the noise generated by a passing ship. The initial results are promising, suggesting that source of opportunity tomography warrants further study, and the use of cost-effective drifting sensors should not be ruled out. It may be possible to establish a large scale ocean monitoring system by fixing hydrophones to drifting buoys and profiling floats and using noise from passing ships as acoustic sources for long term monitoring of ocean structure, for the purpose of adding valuable datasets to the study of the climate system. The goal of Chapter 5 is not to present source of opportunity environmental inversion as a fully developed method, but rather explore the information content of the cross-correlation function waveform of the acoustic energy from ships, tracked using AIS, on a random drifting array of hydrophones; and to examine what, if anything, may be learned from those cross-correlation functions. The findings of this study demonstrate that the cross-correlation waveform contains useful information about the environment.

A preliminary 1-dimensional inversion for vertical sound speed structure using ship noise across an adaptive volumetric array of hydrophones suspended beneath drifting buoys was demonstrated in Chapter 5. The purpose of the study was to explore the feasibility of using ships as sources of opportunity to measure ocean temperature using an array of free floating hydrophones, and the preliminary results indicate that the method warrants further study to determine if it is pos-

sible to perform such environmental characterization in a robust, reliable manner. As part of this study, four field experiments were conducted, off the coast of Connecticut and New York, in the vicinity of Long Island Sound. Each of these four experiments involved deploying four buoys, each with vector sensing hydrophones suspended 20-30 m beneath them, allowing them to drift for several hours, while a R/V drove patterns around the buoys designed to thoroughly sample the ocean. The oceanography was monitored by conducting continuous CTD casts. Between these four experiments there is the potential for doing a variety of geoacoustic inversions, and as well as a full 3D tomography experiment using ship noise, with robust error analysis. Making use of the vector sensors used in the experiment, instead of just the hydrophones, to determine the directionality of the signals on each hydrophone could enhance the method.

There is an ongoing Multidisciplinary University Research Initiative (MURI) entitled "The information content of ocean noise" with the goal to use acoustic sources of opportunity to characterize the environment. One of the objectives of this MURI is to conduct full 3-dimensional robust source of opportunity tomography, with thoroughly examined precision, accuracy and limitations. Most of the work contained in this dissertation is supported fully by this research initiative. This research initiative, involving over 30 researchers from 7 different institutions, has already generated a wide variety of promising results. In an effort to measure ocean temperature to a high degree of fidelity, in 3-dimensions, high resolution, and well understood confidence intervals, an experiment was conducted using the R/V Sally Ride in September of 2016 in the Santa Barbara Channel. Four 32-element vertical line arrays (VLAs), with variable spacing, were deployed in a line approximately 1000 m apart, in approximately 600 m of water, in the center of the Santa Barbara Channel, directly between two shipping lanes. Thermistor strings, spanning the entire water column, were deployed to the north and south of the VLAs to measure the true ocean temperature throughout the experiment. Additionally, CTDs were conducted throughout the experiment for additional sampling of the physical oceanography of the region. Ships moved past the arrays every few hours for the duration of the ten day experiment, and the tracks were recorded

using AIS. Coherent arrivals were detected from these ships on each of the arrays. The experiment has the potential to be one of the first demonstrations of moving source tomography, and the very first true demonstration of source of opportunity tomography.

The work completed in the Santa Barbara channel could benefit from independent experiments which attempt to repeat the findings on different arrays in different marine environments. An exciting possibility for a dataset which could supplement the Santa Barbara Experiment is the AMADEUS acoustic monitoring system on the ANTARES neutrino detection array. The ANTARES array functions as the largest neutrino telescope in the northern hemisphere. It is located off the coast of Toulon, France and installed at a depth of 2500 m in the Mediterranean Sea. In addition to mapping neutrino flux from cosmic origins, ANTARES is also looking to address fundamental particle physics problems, including the search for dark matter. The ANTARES array is home to the acoustic detection system known as AMADEUS. AMADEUS can be used to survey the properties of seawater, including instrumentation for examining salinity and oxygen content, current velocity, light transmission and sound speed. As part of the project there are six acoustic 'storeys', or clusters of 6 hydrophones each, mounted on two vertical arrays with variable spacing between storeys of 15-100 m. The array has been continuously recording since 2013; and the ocean in the area is well characterized through periodic monitoring by research vessels, and an array of sensors including thermistors and ADCPs mounted on one of the instrument lines. Ships have been tracked in the area using AIS since about 2009, so the ship tracking data is available. The experiment has a very different geometry and physical oceanographic environment than the Santa Barbara Experiment and as a result represents a good opportunity for independent verification of the results obtained in Santa Barbara. The dataset can also be used for demonstrating the source localization method described in Chapters 2-4, as well as some of the geoacoustic inversion methods described in the introduction (i.e. bottom-loss estimation).

The ocean sensing discussed in Chapter 5 is accomplished through time-of-arrival tomography, which differences arrival times on a series of hydrophones

in order to gain information about the speed of sound in seawater, and by extension parameters such as temperature. This contrasts tomography in the medical imaging community, which uses the attenuation of X-rays as they travel through human tissue to image the body based on differences in attenuation coefficients for different types of tissue. Chapter 6 of this dissertation works towards using the attenuation of sound waves in seawater, rather than the travel time, to image the ocean for properties including temperature, salinity, and pH. Attenuation tomography is not yet a fully developed method; however, the initial results presented in Chapter 6 show that it is possible to measure the attenuation of sound along eigenray paths in order to estimate attenuation coefficients. If enough rays, with a variety of trajectories and sufficient sampling of the water column are measured, then it will likely be possible to conduct layered inversions for attenuation coefficients which in turn could yield measurements of properties like pH.

It is possible to estimate acoustic volume attenuation coefficients in the ocean by beam-forming onto eigenrays. This technique should be used to quantitatively compare ocean attenuation in different ocean basins under different physical and chemical oceanographic conditions. This will be beneficial for predicting SONAR performance parameters in the detection theory community. Comparisons using the the three Mid-Frequency Noise (MFN) experiments conducted by the Marine Physical Laboratory (MPL) off the coast of California, Oregon, and Iceland should be made. Additionally, it may be possible to combine enough eigenrays to complete a layered inversion of attenuation coefficients, which could be extended to inversions for temperature, salinity, and pH. Progress has been made toward accomplishing this using the dataset collected off the coast of Iceland during the summer of 2015.

7.2 Concluding Thoughts

Acoustic sources of opportunity can be used to localize sources and gain information about the environment. Source of opportunity based acoustic source localization and tomography are far from solved problems, and a great deal of

research remains to be done. This thesis can be thought of as a feasibility study, working towards the use of sources of opportunity in ocean sensing.

Bibliography

[1] Finn B Jensen, William A Kuperman, Michael B Porter, and Henrik Schmidt. *Computational ocean acoustics*. Springer Science & Business Media, 2011.

[2] J D Tippmann, J Sarkar, C M A Verlinden, W S Hodgkiss, and W A Kupermangbd. Toward ocean attenuation tomography : Determining acoustic volume attenuation coefficients in seawater using eigenray amplitudes. 247:1–5, 2016.

[3] A. B. Baggeroer, W. A. Kuperman, and P. N. Mikhalevsky. An overview of matched field methods in ocean acoustics. *IEEE Journal of Oceanic Engineering*, 18(4):401–424, 1993.

[4] Kay L Gemba, William S Hodgkiss, and Peter Gerstoft. Adaptive and compressive matched field processing. *The Journal of the Acoustical Society of America*, 141(1):92–103, 2017.

[5] Karim G Sabra, Bruce D Cornuelle, and William A Kuperman. Sensing deep-ocean temperatures. *Physics today*, 69(2):32, 2016.

[6] Walter Munk and Carl Wunsch. Ocean acoustic tomography: A scheme for large scale monitoring. *Deep Sea Research Part A. Oceanographic Research Papers*, 26(2):123–161, 1979.

[7] Gregory Sinnett and Falk Feddersen. The surf zone heat budget : The effect of wave heating. pages 7217–7226, 2014.

[8] Walter Munk. Acoustic thermometry of ocean climate (ATOC). In *The 3rd Symposium on Integrated Observing Systems*, 1995.

[9] Brian D Dushaw, Peter F Worcester, Walter H Munk, Robert C Spindel, James A Mercer, Bruce M Howe, Kurt Metzger, Theodore G Birdsall, Rex K Andrew, Matthew A Dzieciuch, and Others. A decade of acoustic thermometry in the North Pacific Ocean. *Journal of Geophysical Research: Oceans*, 114(C7), 2009.

[10] ATOC Consortium and Others. Ocean climate change: Comparison of acoustic tomography, satellite altimetry, and modeling. *Science*, 281(5381):1327–1332, 1998.

[11] M. J. Buckingham, B. V. Berkhout, and S. A. L. Glegg. Imaging the Ocean with Ambient Noise. *Journal of the Acoustic Society of America*, 356(March):327–329, 1992.

[12] P. Roux and W. A. Kuperman. Extracting coherent wave fronts from acoustic ambient noise in the ocean. *The Journal of the Acoustical Society of America*, 116(4):1995, 2004.

[13] M. Siderius, C. H. Harrison, and M. B. Porter. A passive fathometer technique for imaging seabed layering using ambient noise. *The Journal of the Acoustical Society of America*, 120(3):1315, 2006.

[14] Martin Siderius, Heechun Song, Peter Gerstoft, William S Hodgkiss, Paul Hursky, and Chris Harrison. Adaptive passive fathometer processing. *The Journal of the Acoustical Society of America*, 127(4):2193–200, apr 2010.

[15] Peter Gerstoft, William S Hodgkiss, Martin Siderius, Chen-Fen Huang, and Chris H Harrison. Passive fathometer processing. *The Journal of the Acoustical Society of America*, 123(3):1297–305, mar 2008.

[16] Lanfranco Muzi, Martin Siderius, and Christopher M A Verlinden. Passive bottom reflection-loss estimation using ship noise and a vertical line array Lanfranco Muzi,. *Journal of the Acoustic Society of America*, SUBMITTED:1–29, 2017.

[17] S. E. Fried, W. A. Kuperman, K. G. Sabra, and P. Roux. Extracting the local Green's function on a horizontal array from ambient ocean noise. *The Journal of the Acoustical Society of America*, 124(4):EL183–8, oct 2008.

[18] A. M. Thode, G. L. D'Spain, and W. A. Kuperman. Matched-field processing, geoacoustic inversion, and source signature recovery of blue whale vocalizations. *The Journal of the Acoustical Society of America*, 107(3):1286–300, mar 2000.

[19] Karim G Sabra, Bruce Cornuelle, William A Kuperman, and William A Kuperman. TEMPERATURES. 69(2), 2016.

[20] Katherine F Woolfe, Shane Lani, Karim G Sabra, and W A Kuperman. acoustic ambient noise. pages 2878–2884, 2015.

[21] Katherine F Woolfe and Karim G Sabra. Optimized extraction of coherent arrivals from ambient noise correlations in a rapidly fluctuating medium. 138(October):375–381, 2015.

[22] Katherine F Woolfe, Shane Lani, Karim G Sabra, and William A Kuperman. Monitoring deep-ocean temperatures using acoustic ambient noise. *Geophysical Research Letters*, 42(8):2878–2884, 2015.

[23] Katherine F Woolfe and Karim G Sabra. Variability of the coherent arrivals extracted from low-frequency deep-ocean ambient noise correlations. *The Journal of the Acoustical Society of America*, 138(2):521–532, 2015.

[24] M B Porter H Schmidt F. B. Jensen W. A. Kuperman. *Computational ocean acoustics*. American Institute of Physics, Woodbury, NY, 2011.

[25] L. T. Fialkowski, M. D. Collins, W. A. Kuperman, J. S. Perkins, L. J. Kelly, A. Larsson, J. A. Fawcett, and L. H. Hall. Matched-field processing using measured replica fields. *The Journal of the Acoustical Society of America*, 107(2):739–46, feb 2000.

[26] Paul Hursky, Michael B. Porter, Martin Siderius, and Vincent K. McDonald. High-frequency (8âĂŞ16 kHz) model-based source localization. *The Journal of the Acoustical Society of America*, 115(June):3021, 2004.

[27] Stephen P. Czenszak and Jeffrey L. Krolik. Robust wideband matched-field processing with a short vertical array. *The Journal of the Acoustical Society of America*, 101(March 1996):749, 1997.

[28] F B Jensen, W A Kuperman, M B Porter, and H Schmidt. Computational ocean acoustics. chapter 2.3.3. American Institute of Physics, Woodbury, NY, 1994.

[29] G. A. Grachev and J. S. Wood. Theory of acoustic field invariants in layered waveguides. *Acoustical physics*, 39(1):33–35.

[30] S S Chuprov. Interference structure of the sound field in a stratified ocean In: Ocean acoustics. *Current status (ed) LM Brekhovskikh [Moscow, Nauka, p. 71–91](in Russian)*, 1982.

[31] W A Kuperman, G L D'Spain, H C Song, A M Thode, and Shallow Water Variability. The Generalized Waveguide Invariant Concept with Application to Vertical Arrays in The Generalized Waveguide Invariant Concept with Application to Vertical Arrays in Shallow Water. In *Ocean Acoustic Interference Phenomena and Signal Processing*, volume 33. American Institute of Physics, 2002.

[32] G L D'Spain and W A Kuperman. Application of waveguide invariants to analysis of spectrograms from shallow water environments that vary in range and azimuth. *Journal of the Acoustical Society of America*, 106(5):2454–2468, 1999.

[33] S. V. Burenkov. Distinctive features of the interference structure of a sound field in a two-dimensionally inhomogeneous waveguide. *Akustičeskij žurnal*, 35(5):797–800, 1988.

[34] W S Hodgkiss, H C Song, W A Kuperman, T Akal, C Ferla, and D R Jackson. A long-range and variable focus phase-conjugation experiment. *Journal of the Acoustic Society of America*, 105(3):1597–1604, 1999.

[35] Seongil Kim, W A Kuperman, W S Hodgkiss, H C Song, G F Edelmann, and T Akal. Robust time reversal focusing in the ocean. *The Journal of the Acoustical Society of America*, 114(1):145–157, 2003.

[36] G.F. Edelmann, W.S. Hodgkiss, S Kim, W.a. Kuperman, H.C. Song, and T. Akal. Underwater acoustic communication using time reversal. *MTS/IEEE Oceans 2001. An Ocean Odyssey. Conference Proceedings (IEEE Cat. No.01CH37295)*, 4:2231–2235, 2001.

[37] W A Kuperman, S Kim, G F Edelmann, W S Hodgkiss, H C Song, and T Akal. *Group and Phase Speed Analysis for Predicting and Mitigating the Effects of Fluctuations*, pages 279–286. Springer Netherlands, Dordrecht, 2002.

[38] C Gervaise, B G Kinda, J Bonnel, Y. SteÌĄphan, and S Vallez. Passive geoacoustic inversion with a single hydrophone using broadband ship noise. *The Journal of the Acoustical Society of America*, 131(3):1999, 2012.

[39] W A Kuperman, G L D'Spain, and K D Heaney. Long range source localization from single hydrophone spectrograms. *J Acoust Soc Am*, 109(5 I):1935–1943, 2001.

[40] Hailiang Tao and Jeffrey L Krolik. Waveguide invariant focusing for broadband beamforming in an oceanic waveguide. *The Journal of the Acoustical Society of America*, 123(3):1338–1346, 2008.

[41] Kevin L Cockrell and Henrik Schmidt. Robust passive range estimation using the waveguide invariant. *Journal of the Acoustic Society of America*, 127(5):2780–2789, 2009.

[42] Aaron M Thode. Source ranging with minimal environmental information using a virtual receiver and waveguide invariant theory. *The Journal of the Acoustical Society of America*, 108(4):1582–1594, 2000.

[43] Altan Turgut, Laurie T Fialkowski, and Jeffrey A Schindall. Measured depth-dependence of waveguide invariant in shallow water with a summer profile. *Journal of the Acoustic Society of America Express Letters*, 139(June):184–189, 2016.

[44] Daniel Rouseff. Effect of shallow water internal waves on ocean acoustic striation patterns. *Waves in Random Media*, 11(4):377–393, 2001.

[45] Daniel Rouseff and Robert C Spindel. Modeling the waveguide invariant as a distribution. *AIP Conference Proceedings*, 621(May 2015):137–148, 2002.

[46] S T Rakotonarivo and W A Kuperman. Model-independent range localization of a moving source in shallow water. *The Journal of the Acoustical Society of America*, 132(4):2218, 2012.

[47] Altan Turgut, Marshall Orr, and Daniel Rouseff. Broadband source localization using horizontal-beam acoustic intensity striations. *Journal of the Acoustic Society of America*, 127(2):73–83, 2010.

[48] Kevin L Cockrell and Henrik Schmidt. A modal Wentzel-Kramers-Brillouin approach to calculating the waveguide invariant for non-ideal waveguides. *Journal of the Acoustic Society of America*, 130(1):72–83, 2011.

[49] A Harms, J L Odom, and J L Krolik. Ocean acoustic waveguide invariant parameter estimation using tonal noise sources. In *2015 IEEE International Conference on Acoustics, Speech and Signal Processing (ICASSP)*, pages 4001–4004, apr 2015.

[50] Christopher M A Verlinden, J Sarkar, W S Hodgkiss, W A Kuperman, and K G Sabra. Passive acoustic source localization using sources of opportunity. *The Journal of the Acoustical Society of America*, 138(1):EL54–9, 2015.

[51] A Turgut and L T Fialkowski. Method of passive acoustic depth determination in shallow water, 2015.

[52] Christopher M A Verlinden, Jit Sarkar, Bruce D. Cornuelle, and William A Kuperman. Determination of acoustic waveguide invariant using ships as sources of opportunity in a shallow water marine environment. *The Journal of the Acoustical Society of America*, (February, 2017):1–7, 2017.

[53] Sydney Levitus and T P Boyer. World Ocean Atlas 1994. Volume 4. Temperature. Technical report, National Environmental Satellite, Data, and Information Service, Washington, DC (United States), 1994.

[54] G. Clifford Carter, Albert H. Nuttall, and Peter G. Cable. The Smoothed Coherence Transform. *Proceedings of the IEEE*, 61(10):1497–1498, 1973.

[55] Michael J Buckingham. Cross-correlation in band-limited ocean ambient noise fields. *The Journal of the Acoustical Society of America*, 131(4):2643–57, apr 2012.

[56] U.S. Coast Guard. United States Coast Guard Navigation Center, Nationwide AIS Database, AIS Messages, 2012.

[57] Karim G Sabra, Stephanie Fried, W A Kuperman, and Mark Prior. On the coherent components of low-frequency ambient noise in the Indian Ocean. *The Journal of the Acoustical Society of America*, 133(1):EL20—-EL25, 2013.

[58] Bruce D Cornuelle. Acoustic tomography. *IEEE Transactions on Geoscience and Remote Sensing*, (3):326–332, 1982.

[59] Paul Hursky, Michael B Porter, Bruce D Cornuelle, William S Hodgkiss, and William A Kuperman. Adjoint modeling for acoustic inversion. *The Journal of the Acoustical Society of America*, 115(2):607–619, 2004.

[60] Michael B Porter. The BELLHOP Manual and User ' s Guide : PRELIMINARY DRAFT. pages 1–57, 2011.

[61] Edwin L Hamilton. Compressional-wave attenuation in marine sediments. *Geophysics*, 37(4):620–646, 1972.

[62] Bikramjit Sarkar. Linear acoustic sensitivity kernels and their applications in shallow water environments. 2011.

[63] Christopher Garrett and Walter Munk. Space-Time scales of internal waves. *Geophysical Fluid Dynamics*, 3(1):225–264, 1972.

[64] Michael D Collins, William A Kuperman, and Henrik Schmidt. Nonlinear inversion for ocean-bottom properties. *The Journal of the Acoustical Society of America*, 92(5):2770–2783, 1992.

[65] A. Tolstoy, O. Diachok, and L. N. Frazer. Acoustic tomography via matched field processing. *The Journal of the Acoustical ...*, pages 1119–1127, 1991.

[66] Bruce D Cornuelle, Carl Wunsch, David Behringer, Theodore Birdsall, Merle Brown, Robert Heinmiller, Ryan Knox, Kurt Metzger, Walter Munk, John Spiesberger, and Others. Tomographic maps of the ocean mesoscale. Part 1: Pure acoustics. *Journal of physical oceanography*, 15(2):133–152, 1985.

[67] Sung-Hoon Byun, Karim G Sabra, Ning Tian, and Justin Romberg. Multichannel blind deconvolution of sound source of opportunity in ocean waveguide. *The Journal of the Acoustical Society of America*, 137(4):2212, 2015.

[68] Michael J Bianco and Peter Gerstoft. Dictionary learning of acoustic sound speed profiles. *The Journal of the Acoustical Society of America*, 140(4):3054, 2016.

[69] Peter Gerstoft. Global inversion by genetic algorithms for both source position and environmental parameters. *Journal of Computational Acoustics*, 2(03):251–266, 1994.

[70] G Jin and P F Worcester. The feasibility of Measuring Ocean pH by Long-Range Acoustics. *Journal of Geophysical Resarch*, 94(C4):4749–4756, 1989.

[71] Timothy F Duda. Revisiting experimental methods for studies of acidity-dependent ocean sound absorption. *The Journal of the Acoustical Society of America*, 125(4):1971–81, apr 2009.

[72] M Ainslie. *Principles of Sonar Performance Modelling*. Springer Praxis Books in Geophysical Sciences. Springer-Verlag Berlin Heidelberg, 2010.

[73] R. E. Francois and G. R. Garrison. Sound absorption based on ocean measurements . Part II : Boric acid contribution and equation for total absorption of sound. *The Journal of the Acoustical Society of America*, 72(6):1879–1890, 1982.

[74] Peter G. Brewer. Ocean chemistry of the fossil fuel co2 signal: The haline signal of âĂIJbusiness as usualâĂİ. *Geophysical Research Letters*, 24(11):1367–1369, 1997.

[75] Keith C. Hester, Edward T. Peltzer, William J. Kirkwood, and Peter G. Brewer. Unanticipated consequences of ocean acidification: A noisier ocean at lower pH. *Geophysical Research Letters*, 35(19):L19601, oct 2008.

[76] D. Benjamin Reeder and Ching-Sang Chiu. Ocean acidification and its impact on ocean noise: Phenomenology and analysis. *The Journal of the Acoustical Society of America*, 128(3), 2010.

[77] Scott C. Doney, Victoria J. Fabry, Richard A. Feely, and Joan A. Kleypas. Ocean acidification: The other co2 problem. *Annual Review of Marine Science*, 1(1):169–192, 2009.

[78] M. A. Ainslie and J. G. Mccolm. A simplified formula for viscous and chemical absorption in sea water. *The Journal of the Acoustical Society of America*, 103(3):1671, 1998.

[79] W. H. Thorp. Deep-Ocean Sound Attenuation in the Sub- and Low-Kilocycle-per-Second Region. *The Journal of the Acoustical Society of America*, (38):648–674, 1965.

[80] R. E. Francois and G. R. Garrison. Sound absorption based on ocean measurements: Part I: Pure water and magnesium sulfate contributions. *The Journal of the Acoustical Society of America*, 72(3):896, 1982.

[81] Matthew A Dzieciuchkgs and Matthew A Dzieciuch. Signal processing and tracking of arrivals in ocean acoustic tomography. 2512, 2014.